Calhoun
Institutional Archive of the Naval Postgraduate School

Calhoun: The NPS Institutional Archive

DSpace Repository

Theses and Dissertations | 1. Thesis and Dissertation Collection, all items

1969

Measurements of half lives of isomeric states in certain off A nuclei.

Peters, James Stephen

Massachusetts Institute of Technology

http://hdl.handle.net/10945/12640

Downloaded from NPS Archive: Calhoun

http://www.nps.edu/library

Calhoun is the Naval Postgraduate School's public access digital repository for research materials and institutional publications created by the NPS community. Calhoun is named for Professor of Mathematics Guy K. Calhoun, NPS's first appointed -- and published -- scholarly author.

Dudley Knox Library / Naval Postgraduate School
411 Dyer Road / 1 University Circle
Monterey, California USA 93943

NPS ARCHIVE
1969
PETERS, J.

MEASUREMENTS OF HALF LIVES OF ISOMETRIC STATES IN CERTAIN ODD A NUCLEI

by

James Stephen Peters

MEASUREMENTS OF HALF LIVES OF ISOMERIC STATES IN CERTAIN ODD A NUCLEI

by

JAMES STEPHEN PETERS

B.S., United States Naval Academy
(1967)

SUBMITTED IN PARTIAL FULFILLMENT OF THE
REQUIREMENTS FOR THE DEGREES OF
MASTER OF SCIENCE AND
NUCLEAR ENGINEER
at the
MASSACHUSETTS INSTITUTE OF TECHNOLOGY
September, 1969

NPS ARCHIVE
1969
PETERS, J.

LIBRARY
NAVAL POSTGRADUATE SCHOOL
MONTEREY, CALIF. 93940

DUDLEY KNOX LIBRARY
NAVAL POSTGRADUATE SCHOOL
MONTEREY, CA 93943-5101

MEASUREMENTS OF HALF LIVES OF ISOMERIC STATES IN CERTAIN ODD A NUCLEI

by

JAMES S. PETERS

Submitted to the Department of Nuclear Engineering on August 18, 1969, in partial fulfillment of the requirements for the degrees of Master of Science and Nuclear Engineer.

ABSTRACT

The determination of nuclear level mean lives is performed by de-excitation gamma ray detection. The high resolution of both the electronic equipment and Ge(Li) detector allow time spectra of the excited level gamma decay to be obtained. After background reduction, a least squares fit of the measured time spectra to the theoretically derived time spectra results in the experimental determination of excited level mean lives. The detection system can be used to measure mean lives between the limits of approximately 200 to 10 nanoseconds.

An immediate value for these mean lives is in the experimental measurement of neutron inelastic scattering cross sections. Since, in the cross section measurements, the background is reduced by time gating, a correction must be made if the nuclear levels do not completely de-excite within this relatively narrow time gate. In order to determine if a correction is warranted and if so, the size, the mean lives of the excited levels must be known.

The mean lives of nuclear levels in F^{19}, Cd^{111}, and Ta^{181} are measured. The measurements compare favorably with the known values. A search for long lived excited levels in Nb^{93} and Sc^{45} was conducted. The experimental results, together with Weisskopf's single particle estimates, showed that none of the levels investigated, with the exception of the .376 MeV level in Sc^{45}, had mean lives greater than the limit of sensitivity of the detection system, about 10 nanoseconds. The .376 MeV level in Sc^{45} was found to have an experimentally observed mean life in the region of 10 nanoseconds. Further work must be conducted to confirm this measurement.

ACKNOWLEDGEMENTS

Sincere appreciation is felt for the many persons who helped with this thesis. Professor Franklyn Clikeman not only aided the author with his duties as thesis supervisor but also contributed encouragement and interest through the exchange of ideas. Acknowledgement is also given to Dr. Leon Beghian whose assistance with both the thesis and the accelerator performance were essential.

Gratitude is extended to Dr. Vern Rogers for his many hours of patience in helping the author understand the experimental system. Further appreciation is acknowledged for the ceaseless efforts of Daniel Sullivan in maintaining and operating of the Van de Graaff Accelerator.

The author thanks Clare Egan for her excellent typing and cheery enthusiasm.

The author acknowledges the support of the Atomic Energy Commission in the form of a fellowship in Nuclear Engineering.

The fortune of having an understanding wife greatly facilitated the completion of this thesis. The continued support from Patricia allowed these two years at M.I.T. to be very enjoyable.

TABLE OF CONTENTS

	Page
ABSTRACT	2
ACKNOWLEDGEMENTS	3
TABLE OF CONTENTS	4
LIST OF FIGURES	6
LIST OF TABLES	10
I. INTRODUCTION	11
II. THEORY	16
III. DESCRIPTION OF EXPERIMENTAL EQUIPMENT	31
3.1 General Arrangement	31
3.2 Neutron Normalization	39
3.3 Electronic Equipment	41
3.3.1 The Time Spectrum	41
3.3.2 Time Gated Energy Spectra	45
3.3.3 Time Resolution	48
3.4 Detector Time Response	55
IV. EXPERIMENTAL METHODS	60
4.1 Introduction	60
4.2 Indirect Method For Excited Level Mean Life Determination	60
4.3 Direct Method of Excited Level Mean Life Determination	61
4.4 Background Subtraction	65
4.4.1 Type of Background	65
4.4.2 Detector Time Response	69
4.4.3 Methods of Background Subtraction	72

		Page
4.5	Analysis of the Two Mean Life Determination Techniques After Background Subtraction	79
4.6	Quick Method for Determining the Presence of Long-Lived Excited Levels	80
4.7	Errors Associated With Experimental Mean Life Measurements	82
V.	EXPERIMENTAL RESULTS AND DISCUSSION	85
5.1	Excited Level Mean Life Determination in F^{19}, Cd^{111}, and Ta^{181}	85
	5.1.1 Indirect Method Results	85
	5.1.2 Direct Method Results	87
	5.1.3 Discussion	102
5.2	The Search for Long Lived Excited Levels in Nb^{93} and Sc^{45}	108
	5.2.1 Niobium Results	109
	5.2.2 Scandium Results	124
VI.	CONCLUSIONS AND RECOMMENDATIONS FOR FURTHER WORK	132
6.1	Conclusions	132
6.2	Recommendations for Further Work	133
	6.2.1 Leading Edge Timing	133
	6.2.2 Double Variable Least Squares Fit	133
	6.2.3 Improvements of Theoretical Detector Time Response	135
REFERENCES		136

LIST OF FIGURES

		Page
1.1	Time Spectrum With Prompt De-excitation Time Gate	12
2.1	Range of Weisskopf Single Particle Estimates	28, 29
3.1	Experimental Setup For De-excitation Gamma Ray Measurements	32
3.2	Neutron Energy As a Function of Proton Energy and Reaction Angle For Li^7	34
3.3	Neutron Energy As a Function of Proton Energy and Reaction Angle For H^3	35
3.4	The Scatterer (Scattering Sample) The Front Shield	37
3.5	Detector Resolution Versus Bias Voltage	38
3.6	Long Counter Used For Neutron Normalization	40
3.7	Electronic Block Diagram For Time Spectra	42
3.8	Time Spectrum	44
3.9	Electronic Block Diagram For Time Gated Energy Spectra	46
3.10	Electronic Block Diagram For Measurements of Time Gated Energy Spectra of De-excitation Gamma Rays	47
3.11	Electronic Diagram For Leading Edge Timing	49
3.12	Timing Signal Characteristics For Identically Shaped Pulses	51
3.13	Timing Signal Characteristics For NOn-identically Shaped Pulses	52
3.14	Time Spectrum From Leading Edge Timing Electronics, Narrow Energy Window (10 keV)	53

		Page
3.15	Time Spectrum From Crossover Pick-off Timing Electronics, Wide Energy Range (170 keV-2.6 MeV)	54
3.16	Time Spectrum From Planar Detector	56
3.17	Time Spectrum From Crystal Used in This Thesis	58
3.18	Asymmetric Exponential Trial on Time Spectrum	59
4.1	Photopeaks From Various Time Gated Energy Spectra.	62
4.2	Time Gate Positions and Reconstructed Time Spectrum	63
4.3	Elimination of Background by Photopeak Area (Indirect) Method	64
4.4	Background Sources	67
4.5	Time Spectrum Showing Background Contributions	71
4.6	Exponential Decay	76
4.7	The Effect of the Detector Mean Life on the Amplitude of the Time Spectrum	78
4.8	Time Spectrum With Prompt and 50 Nanosecond Delayed Time Gates	81
5.1	Normalized Theoretical Time Spectra	86
5.2	F^{19} Energy Level Diagram	88
5.3	F^{19} Time Gated Energy Spectrum, Neutron Energy, 1.41 MeV	89
5.4	Cd^{111} Energy Level Diagram	90
5.5	Cd^{111} Time Gated Energy Spectrum, Neutron Energy, 1.5 MeV	91
5.6	Time Gated Photopeaks For the .197 MeV Gamma Decay in F^{19}	92 - 96

		Page
5.7	F^{19} Time Gate Positions on 125 Nanosecond Period Time Spectrum	97
5.8	F^{19} Reconstructed Time Spectrum	97
5.9	Time Gated Photopeaks for the .247 MeV Gamma Decay in Cd^{111}	98
5.10	Cd^{111} Time Gate Positions on 125 Nanosecond Period Time Spectrum	99
5.11	Cd^{111} Reconstructed Time Spectrum	99
5.12	Ta^{181} Energy Level Diagram	100
5.13	Ta^{181} Time Gated Energy Spectrum, Neutron Energy, 1.41 MeV	101
5.14	F^{19} Direct Method Time Spectrum, No Background Subtraction	103
5.15	F^{19} Direct Method Time Spectrum, Background Subtracted	104
5.16	Ta^{181} Direct Method Time Spectrum, No Background Subtraction	105
5.17	Ta^{181} Direct Method Time Spectrum, Background Subtracted	106
5.18	Nb^{93} Energy Level Diagram	110
5.19	Nb^{93} Time Gated Energy Spectrum, Neutron Energy, 1.79 MeV	111
5.20	Sc^{45} Energy Level Diagram	112
5.21	Sc^{45} Time Gated Energy Spectrum, Neutron Energy, 1.69 MeV	113
5.22	F^{19}, 197 keV Level, Prompt Versus Delayed Photopeaks	114
5.23	Nb^{93}, 742 keV Level, Prompt Versus Delayed Photopeaks	115

	Page
5.24 Nb^{93}, 808 keV Level, Prompt Versus Delayed Photopeaks	116
5.25 Nb^{93}, 809 keV Level, Prompt Versus Delayed Photopeaks	117
5.26 Nb^{93}, 952 keV Level, Prompt Versus Delayed Photopeaks	118
5.27 Nb^{93}, 1080 keV Level, Prompt Versus Delayed Photopeaks	119
5.28 Nb^{93}, 1295 keV Level, Prompt Versus Delayed Photopeaks	120
5.29 Nb^{93}, 1337 keV Level, Prompt Versus Delayed Photopeaks	121
5.30 Sc^{45}, 376 keV Level, Prompt Versus Delayed Photopeaks	125
5.31 Sc^{45}, 544 keV Level, Prompt Versus Delayed Photopeaks	126
5.32 Sc^{45}, 722 keV Level, Prompt Versus Delayed Photopeaks	127
5.33 Sc^{45}, 1238 keV Level, Prompt Versus Delayed Photopeaks	128
6.1 Improved Leading Edge Timing	134

LIST OF TABLES

		Page
4.1	Photon Background Sources	66
4.2	Time Dependence of Photon Background	70
5.1	Comparison of Experimental Measurements to Well Determined Mean Life Values	107
5.2	Excited Levels Investigated ^{3} in Nb^{93}	123
5.3	Excited Levels Investigated ^{3} in Sc^{45}	130

CHAPTER 1

INTRODUCTION

In the Ph.D. theses of Hoffman [1] and Mahoney [2], it was suggested that mean lives of excited states of the nucleus could be measured in the 10-120 nanosecond region using the pulsed neutron source and high resolution electronics available at the M.I.T.'s Rockefeller Van de Graaff Accelerator.

The nuclei to be investigated are bombarded with neutron bursts produced by the reaction of a pulsed proton beam from the accelerator (4 nanoseconds pulse width, 125 nanosecond period) on a tritium ($H^3(p,n)\ He^3$) or lithium ($Li^7(p,n)\ Be^7$) target. A high resolution solid state lithium drifted germanium, Ge(Li), detector is placed 40 cm from the sample. Due to this relatively large distance between sample and detector, the faster speed of the photons with respect to the neutrons causes the gamma ray time spectrum over the 125 nanosecond period to be resolved into two distinct peaks (Figure 1.1). The first peak in time, (A), corresponds to the prompt gamma rays from the de-excitation of the excited states produced by the neutron inelastic scattering in the sample. The second peak, (B), represents the gamma rays produced by the interaction of all neutrons, elastic and inelastic, incident on the detector and its auxilary equipment.

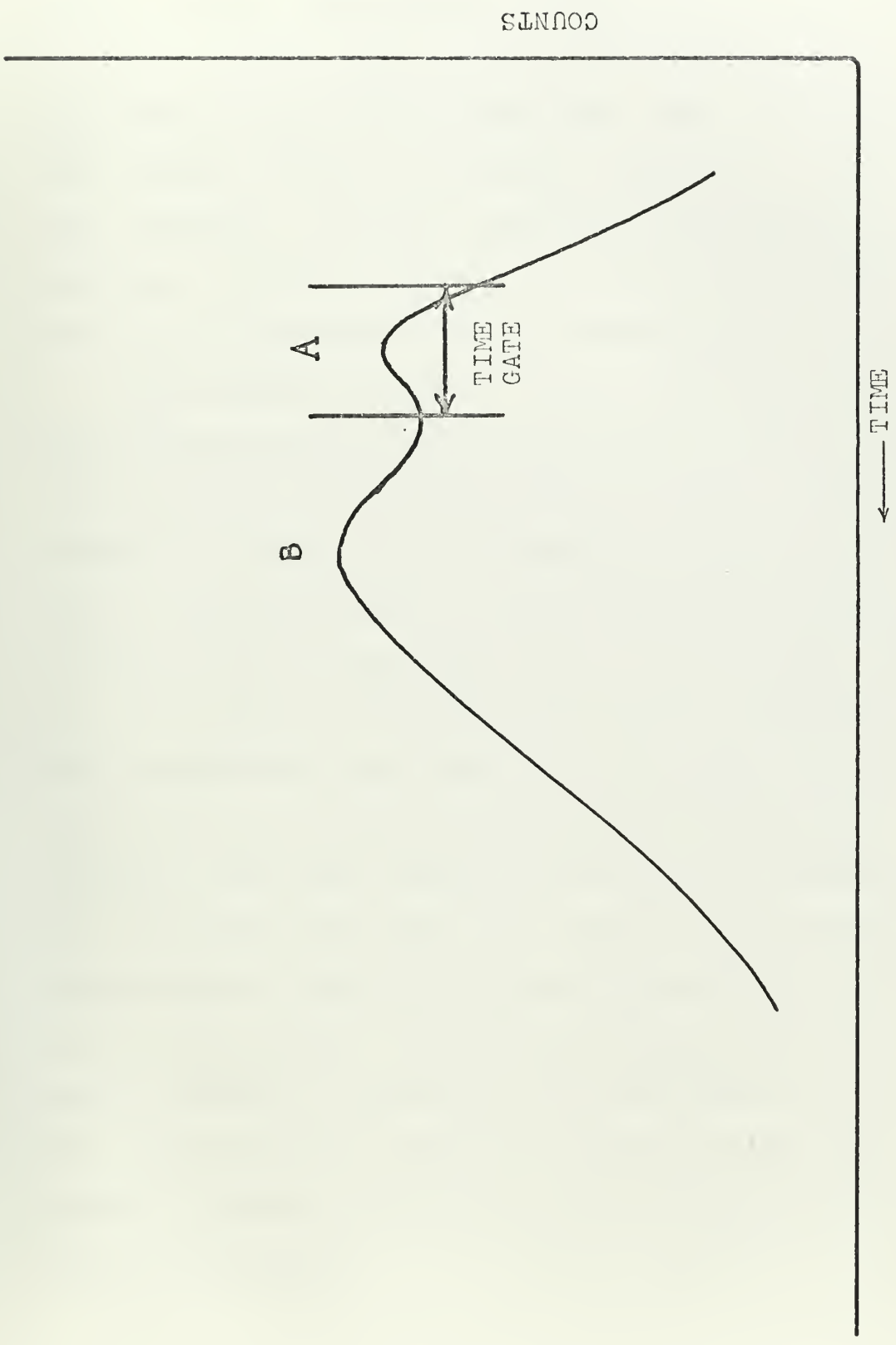

1.1 Time Spectrum With Prompt De-excitation Time Gate

In order to measure the mean life of a particular excited level, the analyzing system must be energy gated to accept photons only with the approximate energy of the particular de-excitation gamma ray. Next the time dependent, fast neutron induced, background peak (B), is measured and subtracted. From the remaining prompt gamma ray time spectrum, the decay constant (λ), and thus the mean life ($\tau = 1/\lambda$), of the excited state is determined.

One immediate value of the mean life measurements is their importance in determining accurate neutron inelastic cross-sections. The method used by Hoffman, Mahoney, and Rogers [3] to obtain neutron inelastic cross section values was to experimentally measure the gamma ray production cross section for each gamma ray of a particular nuclide. From the energy of the gamma rays and the thresholds of their production cross sections, the nuclear level structure and the level excitation functions were determined. These functions were then compared with similarly measured gamma ray excitation functions for a material with known inelastic cross section values (in the work referenced above Fe^{56} was used as the known). After determining the correct level cross sections by comparison with the known, the values for the various nuclear levels were added to obtain the total neutron inelastic cross section for the particular nucleus being investigated.

In experimentally detecting the de-excitation gamma rays from the sample, the background peak (B) was eliminated by time gating, and accepting for analysis, only the desired prompt gamma ray portion of the time spectrum (Figure 1.1). However with such time-gating, if the mean life of the excited level is of the same order of magnitude or larger than the time gate, a portion of the de-excitation gamma rays will be radiated at a later time not included in the time gate. In order to determine the actual level inelastic scattering cross section, the ratio of the de-excitation gamma rays detected in the time gate to those detected over the entire 125 nanosecond period must be known. To calculate this ratio, the mean life of the excited level must be determined.

The elements to be investigated are F^{19}, Cd^{111}, Ta^{181}, Sc^{45}, and Nb^{93}. The levels investigated in cadmium, tantalum, and fluorine are well known and are used to determine the accuracy of the experimental methods. Each has and excited level mean life in 10 - 150 nanosecond region. Scandium and niobium are viewed with the purpose of determining if the mean lives are long enough to warrant a correction in their experimentally measured neutron inelastic scattering cross section.

The remainder of the thesis is presented in the following chapters.

Chapter II points out the dependence of the mean lives on various properties of the nucleus and provides a derivation of Weisskopf's extreme single particle estimate for theoretical values of the mean lives of nuclear levels.

Chapter III describes in detail the properties of the experimental equipment used in this project.

Chapter IV presents the different experimental procedures and background subtraction methods employed in evaluating the mean lives.

Chapter V discusses the results obtained and compares them to the theoretical Weisskopf single particle estimates.

Chapter VI gives conclusions and recommendations for further optimization of the experimental system.

CHAPTER II

THEORY

With the advent of high resolution electronics the measurable lifetimes are not longer bound to the long lived excited levels but indeed are being accurately determined in the nano- and pico-second region. Consequently, the definition of a nuclear isomeric state is any excited level of the nucleus whose mean life can be experimentally measured.

The mean life, τ, of a particular excited state is inversely proportional to the transition probability (λ) from that excited level to a lower level or ground state.

$$\tau = 1/\lambda \, . \qquad (2.1)$$

The transition probability depends strongly on three factors, the change in the angular momentum (ℓ) between the initial and final states, the de-excitation gamma ray energy, and the atomic number or radius of the nuclei in question. Taken independently the effects of these three factors are as follows:

1. The greater the change in angular momentum (ℓ) or, in other words, the higher the multipolarity (e.i., E1, M1, E2, M2, E3....) of the radiation, the smaller the transition probability.

2. The greater the energy difference between the initial and final states, the higher the transition probability.

3. The larger the atomic number or nuclear radius ($R \simeq A^{1/3} \times 10^{-13}$ cm.), the greater the transition probability.

The type of multipolarity of the radiation is dependent on the relationship of the angular momentum change and the parity requirements. This dependence is represented in the familiar "selection rules" for gamma ray transitions.

The multipolarity, ℓ, is determined by the relationship

$$|J_{INITIAL} - J_{FINAL}| \leq \ell \leq J_{INITIAL} + J_{FINAL}$$

where

ℓ = an integer

$\ell \neq 0$

and J = angular momentum.

Therefore a transition between two states having angular momenta of 1/2 and 5/2 could have an ℓ of 3 or 2 with the type of multipole, electric or magnetic, depending on whether or not parity is conserved.

Theoretical estimates of these transition probabilities have been calculated. The approximation presented in this chapter will be Weisskopf's single particle estimate of multipole transition probability [4].

Although the extreme single particle theory limits

the accuracy of this approximation, Weisskopf's formulas are developed [5,6] here because of their relative simplicity in derivation and due to the fact that most experimental works compare their results in terms of the well known Weisskopf transition probabilities.

To find the probability of emission of a quantum of radiation per unit time, it is desired to find the rate of energy emission and divide it by the quantum energy, $\hbar\omega$.

In electromagnetic theory, the energy flux $\left(\frac{\text{energy}}{\text{cm}^2 - \text{sec}}\right)$ is given by the absolute value of the Poynting vector $\underline{S}$,

$$|\underline{S}| \cong \frac{c\mathcal{E}^2}{4\pi} \cong \frac{c}{4\pi}\mathcal{H}^2 , \tag{2.2}$$

assuming the source of radiation is far away.
Given the fields as

$$\underline{\mathcal{E}}(\underline{r},t) = \underline{\mathcal{E}}(\underline{r})e^{-i\omega t} + \underline{\mathcal{E}}^*(\underline{r})e^{i\omega t} , \tag{2.3}$$

and

$$\underline{\mathcal{H}}(\underline{r},t) = \underline{\mathcal{H}}(\underline{r})e^{-i\omega t} + \underline{\mathcal{H}}^*(\underline{r})e^{i\omega t} , \tag{2.4}$$

where * implies the complex conjugate, the average values for $\underline{\mathcal{E}}^2$ and $\underline{\mathcal{H}}^2$ are

$$\langle \mathcal{E}^2(\underline{r},t)\rangle_{ave} = 2\,\underline{\mathcal{E}}^*(\underline{r})\cdot\underline{\mathcal{E}}(\underline{r}) , \tag{2.5}$$

and

$$\langle \mathcal{H}^2(\underline{r},t)\rangle_{ave} = 2\,\underline{\mathcal{H}}^{*}(\underline{r})\cdot\underline{\mathcal{H}}'(\underline{r}) \quad . \tag{2.6}$$

Due to the close parallel in the derivations of both types of multipole transition probabilities, only the electric transition solution will be carried out from this point.

In quantum theory, the time independent magnetic and electric field vectors are not only functions of position but also functions of the quantum numbers ℓ and m, generated from the spherical coordinate solution of the wave equation. Therefore [5]

$$\underline{\mathcal{H}}_E(\ell,m;\underline{r}) = \frac{\mu_\ell^{(+)}(r)}{kr}\,\underline{X}_{\ell,m}(\theta,\phi) \quad , \tag{2.7}$$

where

$\mu_\ell^{+}(r)$ = the solution of the radial equation (outgoing = +),

$$\left[\frac{d^2}{dr^2} - \frac{\ell(\ell+1)}{r^2} + k^2\right] f(\ell,m;r) = 0 \quad ,$$

$\underline{X}_{\ell,m}(\theta,\phi)$ = the vector spherical harmonic

and,

$$\underline{\mathcal{H}}(\underline{r}) = a_E(\ell,m)\,\underline{\mathcal{H}}_E(\ell,m;r) \tag{2.8}$$

where

$a_E(\ell,m)$ = the amplitude of the pure electric multipole radiation ℓ,m.

To get the emission rate, $U(\ell,m)$, into the solid angle $d\Omega$, the absolute value of the Poynting vector is multiplied by $R^2 d\Omega$, the area subtended by $d\Omega$.

$$U_E(\ell,m;\Omega)d\Omega = |S| R^2 d\Omega = \frac{c}{4\pi} \mathcal{H}^2(r) R^2 d\Omega \,. \tag{2.9}$$

From equations (2.5, 2.7, 2.8, 2.9) the rate of emission of energy is

$$U(\ell,m;\Omega) = \frac{c}{2\pi k^2} \mathcal{Z}_{\ell,m}(\theta,\phi) \left| a_E(\ell,m) \right|^2 \,, \tag{2.10}$$

where

$$k = \omega/c$$

and

$\mathcal{Z}_{\ell,m}(\theta,\phi)$ = the angular distribution function $\underline{\chi}^*_{\ell,m} \cdot \underline{\chi}_{\ell,m}$

Since the integral of $\mathcal{Z}_{\ell,m}(\theta,\phi)$ is normalized [5] over $d\Omega$,

$$\int \mathcal{Z}_{\ell,m}(\theta,\phi)\, d\Omega = \int \underline{\chi}^*_{\ell,m} \cdot \underline{\chi}_{\ell,m}\, d\Omega = 1 \,, \tag{2.11}$$

the total energy emitted per unit time can be expressed as

$$U_E(\ell,m) = \frac{c}{2\pi k^2} \left| a_E(\ell,m) \right|^2 . \tag{2.12}$$

Likewise, the rate of energy emission associated with the magnetic field is

$$U_M(\ell,m) = \frac{c}{2\pi k^2} \left| a_M(\ell,m) \right|^2 . \tag{2.13}$$

The problem now is to solve for the amplitude of the electric radiation, $a_E(l,m)$. A detailed solution for $a_E(l,m)$ is given in Appendix B[5] of Theoretical Nuclear Physics by Blatt and Weisskopf. Briefly the method is described below.

Using Maxwell's equations, the wave equations at the source,

$$\nabla \times \nabla \times \underline{\mathcal{H}} - k^2 \underline{\mathcal{H}} = \frac{4\pi}{c} \left(\nabla \times \underline{j} + ck^2 \underline{M} \right) , \qquad (2.14)$$

and far from the source,

$$\nabla \times \nabla \times \underline{\mathcal{H}} - k^2 \underline{\mathcal{H}} = 0 \qquad (2.15)$$

are derived. The solutions to these equations are of the form

$$\mathcal{H}_E(r) = f(a_E(l,m)) \underline{\mathcal{H}}_E(l,m;r) . \qquad (2.16)$$

$a_E(l,m)$ is found by comparing the asymptotic solution ($r \to \infty$) of the magnetic field ($\underline{\mathcal{H}}$) at the source with the solution for $\underline{\mathcal{H}}$ far from the source. This comparison yields

$$a_E(l,m) = \frac{4\pi}{c} \int r^{-1} F_l(r) Y^*_{lm} \left(\nabla \times \underline{j} + ck^2 \underline{M} \right) dV \qquad (2.17)$$

where

$$F_l(r) = kr\, j_l(kr) ,$$

$$j_l(kr) \equiv \sqrt{\frac{\pi}{2kr}}\, J_{l+\frac{1}{2}}(kr) ,$$

$\equiv$ "spherical Bessel function" of the first kind of order ℓ.

Assuming the wave length of the photon is large compared to the dimensions of the source ($kr \ll 1$),

$$F_\ell(r) \longrightarrow \frac{(kr)^{\ell+1}}{(2\ell+1)!!}$$

where

$$(2\ell+1)!! = (1\times3\times5\times7\ldots.\,2\ell+1).$$

After the application of various vector identities, the amplitude of the electric radiation can be expressed as

$$a_E(\ell,m) \simeq \frac{-4\pi}{(2\ell+1)!!}\left(\frac{\ell+1}{\ell}\right)^{1/2} k^{\ell+2}\left(Q_{\ell,m} + Q'_{\ell,m}\right) \quad (2.18)$$

where

$Q_{\ell,m}$ = electric multipole moment of order due to current and charge distribution.

$Q'_{\ell,m}$ = electric multipole moment of order due to varying density of magnetization, $\underline{M}(r,t)$.

The energy emitted per unit time from the source of radiation can now be written as

$$U_E(\ell,m) = \frac{8\pi c}{[(2\ell+1)!!]^2}\left[\left(\frac{\ell+1}{\ell}\right) k^{2\ell+2} \left| Q_{\ell,m} + Q'_{\ell,m}\right|^2\right] \quad (2.19)$$

and again for the magnetic radiation,

$$v_M(l,m) = \frac{8\pi c}{[(2l+1)!!]^2}\left[\left(\frac{l+1}{l}\right)k^{2l+2}\left|M_{l,m}+M'_{l,m}\right|^2\right] \qquad (2.20)$$

where M = magnetic multipole moment.

As stated earlier, to find the probability of emission of a quantum of energy per second, the rate of energy emission is divided by the energy per quantum. Therefore the transmission probabilities are calculated by dividing into equations (2.19) and (2.20).

$$\lambda_{E(l,m)} = \frac{8\pi(l+1)}{l[(2l+1)!!]^2}\,\frac{k^{2l+1}}{\hbar}\left|Q_{l,m}+Q'_{l,m}\right|^2. \qquad (2.21)$$

$$\lambda_{M(l,m)} = \frac{8\pi(l+1)}{l[(2l+1)!!]^2}\,\frac{k^{2l+1}}{\hbar}\left|M_{l,m}+M'_{l,m}\right|^2. \qquad (2.22)$$

It is now necessary to determine a value for the multipole moments. In the electric case, the contribution of $Q'_{l,m}$ (due to spin) is quite small compared to that of $Q_{l,m}$ (due to charge density), thus the former is neglected. In the magnetic case the contribution of $M'_{l,m}$ is believed to be roughly 2 to 3 times the contribution of $M_{l,m}$[5].

In cartesian coordinates, a multipole moment may be expressed as

$$M_x(l) = \int x^l \rho\, d\tau \qquad (2.23)$$

where

$M_x(\ell)$ = the x component of the multipole moment of order ℓ

ρ = the change density

and

$d\tau$ = the volume element

In spherical coordinates, the electric multipole moment is defined as

$$Q_{\ell,m} = \int r^{\ell} Y^{*}_{\ell m}(\theta,\phi)\rho\, d\tau. \qquad (2.24)$$

In order to transform equation (2.24) to conform to a quantum mechanical system, the charge density is redefined in terms of the unit charge times the wave equation probability density, $\psi\psi^*$. Another change is due to the fact that equation (2.24) expresses the moment at only one state. However, in transition theory, a matrix element is needed to express the jump from the initial state, 1, to the final state, 2. Therefore the "quantized" definition for the electric multipole matrix element is

$$Q_{\ell,m}(1\to 2) = e\sum_{k=1}^{z}\int r_k^{\ell}\, Y^{*}_{\ell,m}(\theta_k,\phi_k)\,\psi_2^{*}\psi_1\, d\tau\,. \qquad (2.25)$$

With the exception of deuteron, the exact wave equation for the excited levels are unknown. Hence only an order of magnitude approximation can be made for the transition probabilities. In his estimates, Weisskopf used the simple shell and single particle model in order to obtain an

approximation of the wave functions, ψ_1 and ψ_2. The single particle model assumes that the angular momentum and parity are carried only by the odd nucleon and that the remaining nucleons form a spherically symmetric charge distribution. The initial wave function, ψ_1, of the odd nucleon is

$$\psi_1 = R_1(r) Y_{l,m}(\theta,\phi) . \tag{2.26}$$

The final state is assumed to be an s-state $(l=0)$ with spin parallel to the initial state. The final wave function, ψ_2, is

$$\psi_2 = \frac{R_2(r)}{\sqrt{4\pi}} . \tag{2.27}$$

Another assumption is that $R_1(r)$ and $R_2(r)$ are constants inside the nucleus and zero outside.

If these radial wave equations are normalized,

$$\int_0^R |R_1(r)|^2 r^2 dr = 1$$

$$\int_0^R |R_2(r)|^2 r^2 dr = 1$$

the integration yields $R_1(r) = R_2(r) = \sqrt{3/R^3}$. The electric multipole matrix element now becomes

$$Q_{l,m}(1\to 2) = \frac{e}{\sqrt{4\pi}} \int_{\text{Volume}} r^l \frac{3}{R^3} Y^*_{l,m}(\theta,\phi) Y_{l,m}(\theta,\phi) \cdot r^2 \sin\theta \, dr \, d\theta \, d\phi . \tag{2.28}$$

(The "k's" from equation (2.25) are, of course, eliminated because of the use of the single particle model.)

Due to the normalization of the spherical harmonic function, equation 2.11, the integral over θ and ϕ equal unity. The integral of the radial component, from 0 to R, yields

$$Q_{l,m}(1\to 2) = \frac{e}{\sqrt{4\pi}} \frac{3R^l}{(l+3)} \quad . \tag{2.29}$$

Inserting the above equation into equation (2.21), results in the Weisskopf single particle estimate of the electric multipole radiation transition probability.

$$\lambda_{E_W}(l) = \frac{2(l+1)}{l[(2l+1)!!]^2}\left(\frac{3}{l+3}\right)^2 \frac{e^2R^2}{4\pi\epsilon_0\hbar}\left(\frac{\omega}{c}\right)^{2l+1} \cdots\cdots \left[\frac{1}{sec}\right] \quad , \tag{2.30}$$

or, more commonly,

$$\lambda_{E_W}(l) = \frac{4.4\,(l+1)\,10^{21}}{l[(2l+1)!!]^2}\left(\frac{3}{l+3}\right)^2\left(\frac{E_\gamma}{197}\right)^{2l+1} R^{2l} \tag{2.31}$$

where E_γ is in Mev.

R is in fermis $[10^{-13}\,cm]$.

Likewise the magnetic transition probability is

$$\lambda_{M_W}(l) = \frac{1.9\,(l+1)\,10^{21}}{l[(2l+1)!!]^2}\left(\frac{3}{l+3}\right)^2\left(\frac{E_\gamma}{197}\right)^{2l+1} R^{2l-2} \tag{2.32}$$

From equation (2.1) the mean life can be determined.

It must be pointed out that the probabilities derived above are only for transitions by multipole radiation or gamma decay. However, if another process such as internal conversion or beta decay is in competition with the gamma transition, the experimentally observed mean life will be shorter. In the case of internal conversion, the observed mean life can be expressed as

$$\tau_{obs.} = (1+\alpha)\tau_W \qquad (2.33)$$

where α is the internal conversion coefficient and τ_W is the Weisskopf estimate.

The accuracy of the Weisskopf estimates when compared to experimental data depend on the multipolarity of the transition. Figure 2.1 shows the range of accuracy for the various types of radiation[7]. The terms "enhanced" or "hindered" are commonly used to express experimental results with reference to Weisskopf estimates.

The large discrepancies between experimental data and Weisskopf's theoretical probabilities are largely due to the insufficiency of the single particle model. The collective model with its rotational levels would be more appropiate for even-even nuclei [3]. Yet, for odd A nuclei, one might suppose that the single particle model would give comparable results. Even if the odd nucleon was not the only

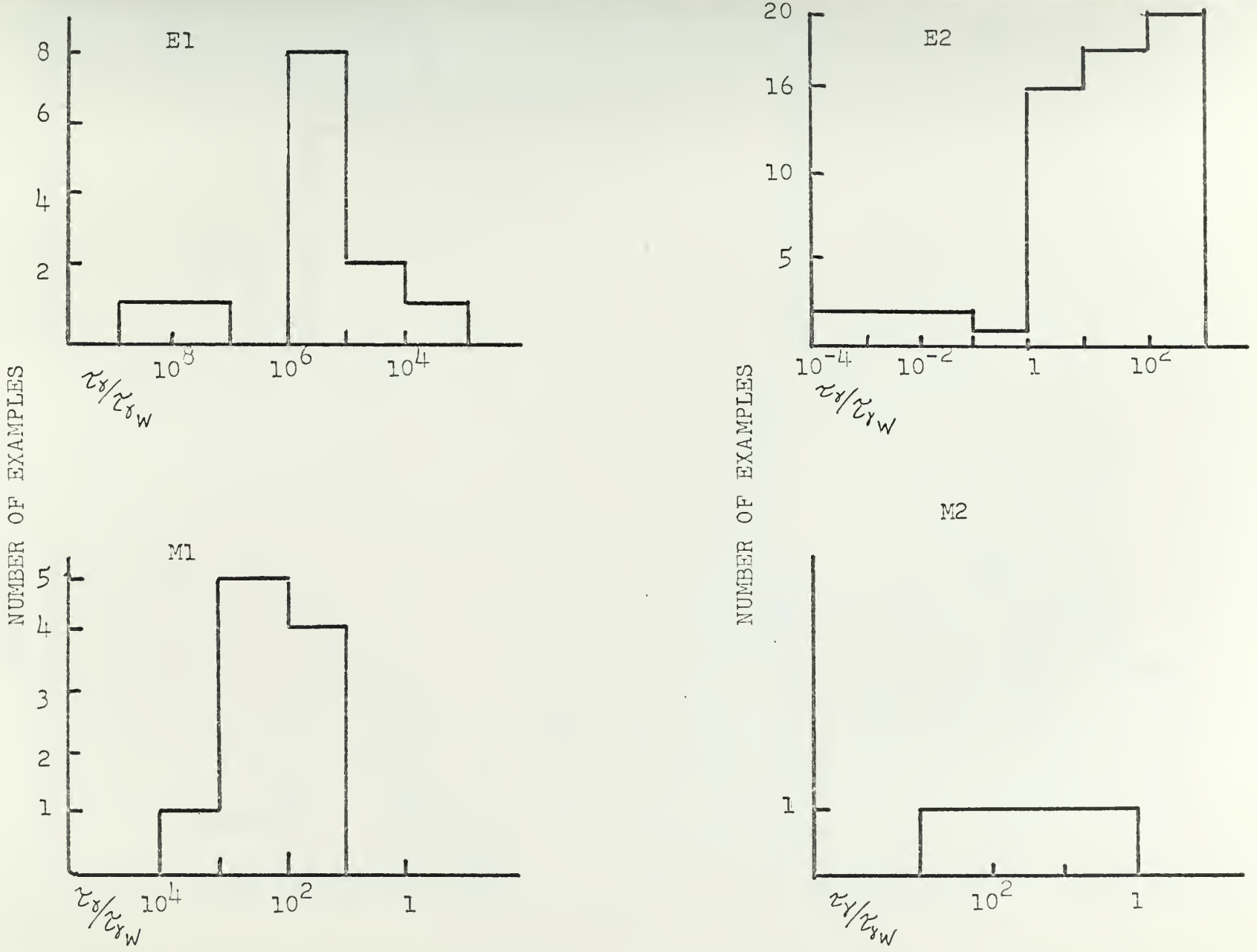

2.1a Range of Weisskopf Single Particle Estimates

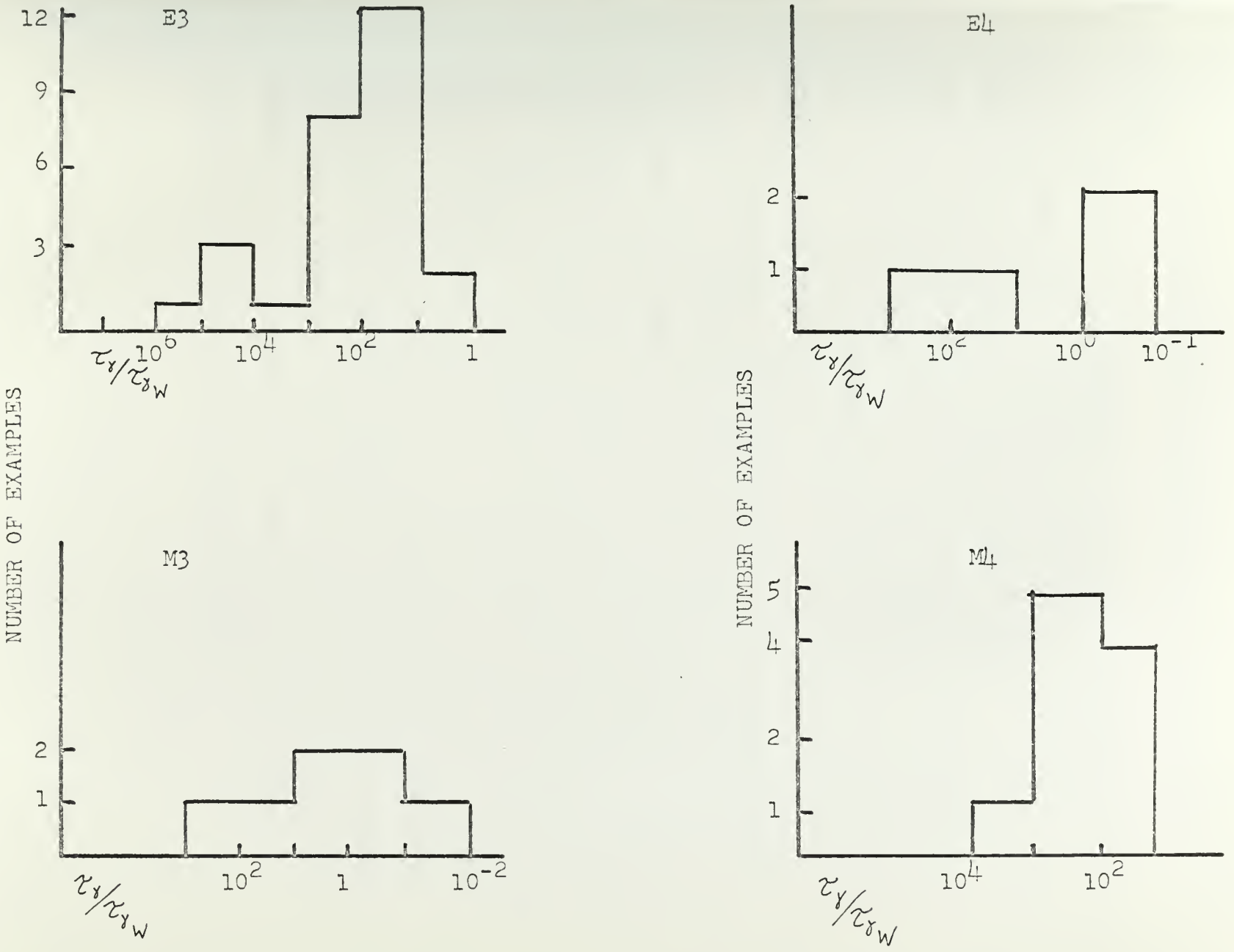

2.1b Range of Weisskopf Single Particle Estimates

particle in its particular shell, the other members of that shell would be partially bound by the nuclear pairing energy.

Difficulty in obtaining reasonable theoretical estimates of the mean lives is also encountered when the de-excitation occurs with a mixing of the multipole types (i.e., an excited state may decay by both M 1 and E 2 transitions). Unless the branching ratios of the competing multipole types are known, Weisskopf estimates can not accurately determine the mean life.

Nevertheless, regardless of the over-simplification of the single particle model, Weisskopf's theoretical estimates are a powerful tool for determining the type of multipolarity of low energy (< 2 Mev) transitions. Due to the extreme dependence of the transition probabilities on ℓ, there is a difference of about 10^2 to 10^4 between each type of multipole radiation. Therefore the multipolarity of the transition can often be predicted by matching the experimentally observed result to the numerically closest Weisskopf estimate. Knowledge of the multipolarity of the radiation can then be used in determining the angular momentum and parity of the excited levels.

CHAPTER III

DESCRIPTION OF EXPERIMENTAL EQUIPMENT

3.1 General Arrangement

Figure 3.1 presents a diagram of the arrangement of the experimental equipment.

A Van de Graaff accelerator produces a pulsed beam of monoenergetic protons with a pulse width (FWHM) of about 4 nanoseconds and a repetition rate of 8 megacycles/sec. The accelerator, built in 1947, has a maximum energy of 3 Mev.

Neutrons are generated by the (p,n) reaction of the proton beam on a Li^7 or H^3 target. The $Li^7(p,n)Be^7$ and $H^3(p,n)He^3$ sources provide neutrons with energies between 100 kev and 2 Mev. The proton-neutron energy relationship is derived from the conservation of mass and momentum [8].

$$E_n = E_p \left[\frac{(M_p M_n)^{1/2}}{(M_n + M_R)} \cos\theta \pm X \right]^2 , \qquad (3.1)$$

where

$$X = \left[\frac{M_p M_n}{(M_n + M_R)^2} \cos^2\theta + \frac{(M_R - M_p)}{(M_n + M_R)} + \frac{M_R q}{(M_n + M_R) E_p} \right]^{1/2} . \qquad (3.2)$$

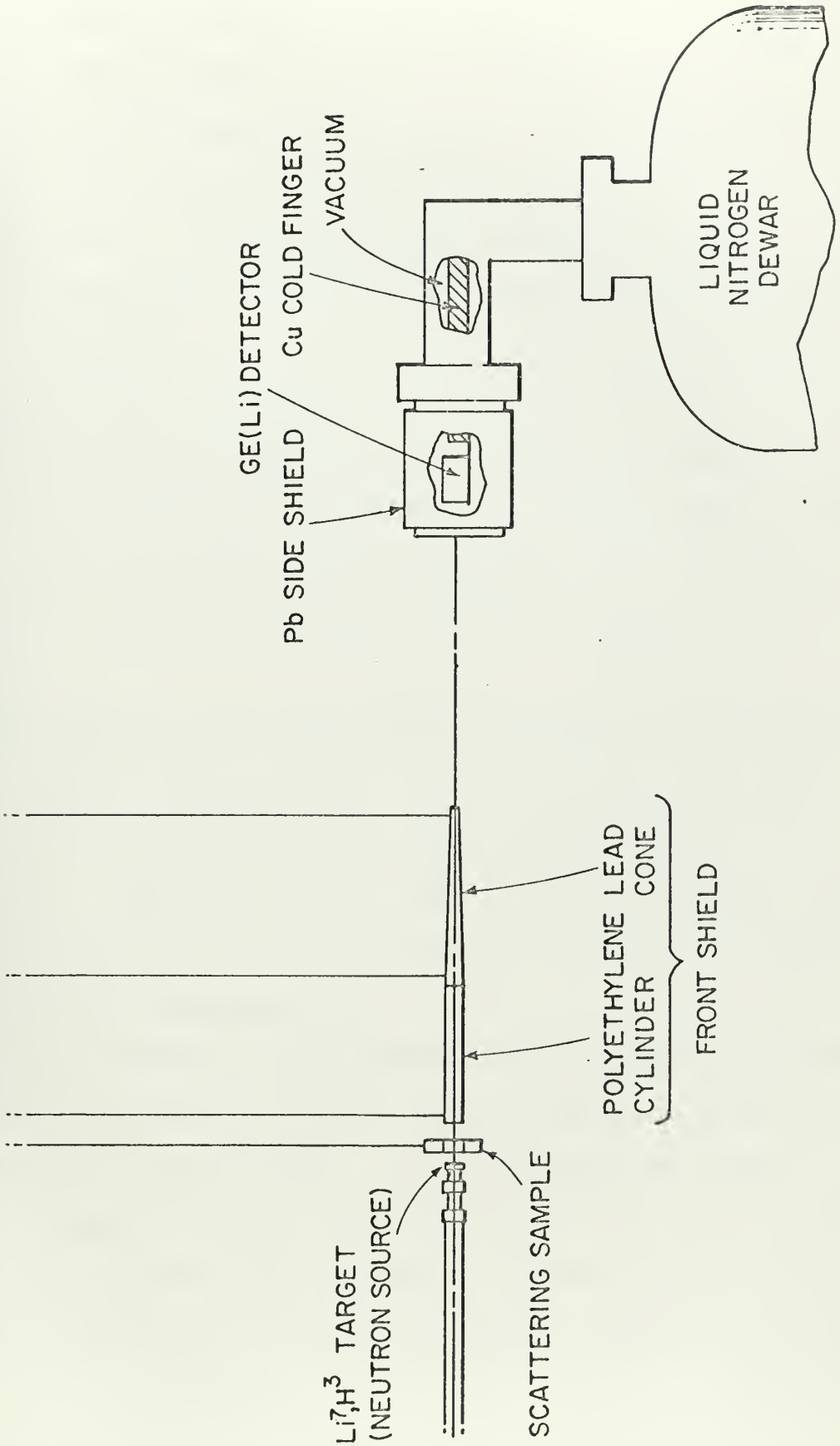

3.1 Experimental Setup For De-excitation Gamma Ray Measurements

E_n= neutron energy.

E_p= proton energy.

M_n= neutron mass.

M_p= proton mass.

M_R= mass of residual nucleus, either Li^7 or He^3.

θ = laboratory angle between proton and neutron flight paths.

q= nuclear disintegration energy.

Plots of this relationship are shown in Figures 3.2 and 3.3 for Li^7 and H^3 respectively. Further target information regarding (p, n) cross sections, angular distributions, and neutron energy spread may be found in references [1], [2], and [3].

The neutrons from the target next strike the scattering sample.which is 2.6 cm from the (p, n) source. The geometry of the ring scattering sample is diagramed in Figure 3.4. Neutrons emitted from the source between the angles of 20.1^o and 44.5^o with respect to the proton beam enter the scattering sample.

Of the neutrons which traverse the sample, some undergo inelastic scattering with the sample nuclei, leaving the nuclei in an excited state. These excited nuclei then decay by gamma emission characteristic of the energy of the particular nuclear level excited. A portion of the gamma rays are detected by the Ge(Li) detector located .40 cm from

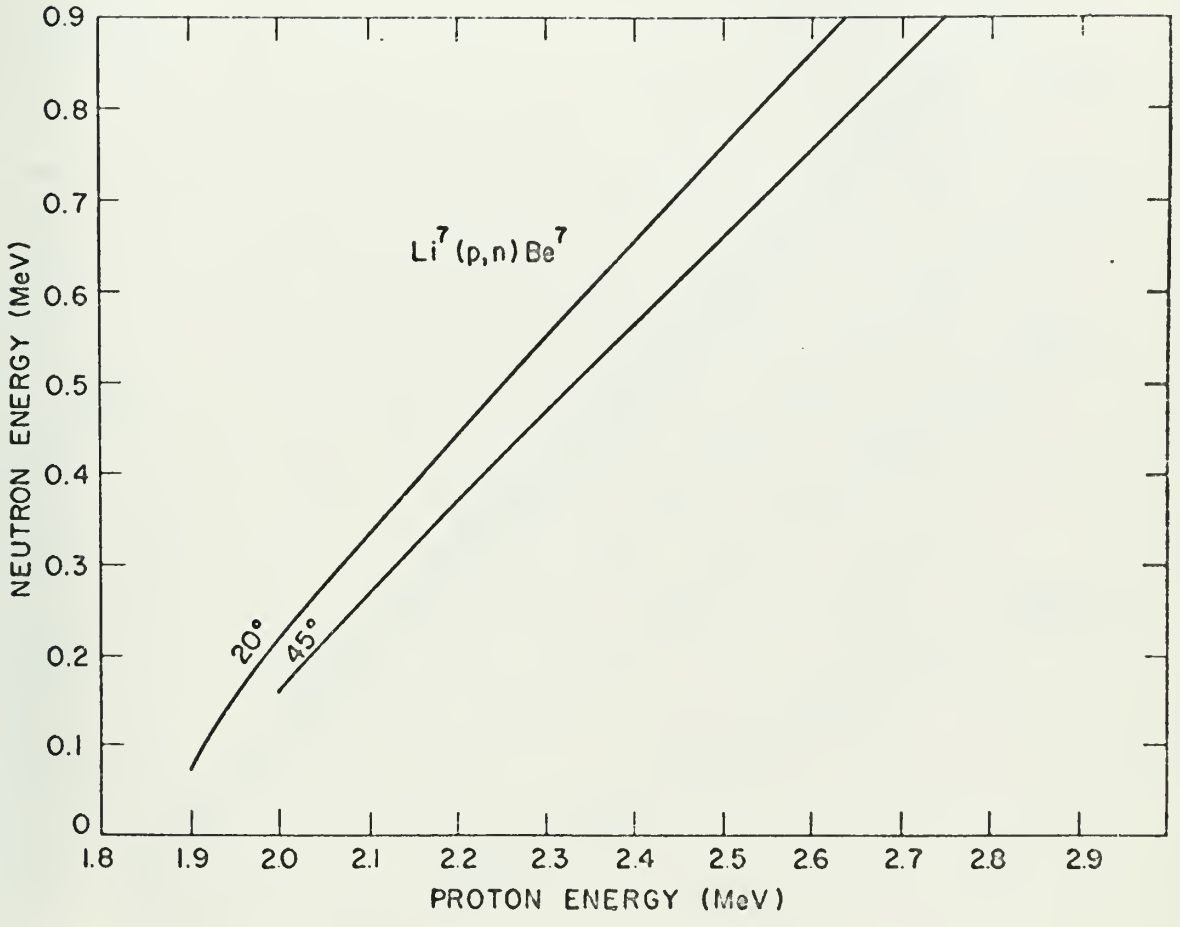

3.2 Neutron Energy As A Function of Proton Energy and Reaction Angle For Li^7

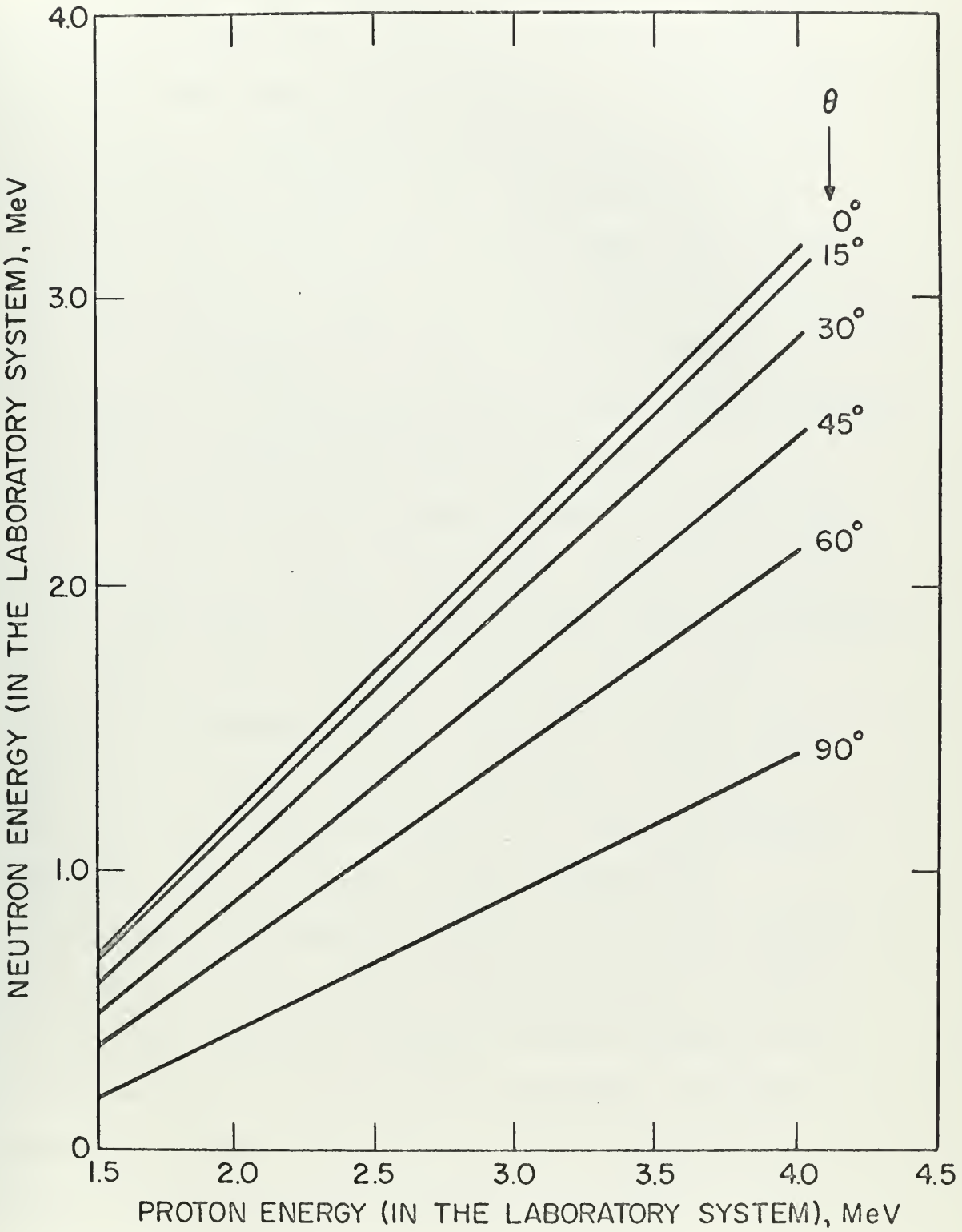

3.3 Neutron Energy As A Function of Proton Energy Energy and Reaction Angle For H^3

the scattering sample.

To prevent direct neutron irradiation of the detector, a 27.5 cm long, tapered cylindrical shield is placed between the scatterer and the detector. The front portion of the shield is polyethylene and the back portion is a lead-epoxy mixture (Figure 3.4). In addition to the polyethylene-lead front shield, a 6 mm lead side shield is wrapped around the Ge(Li) detector. The side shield thickness is optimized [3] to reduce the low energy gamma ray background from the room without appreciably increasing the inelastic neutron scattering in the lead.

The lithium drifted germanium detector is the same crystal used by V. Rogers in his Ph.D. thesis [3]. It is a single-open ended coaxial type crystal with a trapezoidal cross section. Its sensitive volume is 17 cc. To minimize the leakage current, the Ge(Li) crystal is maintained at liquid nitrogen temperature ($77^{\circ}K$). It is also kept in a vacuum of about 10^{-6} torr to prevent condensation and to provide thermal insulation.

The energy resolution of the detector is a function of the applied bias voltage. Figure 3.5 shows a graph of the energy resolution versus the bias voltage using the 662 keV peak of Cs^{137} as the reference. The plot reveals an unusual situation in which the resolution maximizes at two applied voltages. Repetition of the

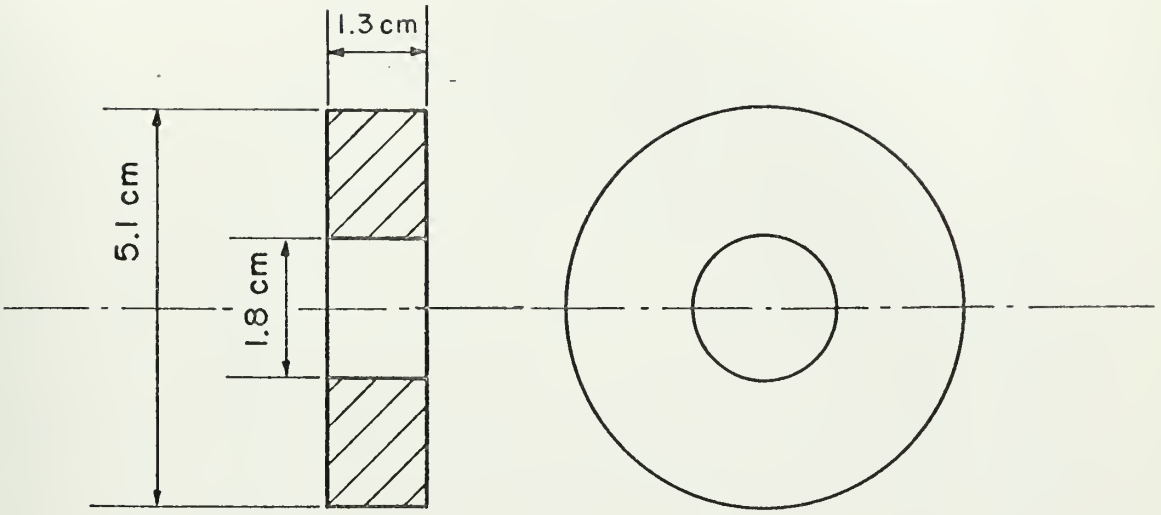

3.4 The Scatterer (Scattering Sample)

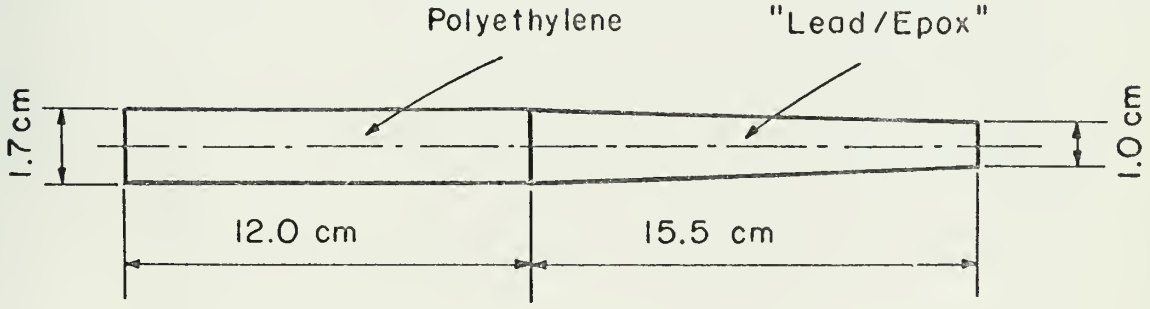

3.4 The Front Shield

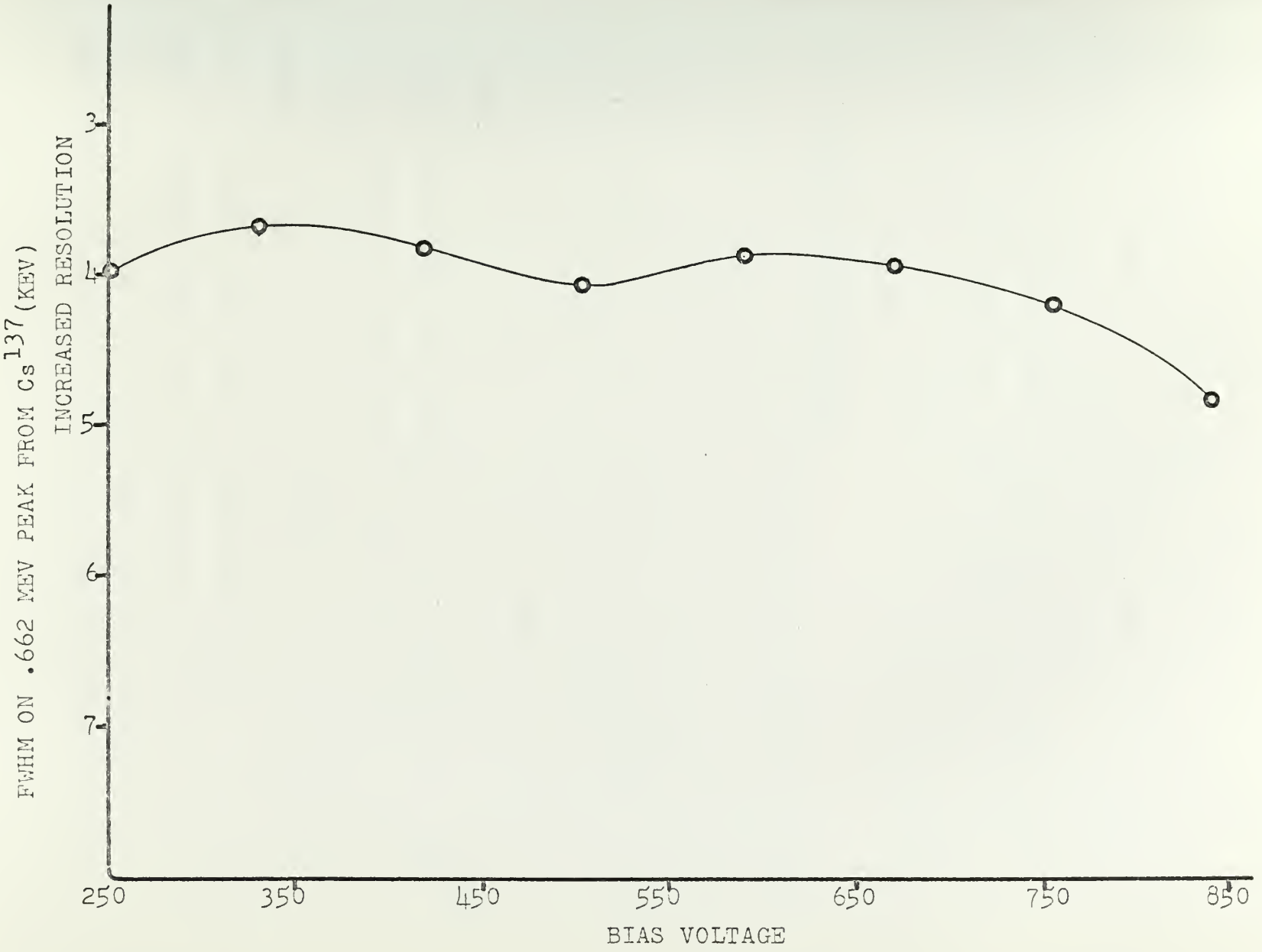

3.5 Detector Resolution Versus Bias Voltage

experiment verified this peculiarity. The best resolution (3.62 keV) is obtained at 330 volts while the second maximum gives a 3.87 keV FWHM at 590 volts. However since the time response of the crystal is important in these mean life measurements, the higher bias voltage of 590 volts was chosen as the operating voltage. In a solid state detector, the larger the bias voltage the faster the electron-hole pair collection time and thus the faster the time response.

3.2 Neutron Normalization

In order to aid in determining the relative duration of experimental data runs, a system is used to integrally monitor a fraction of the incident neutron beam (Figure 3.6). A long counter, BF_3 tube inserted in a polyethylene shield, is placed at an angle of 90^o and at a distance of 125 cm from the (p,n) target. The total number of thermal neutrons detected by the BF_3 tube is measured on a scaler. Since the angular distribution of the neutrons from the (p,n) target is constant for identical energies, the relative number of neutrons incident on the scattering sample in each run can be determined by the normalizing of the counts registered by the long counter. For identical beam energies, data runs are defined as neutron normalized when the total count on the long counter scaler records the same for each run. A slight error is present when

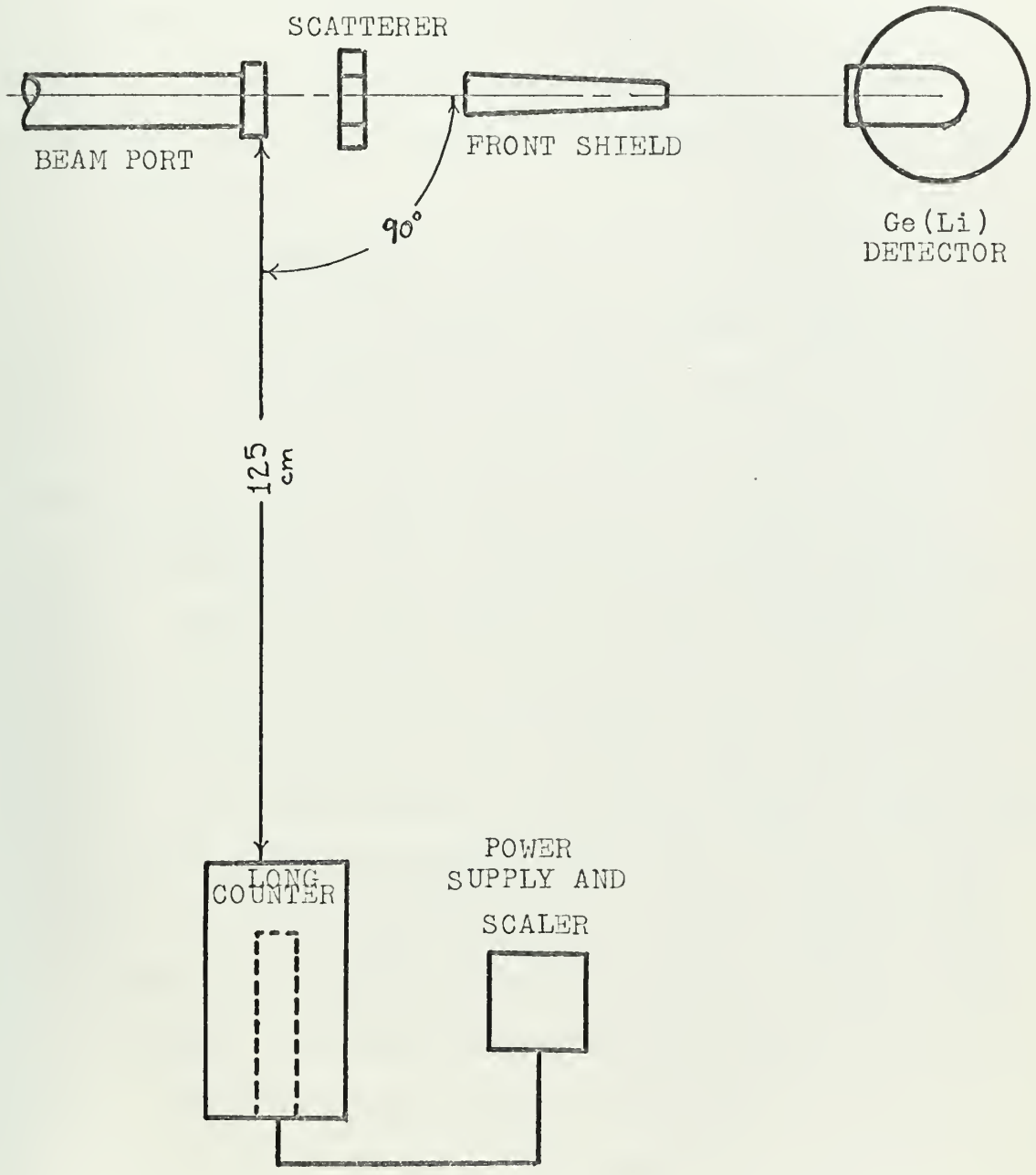

3.6 Long Counter Used For Neutron Normalization

different scattering samples are used due to the different elastic scattering cross sections of the scatterer materials.

3.3 Electronic Equipment

The methods used for measurement of the mean lives of the nuclear levels require the determination of the slope of the de-excitation gamma decay time spectrum. The electronic equipment employed to provide these time spectra is described below.

3.3.1 The Time Spectrum A simple time spectrum can be obtained using the electronic block diagram depicted in Figure 3.7. The output of the Ge(Li) detector is first amplified by a low noise, field effect transistor (F.E.T.) preamplifier. The signal then passes through a time optimized amplifier for further amplification and pulse shaping. Next the pulse enters a timing single channel analyzer which provides an energy discrimination capability. This unit also produces a fast output logic pulse with a definite time relationship to the input pulse irregardless of the input pulse amplitude. This logic pulse is used to start the time-to-pulse height converter (TAC). The stop signal for the TAC is derived from the pulsed proton beam by means of a capacitor pickup just before the (p,n) target. The beam pickup signal is not used to turn on the TAC since the extremely high repetition rate of 8 megacycles per second exceeds the rated input of the

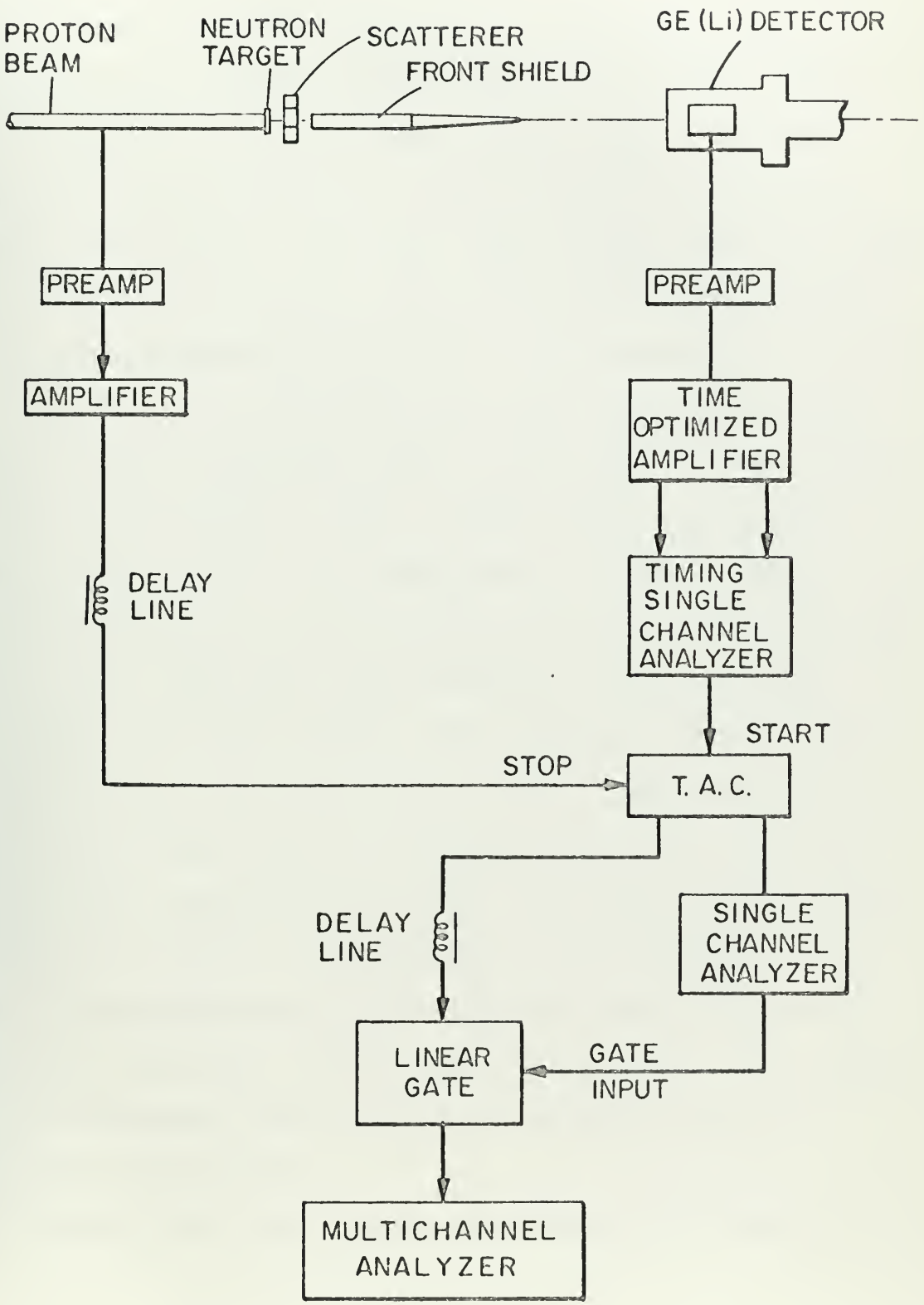

3.7 Electronic Block Diagram For Time Spectra

circuit. The TAC output consists of two pulses. One is sent to a single channel analyzer (SCA), whose output goes to the coincidence input of a linear gate. The other TAC output passes through delay lines which approximate the delay time of the SCA. If the first TAC output satisfies the discrimination level of the SCA (determines maximum time period), the pulse from the SCA opens the linear gate and allows the second pulse from the TAC to proceed to the multichannel analyzer (MCA) for analysis.

Figure 3.8 is an example of a time spectrum obtained from the system described above. Note that the time scale increases from right to left. Since the beam pick-up is used to stop the TAC, the amplitudes of the TAC output pulses are inversely proportional to the time of detection. That is, if a gamma ray was detected a relatively long time after the neutron burst, the time difference in the TAC between the start pulse and the stop pulse from the next neutron burst would be shorter than if the gamma ray was detected instantaneously after the first neutron burst. Therefore the longer the delay time in de-excitation, the smaller the amplitude of the TAC output, resulting in the time scale inversion. The maximum range of the time spectra is 125 nanoseconds due to the beam repetition rate of 8 megacycles per second.

Energy gated time spectra are obtained by placing the

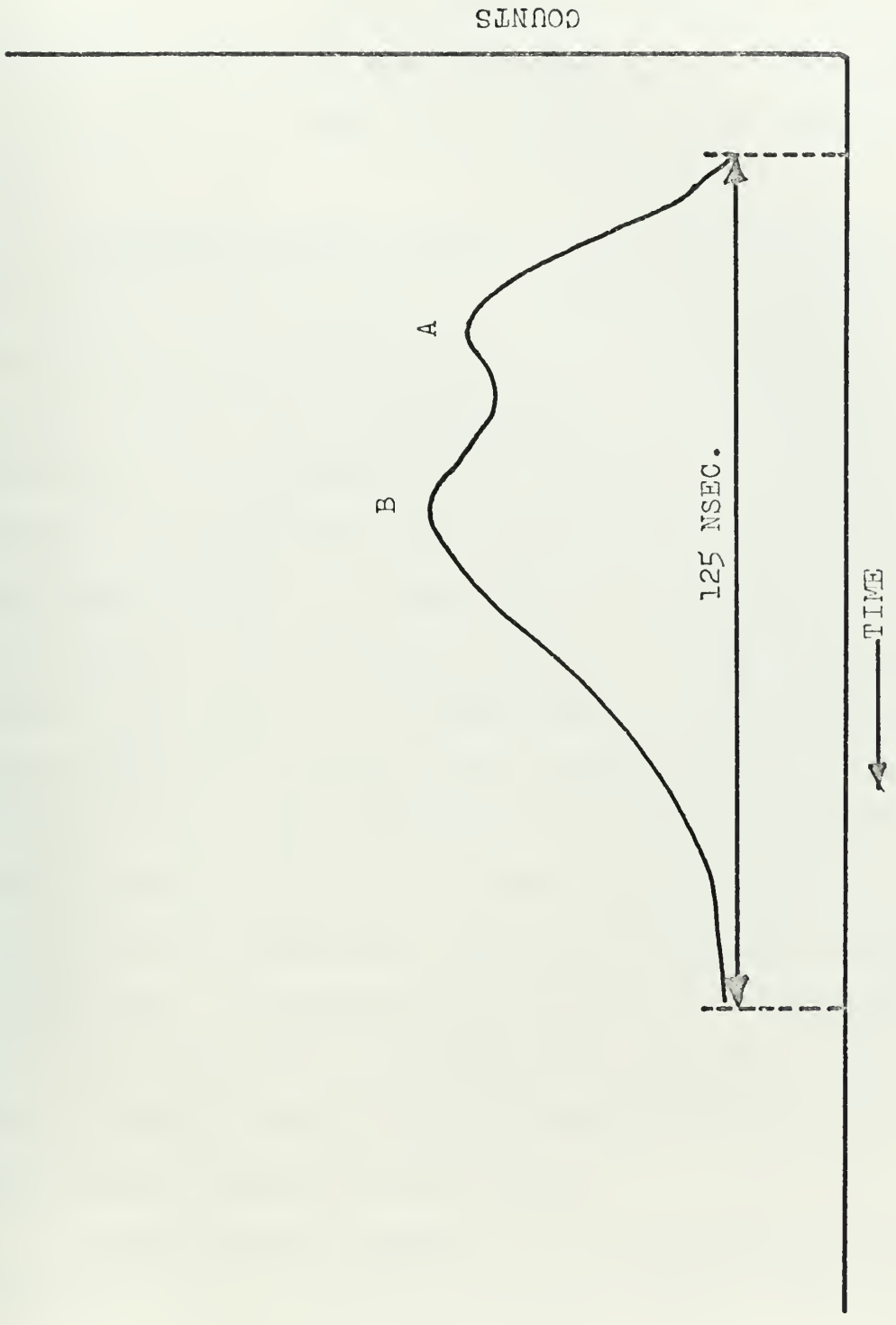

3.8 Time Spectrum

energy window of the discrimination unit in the timing single channel analyzer around the de-excitation photopeak of interest. After background subtraction, the spectrum remaining is the time decay of only that particular de-excitation gamma ray accepted by the energy restriction.

3.3.2 Time Gated Energy Spectra By modifying the system described in section 3.3.1, one obtains the capability of measuring energy spectra with a time discrimination. Figure 3.9 shows the block diagram of the electronics necessary for time-gated energy spectra. A pulse which leaves the preamplifier now travels to an energy optimized amplifier as well as a time optimized amplifier. After the amplifier the energy-side pulse is delayed so that it reaches the input of the linear gate in coincidence with the gating pulse from the SCA following the TAC. This SCA can place a time discrimination window anywhere within the 125 nanosecond period between neutron bursts. In order for the energy-side pulse to be accepted by the linear gate, the time-side pulse from the TAC must meet the time restriction set by the SCA. With this arrangement an energy spectrum can be obtained for any time interval over the 125 nanosecond time period.

A more detailed diagram of the electronics is shown in Figure 3.10. A switch is used to set the electronic

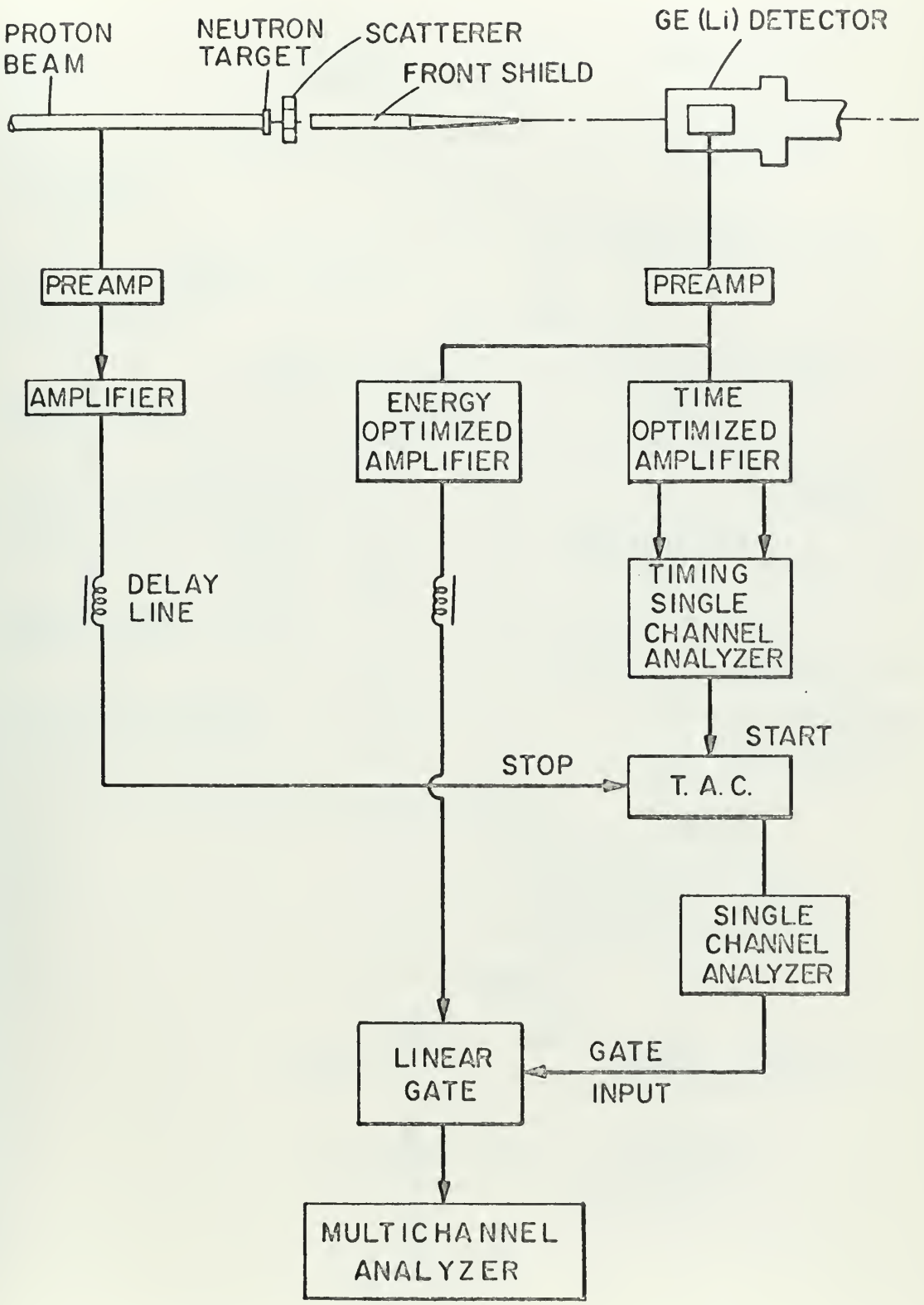

3.9 Electronic Block Diagram For Time Gated Energy Spectra

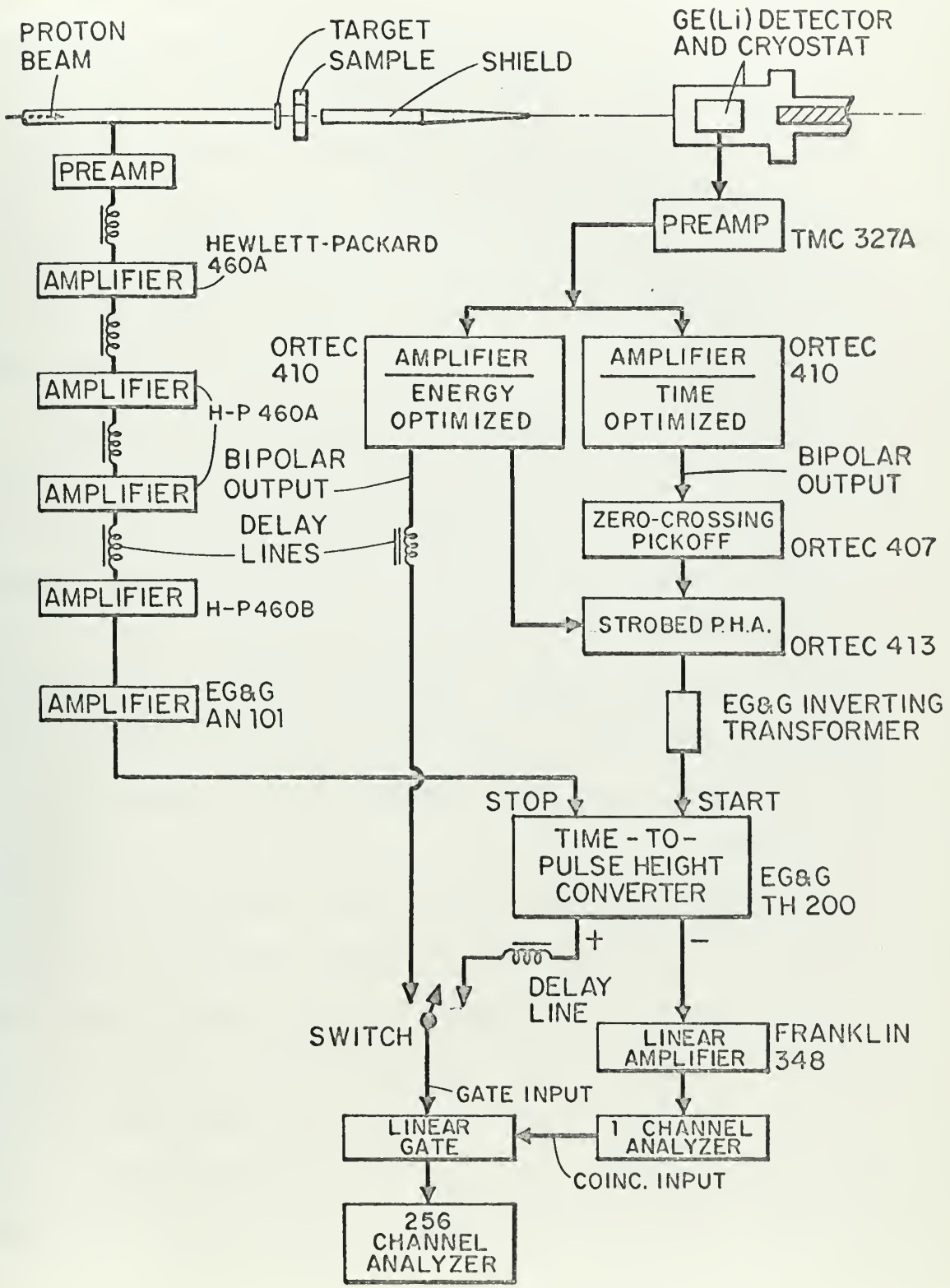

3.10 Electronic Block Diagram For Measurements of Time Gated Energy Spectra of De-excitation Gamma Rays

equipment for either a time or energy spectrum.

3.3.3 Time Resolution The time resolution of the above system depends critically on the uniformity of the timing signal derived from each input pulse. Since the shape, rise time, and voltage height of the pulses from the Ge(Li) detector may vary significantly, it becomes a problem to insure accurate, consistent timing signals. Two timing methods, leading edge and crossover pick-off were reviewed.

Leading edge timing [9, 10] consists of triggering a uniform fast rise time signal when the leading edge of the detector output pulse reaches a certain minimum voltage level. In order to insure consistency in the start of the triggered time signals, the rise time of the pulses must be fairly constant. Figure 3.11 is an electronics diagram for measuring leading edge timing spectra.

Crossover pick-off timing makes use of the fact that the time at which the second derivative with respect to time of the detector pulse crosses zero is nearly the same for identically shaped pulses, regardless of their rise times or amplitudes. Referring to Figure 3.10, a pulse from the detector preamplifier is double differentiated in the Ortec 410 amplifier and a bipolar output is sent to the corssover pick-off unit. Here,a uniform fast rise time output pulse is generated at the time when the

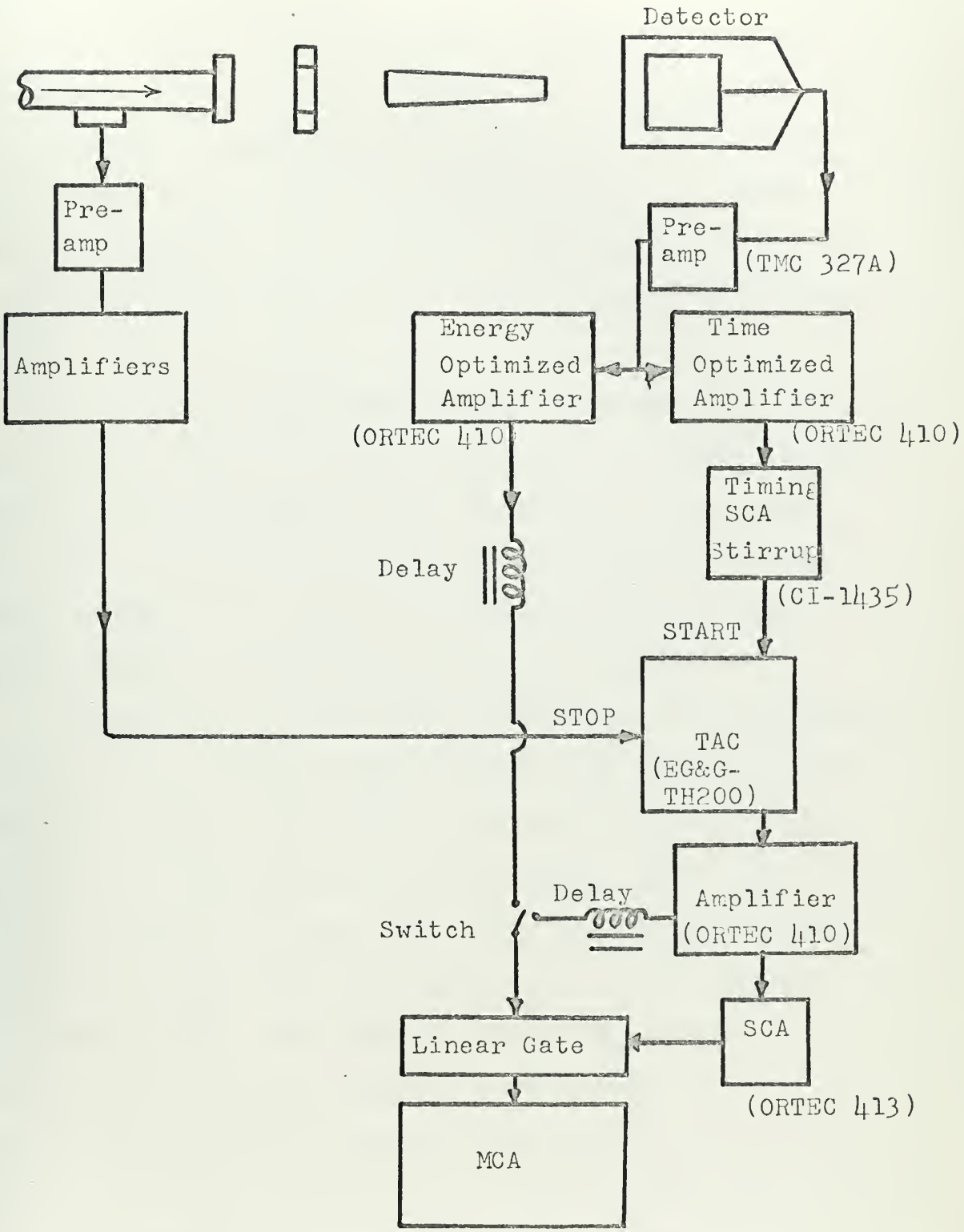

3.11 Electronic Diagram For Leading Edge Timing

bipolar pulse crosses zero.

In the case of identical pulse shapes with varying amplitudes and rise times (Figure 3.12), the crossover pick-off method generates a more consistent time signal. Leading edge timing appears feasible only when a narrow range of amplitudes are accepted. This can be accomplished by admitting only pulses from a narrow energy discrimination window.

However the pulses from a Ge(Li) detector are not identical in shape. For this situation, the doubly differentiated detector pulses do not cross zero at the same time, thus introducing a non-uniformly generated timing signal. Figure 3.13 depicts a typical example of the timing problems for non-identical pulse shapes.

Determination of the better timing method is dependent on the type of detector used and the sophistication of the timing electronics. For the two systems shown in Figures 3.11 and 3.10, the experimentally measured time spectra are shown in Figures 3.14 and 3.15. The leading edge timing plot was performed with a 10 keV window on the 847 keV photopeak of Fe^{56}. The FWHM was about 19 nanoseconds. The statistics are poor due to the relatively short counting time and the narrow energy restriction. The crossover pick-off spectrum was taken for an energy range from 170 keV to 2.6 MeV with a resulting FWHM of 29 nanoseconds.

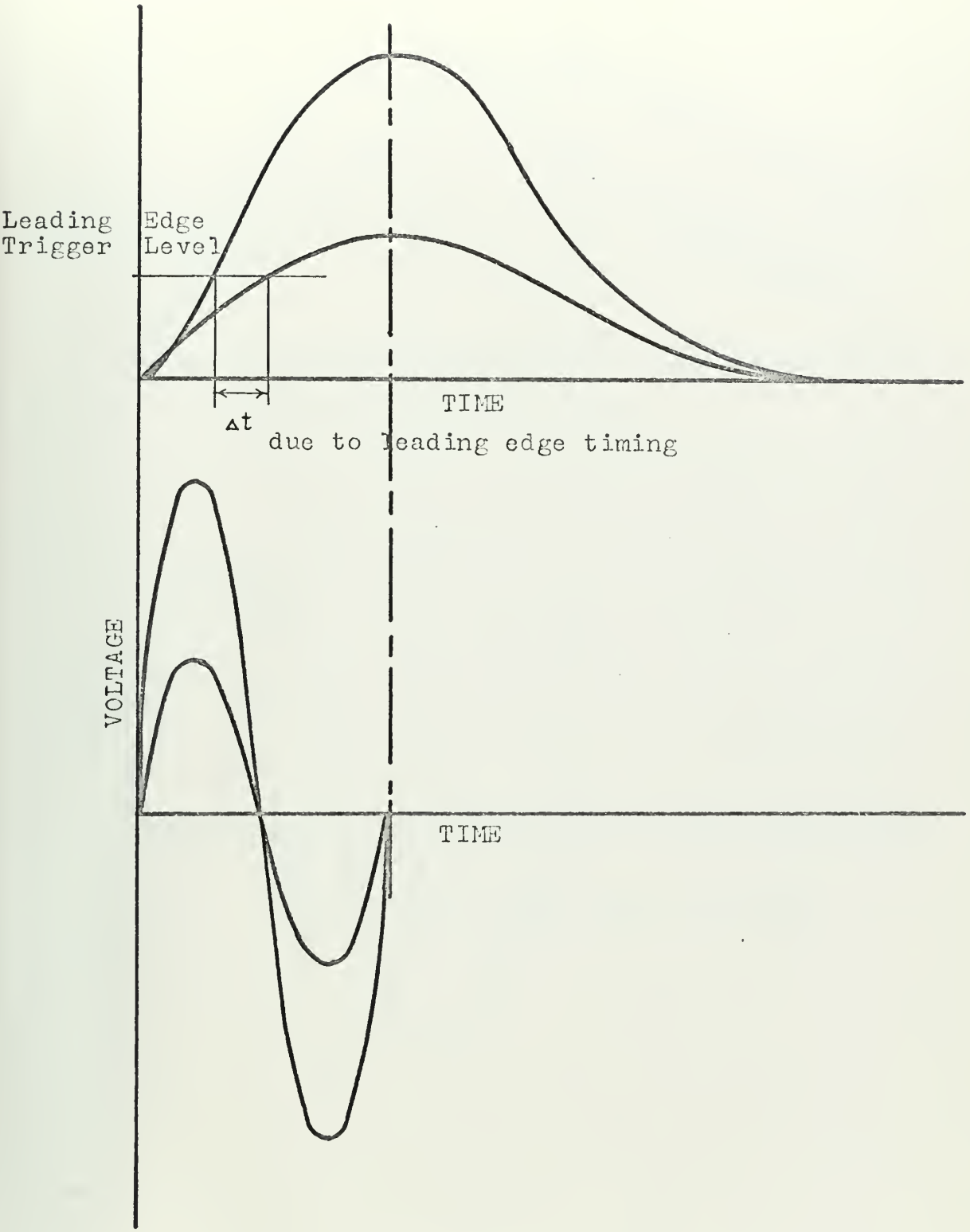

3.12 Timing Signal Characteristics For
Identically Shaped Pulses

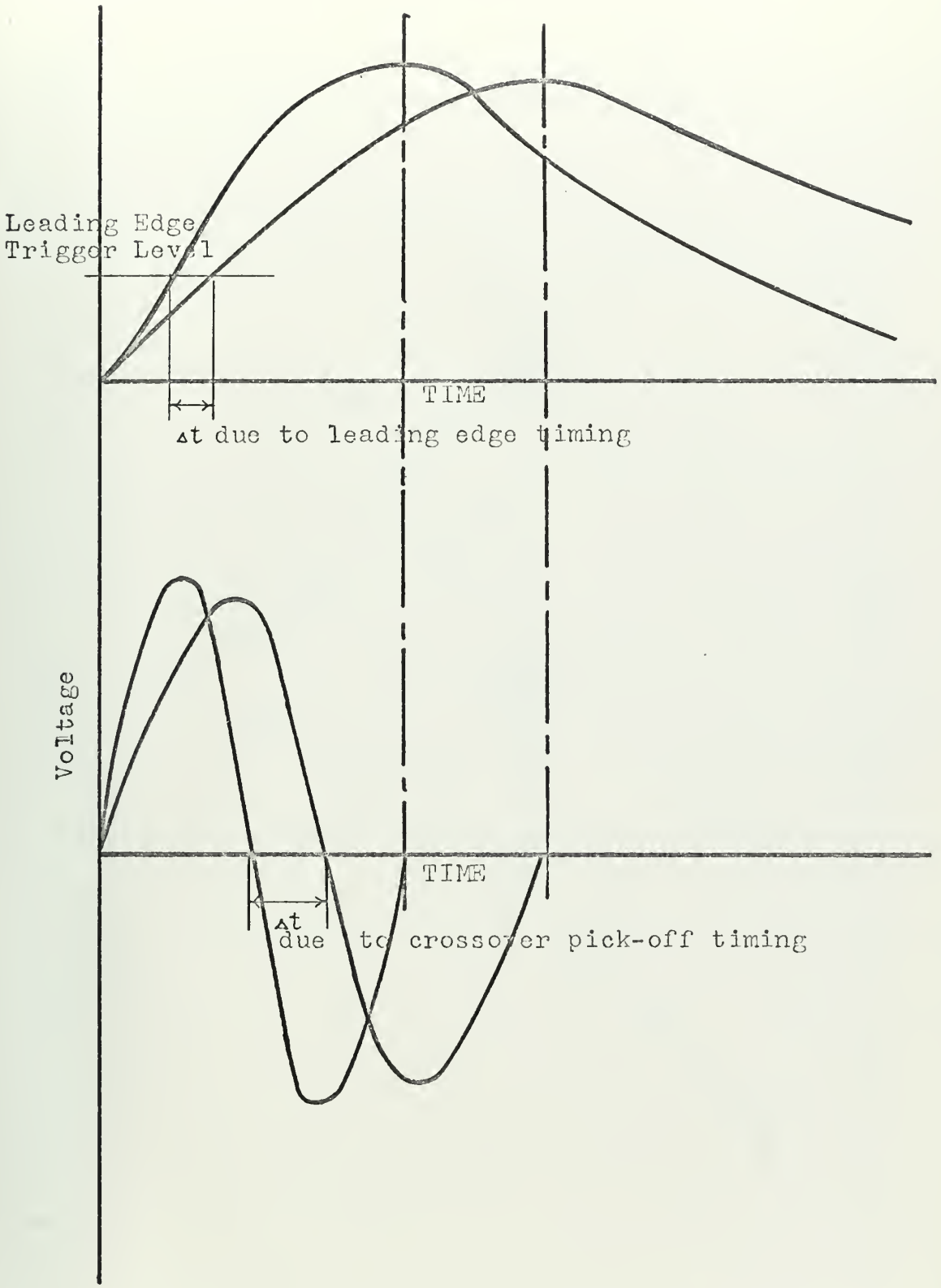

3.13 Timing Signal Characteristics For
Non-identically Shaped Pulses

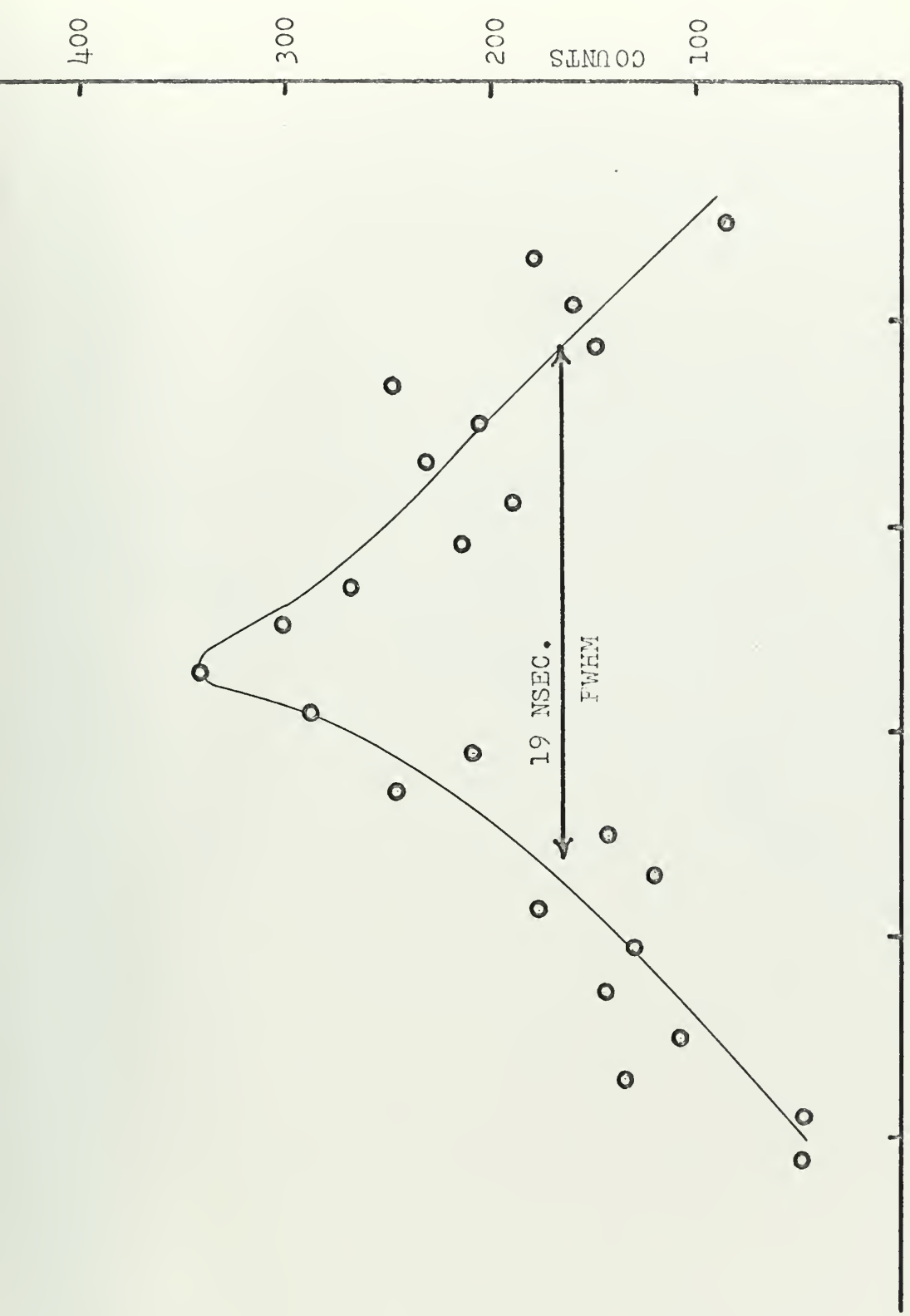

3.14 Time Spectrum From Leading Edge Timing Electronics, Narrow Energy Window (10 keV)

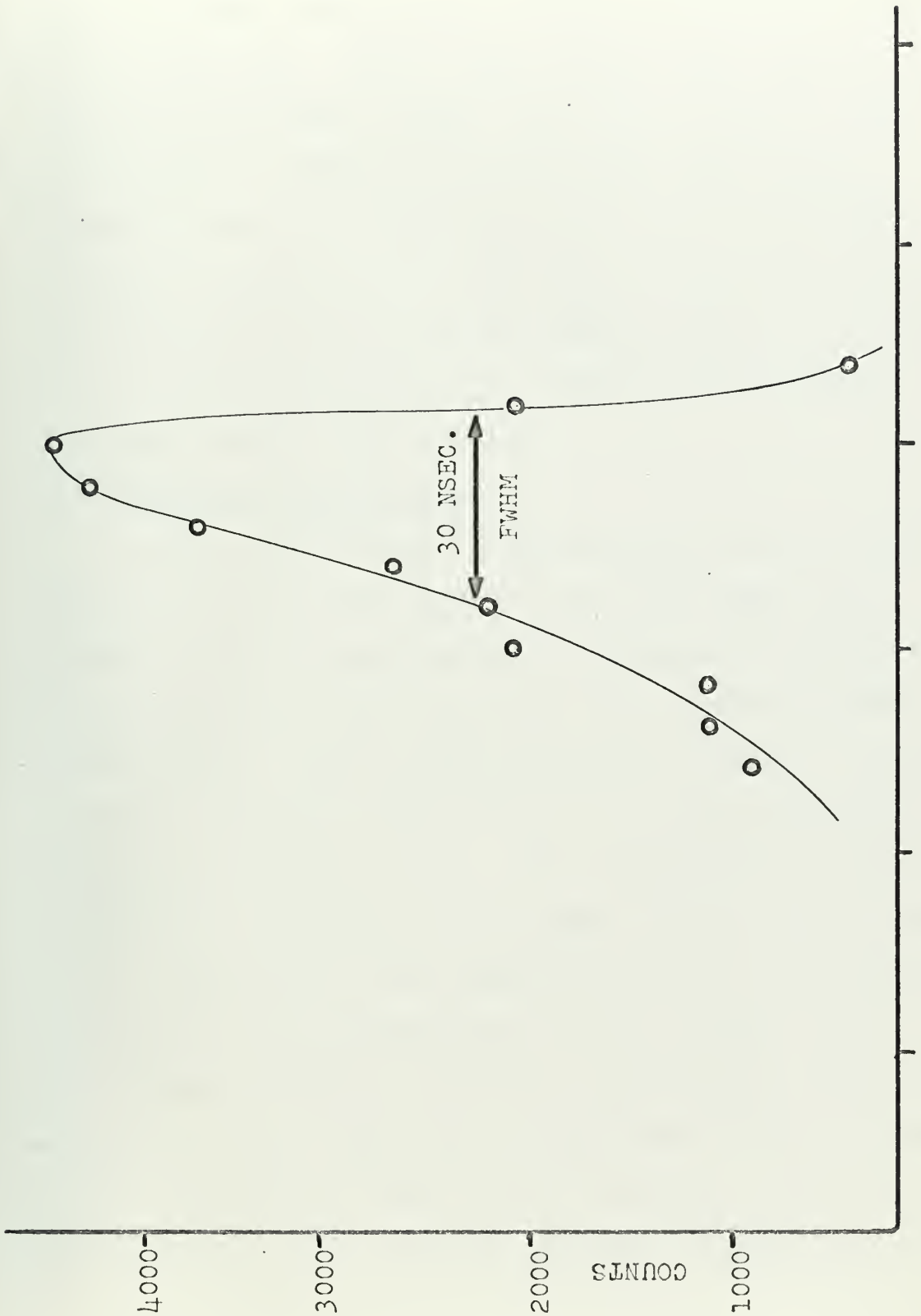

3.15 Time Spectrum From Crossover Pick-off Timing Electronics, Wide Energy Range (170 keV - 2.6 MeV)

It appears that, for narrow energy ranges and long counting times, leading edge timing may provide a better time resolution. However when leading edge timing was used over the larger energy (170 keV - 2.6 MeV) range, the resulting spectrum was practically unresolvable. Therefore when the electronic timing systems diagramed above are employed and a wide range of pulses are accepted, the crossover pick-off method usually results in a more uniform timing signal and thus better time resolution than the leading edge technique.

3.4 Detector Time Response

If one could assume an instantaneous collection time for the electron hole pairs in the solid state Ge(Li) crystal, the time spectrum for an immediate or picosecond range mean life decay gamma ray (such as from the 847 keV level in Fe^{56}) would appear guassian in nature. The width of such a spectrum would be due to the time resolution discussed in section 3.3.3. This instantaneous collection time can be approximated in a small planar crystal because of the uniformity of its electric field and the short travel distances for the electron-hole pairs (Figure 3.16). However due to the weak electric field regions and odd geometry of the single open-ended coaxial Ge(Li) crystal used in this thesis, the charge collection times are relatively long. This poor time response results in an un-

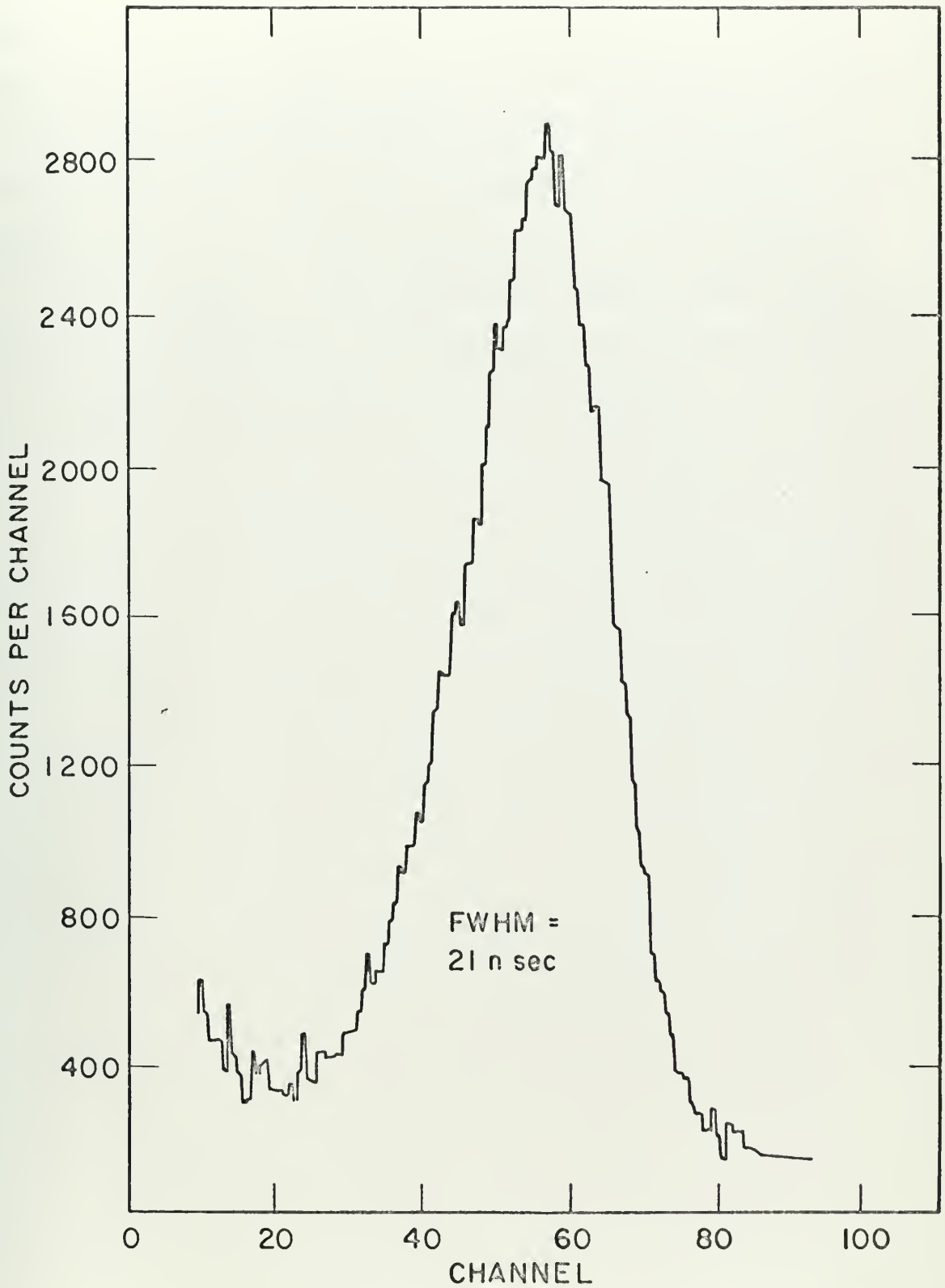

3.16 Time Spectrum From Planar Detector

symmetric time spectrum as shown in Figure 3.17. The extended tail on the longer time side can be fit to an exponential with a decay time of 29 nanoseconds [3] (Figure 3.18). An interesting feature is the fact that the 29 nanosecond decay time of the exponential tail proves to be independent of the energy of the gamma ray time spectra.

The problem of eliminating the detector time response from the experimentally determined time spectra of nuclear level decay is discussed in section 4.4.4c.

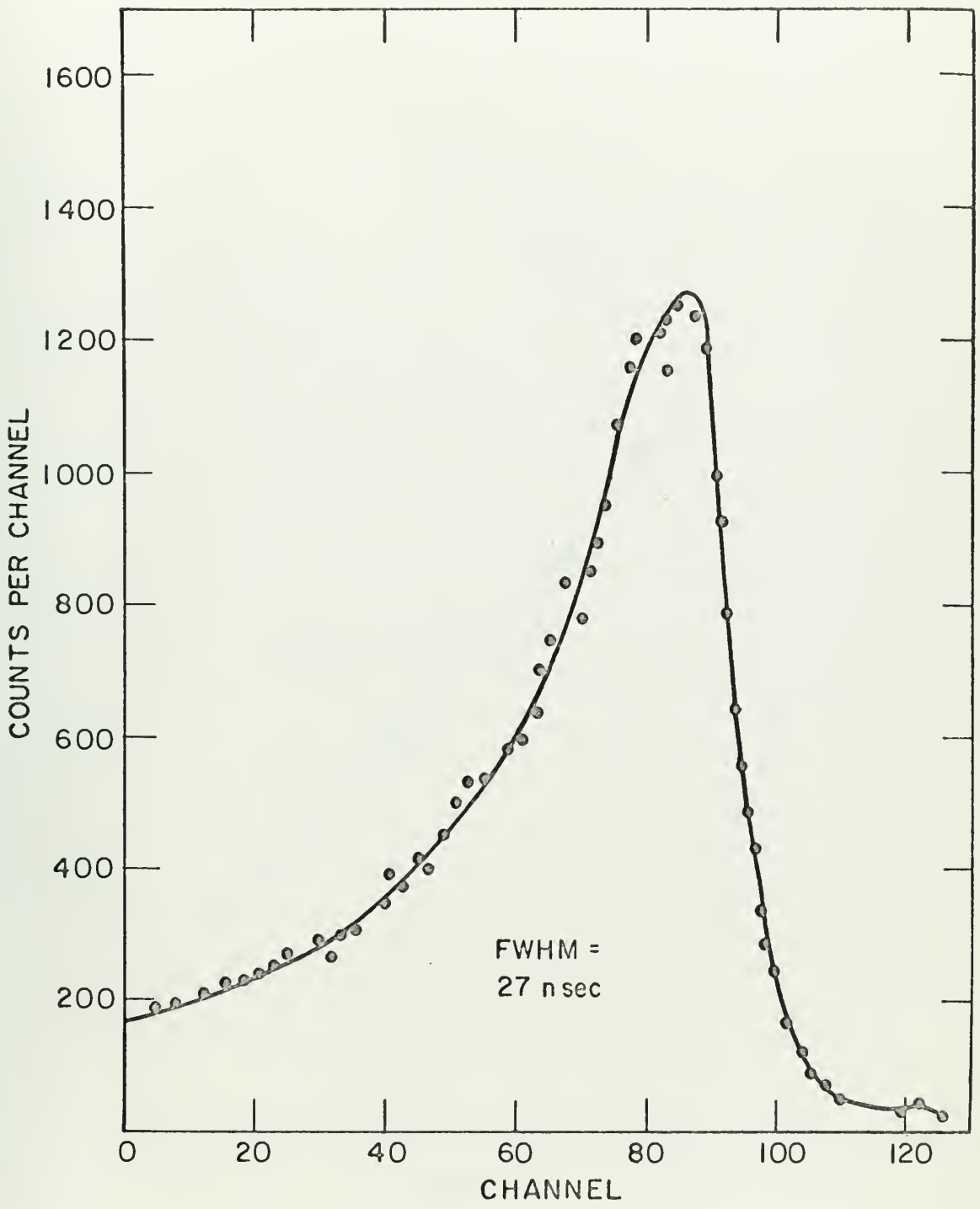

3.17 Time Spectrum From Crystal Used in This Thesis

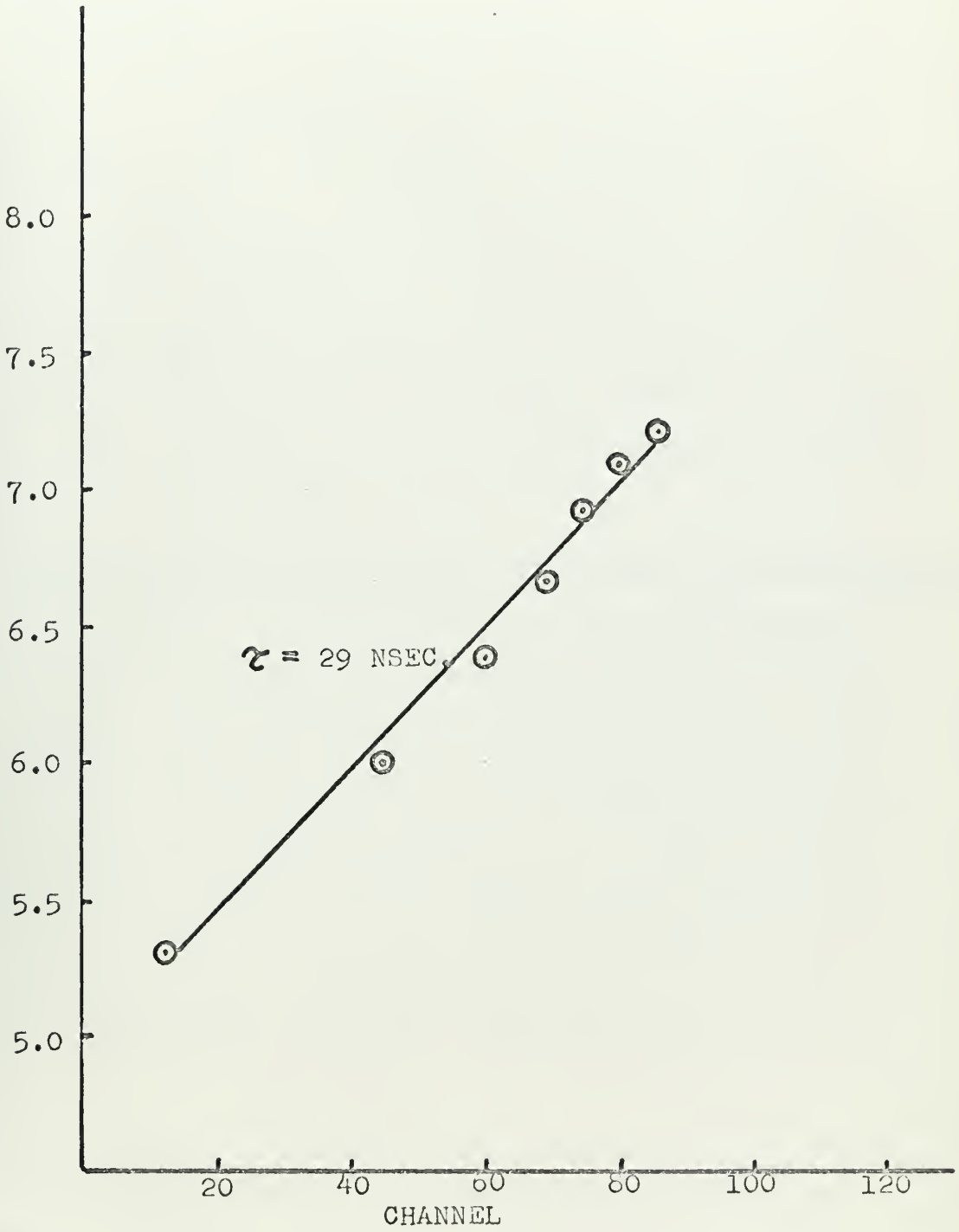

3.18 Asymmetric Exponential Trial on Time Spectrum

CHAPTER IV

EXPERIMENTAL METHODS

4.1 Introduction

This chapter is divided into four parts. First, two techniques for experimental mean life determination will be described. Next, the methods of background subtraction are discussed and the above two techniques are analyzed for their advantages and disadvantages. Thirdly, a quick technique for discerning if an isotope has any long-lived excited levels is reviewed. Lastly, the experimental errors involved in the equipment and the background subtraction are presented.

4.2 Indirect Method For Excited Level Mean Life Determination

The technique is to reconstruct the time spectrum of the prompt de-excitation gamma ray peak (peak A on Figure 1.1) without the interferring background peak due to fast neutron excitation and capture in the detector and laboratory environment (peak B on Figure 1.1). Once the time spectrum of the de-excitation gamma ray of interest has been reconstructed, the experimental mean life, τ, can be simply obtained from the decay constant, λ, of the plot.

$$\tau = 1/\lambda \, . \qquad (4.1)$$

The construction of the time spectrum is performed by taking time gated energy spectra at various times in the 125 nanosecond period between neutron bursts. The

different energy spectra are neutron normalized and the time window size is kept the same, <20 nanoseconds, for each run. For each energy spectrum the area, or total number of counts, under the photopeak of the de-excitation gamma ray of interest is measured. These areas are then plotted against their respective time window positions (Figure 4.1 and 4.2). The slope of the plot of the natural logarithm of the area under the photopeaks versus time yields the experimental value of the decay constant λ.

Since the areas under the energy peaks are defined as the number of counts above the normal background spectrum in that particular energy range (Figure 4.3), separate data runs for the subtraction of background from the initial energy spectra are normally not required. Only if the gamma ray of interest is also found in the background or if the energy peak of the gamma ray of interest is not resolved due to the overlap of a background energy peak must background runs be taken and subtracted from the data runs.

4.3 Direct Method of Excited Level Mean Life Determination

This technique provides for the measurement of τ directly from the experimental time spectra. An energy window is placed around the de-excitation gamma ray energy of interest and a time spectrum is taken. The energy window is controlled by the energy discrimination unit in the strobed SCA (Figure 3.10). The background time spectrum

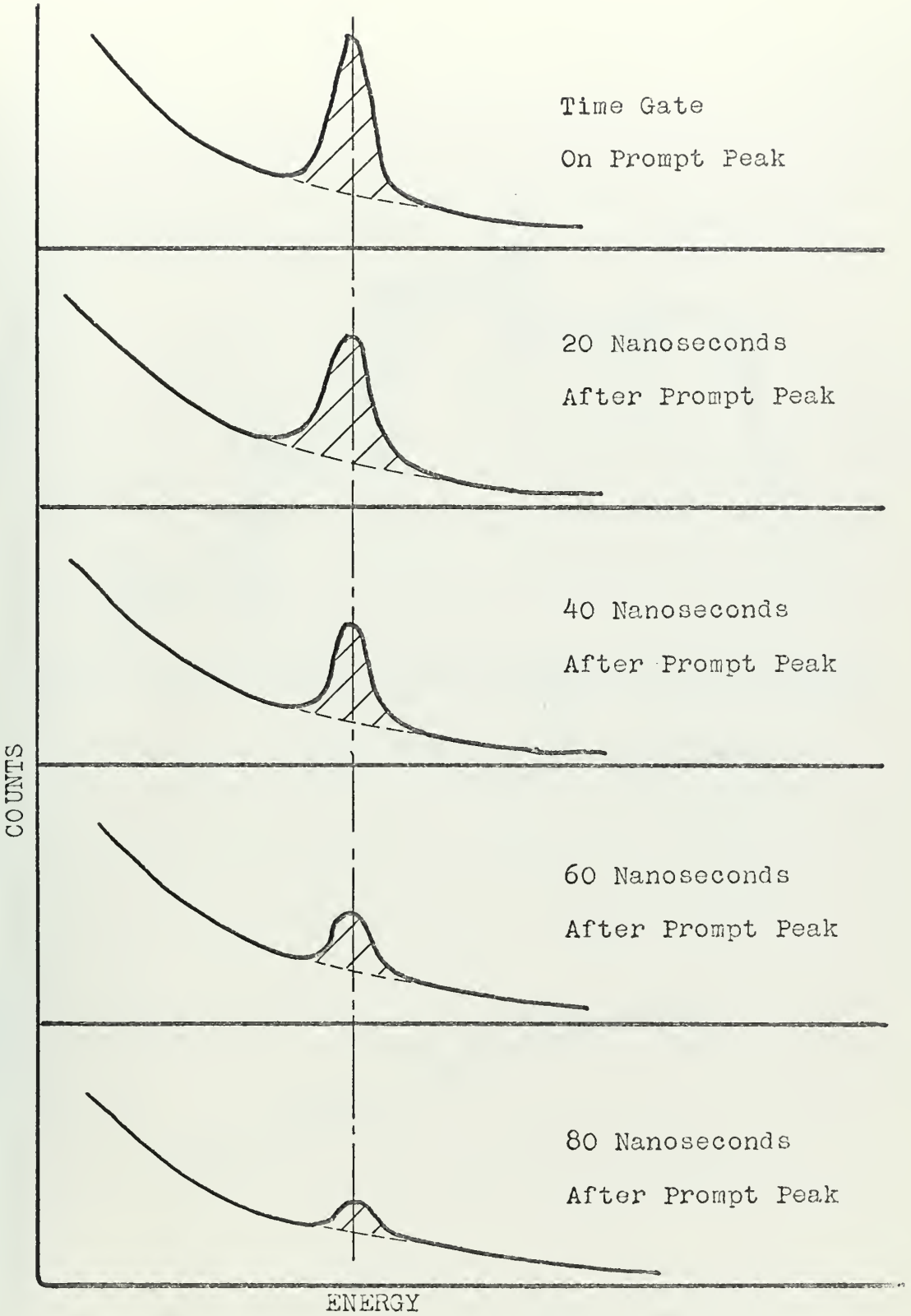

4.1 Photopeaks From Various Time Gated Energy Spectra

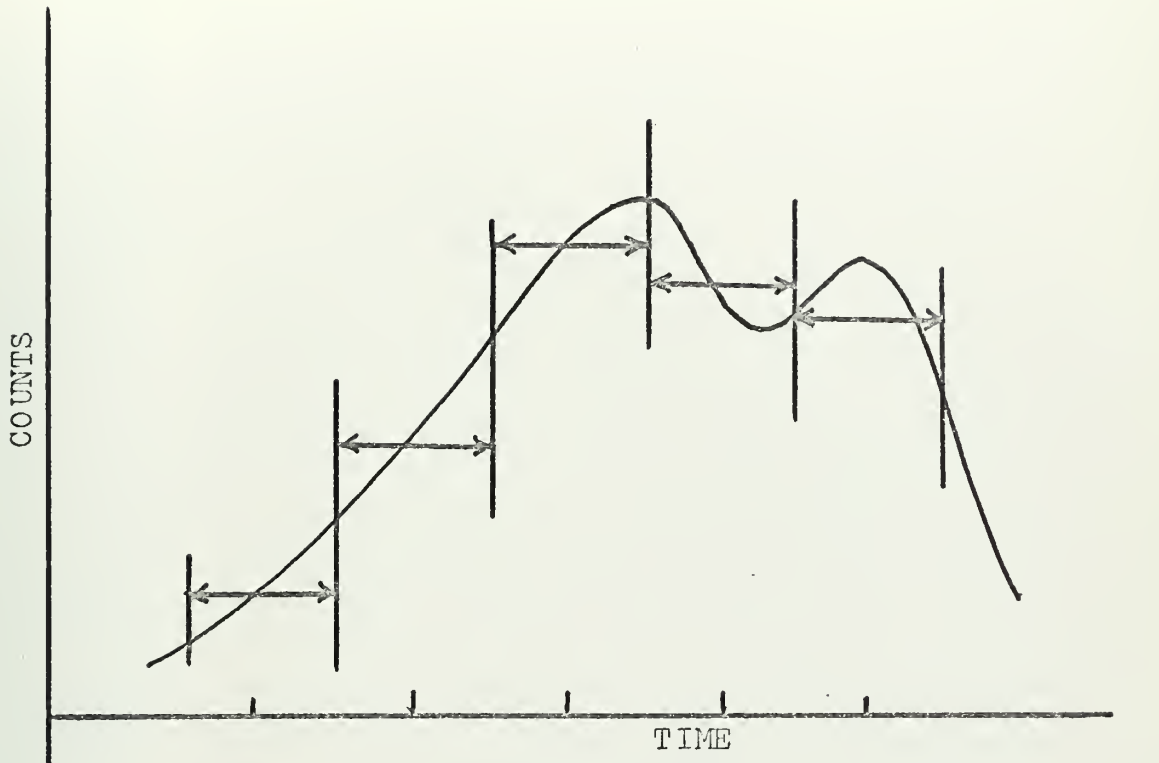

TIME SPECTRUM WITH TIME GATES

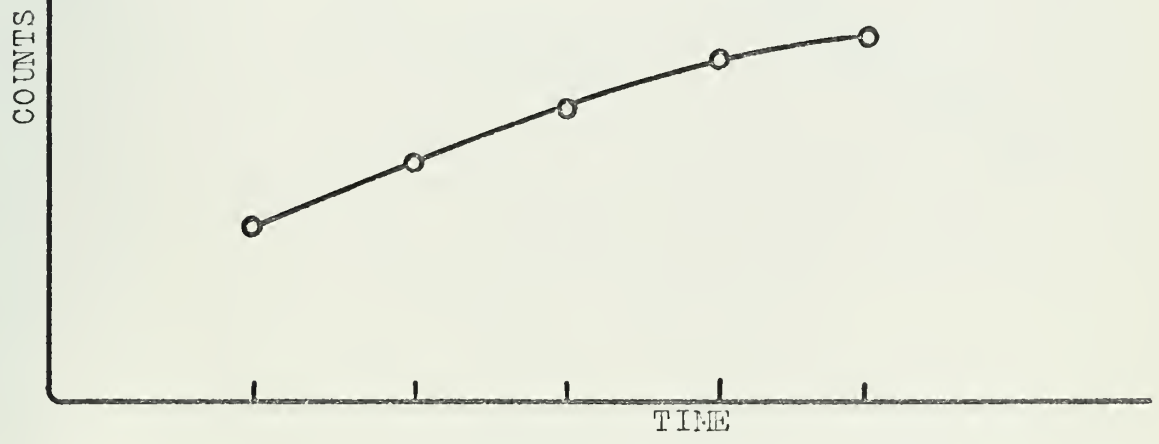

RECONSTRUCTED TIME SPECTRUM

4.2 Time Gate Positions and Reconstructed Time Spectrum

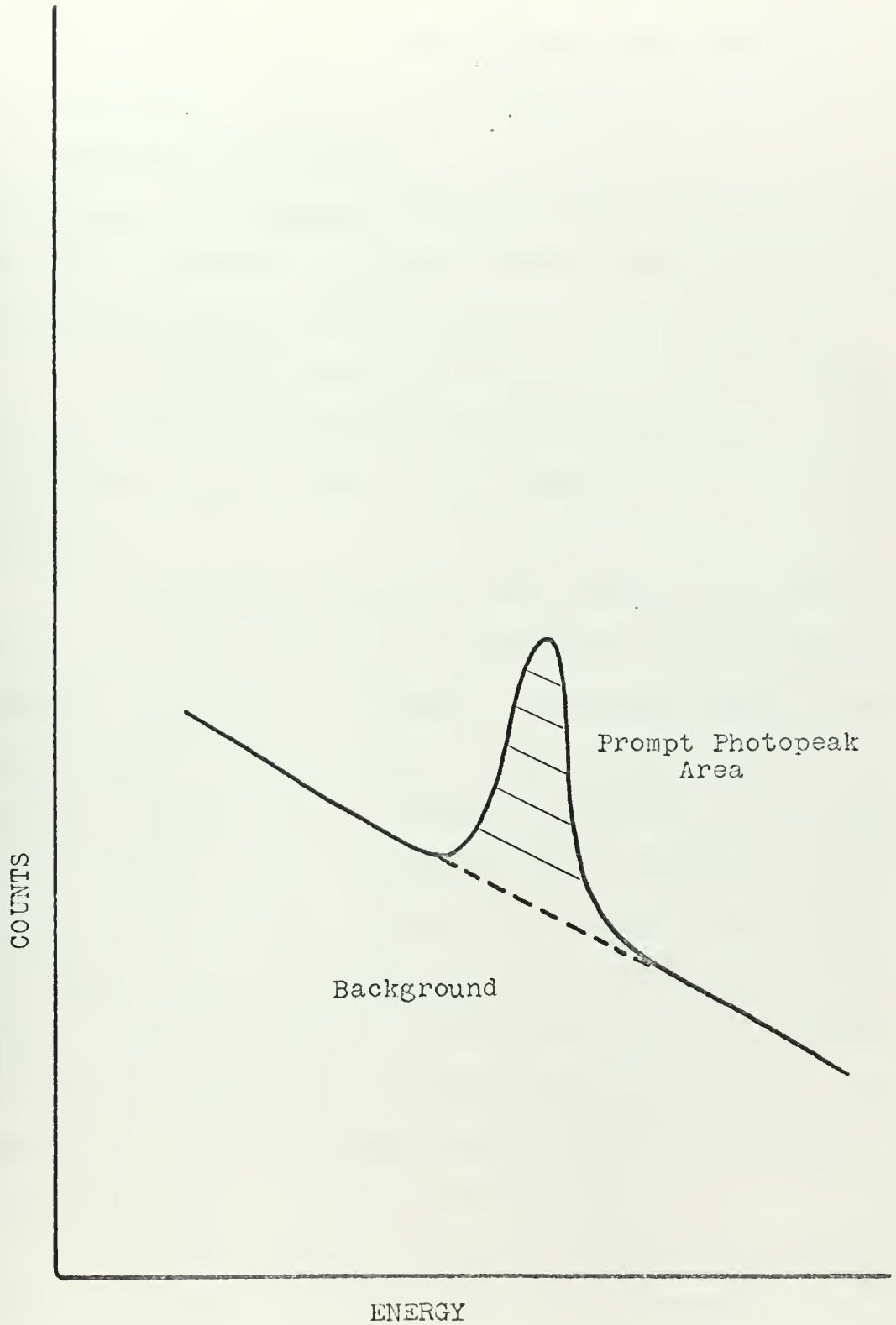

4.3 Elimination of Background by Photopeak Area (Indirect) Method

is then subtracted out by one of several methods presented later. From the slope of the resulting time spectrum the experimental value of λ is found.

4.4 Background Subtraction

4.4.1 Types of Background The background superimposed onto the prompt de-excitation gamma ray time spectrum can be attributed to three sources (Table 4.1 and Figure 4.4)

a. The first, cosmic radiation [11], is self-explanitory. The photons detected from this source have a constant distribution in time and an approximate $1/E^2$ distribution in energy.

b. Background produced by the Van de Graaff accelerator is two-fold. X-rays are generated by atomic excitation during the accelerator operation. Assuming that the beam characteristics remain stable, these X-rays are time independent. Another form of machine background is the gamma ray bursts which result from the (p,n) reactions at the neutron source target. These time dependent gamma rays are produced every 125 nanoseconds and are detected in the Ge(Li) crystal a couple of nanoseconds before the prompt de-excitation gamma rays from the scattering sample. The majority of these gamma rays are attenuated by the parafin-lead epoxy shield in front of the crystal.

c. The fast neutrons which are emitted from the (p,n) target contribute to several types of background.

Table 4.1

Photon Background Sources

1. Cosmic Radiation.

2. Accelerator Background.
   a. Atomic Excitation X-rays.
   b. Gamma Burst Due to Neutron Target (p,n) Reaction.

3. Neutron Indued Background.
   a. Fast Neutron Excitation andCapture in Detector and Nearby Auxilary Equipment.
   b. Fast Neutron Excitation and Capture in Room Environment.
   c. Induced Activity in Room Due to Neutron Capture.

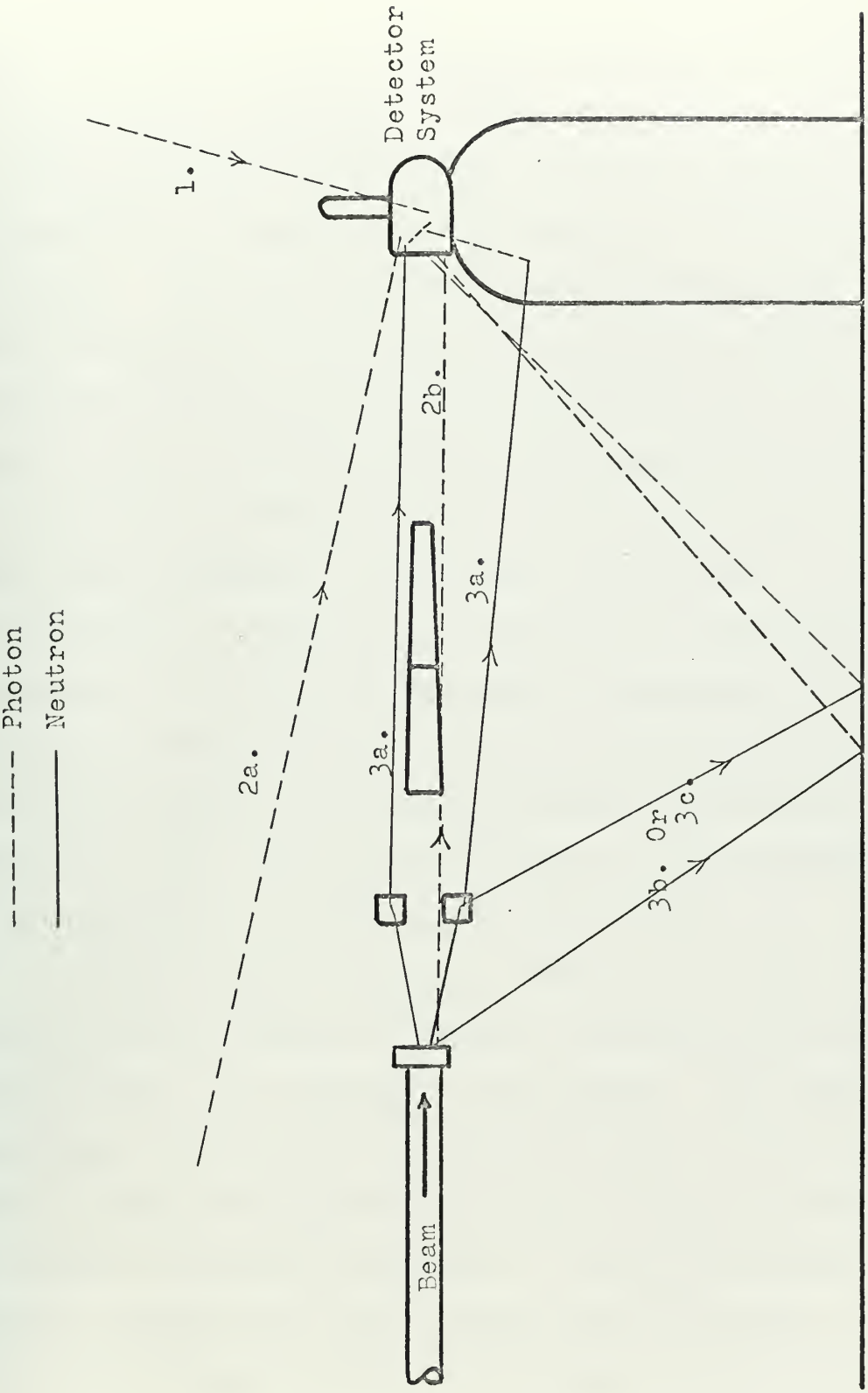

4.4 Background Sources

The first type is caused by fast neutrons which are scattered by the scattering sample directly onto the detector and its auxilary equipment. These fast neutrons produce a gamma ray background by either inelastic scattering and subsequent de-excitation or by capture in the detector system materials. The gamma rays are time dependent since the fast neutrons which generate the photons are directly scattered from the periodic neutron bursts into the detector area. The energies of the gammas are characteristic of the excited levels and (n,γ) reactions of the various metals and materials in and around the detector. The energy distribution is continuous, however, due to the Compton scattering, thus preventing complete background reduction by energy discrimination. One also should be aware that the Compton edges in time-gated energy spectra have a time dependence due to the decay mean life of the excited level which generates the particular Compton edge.

Another similar background caused by the fast neutrons are gamma rays produced by neutron inelastic scattering and capture in the laboratory environment. The only difference between this type of background and the fast neutron induced background discussed in the proceeding paragraph is the time dependence. The fast neutrons which scatter directly into the detector area all travel about the same distance and thus the resultant capture and nuclear

de-excitation gamma rays are detected at about the same time. This results in a well-defined background peak (labeled B in Figure 1.1) on the time spectra. However the fast neutrons, which are scattered into other areas in the laboratory, travel different distances and thus results in a very broad background peak on the time spectra (Figure 4.5).

The third type of background consists of neutron induced radioactivity in the laboratory due to neutron capture. The photons detected from the resultant nuclear decay have roughly a $1/E^2$ energy distribution. When activity equilibrium has been reached this background appears constant in time over the 125 nanosecond range.

The different types of background discussed above and shown in Table 4.1 can now be arranged according to their time characteristics, either time independent or time dependent (Table 4.2). The contribution of these backgrounds to the time spectrum is depicted in Figure 4.5.

Since the decay constant of the time spectra is determinded from a semi-logarithm plot, the time independent, as well as the time dependent background, must be eliminated from the raw experimental data.

4.4.2 Detector Time Response A separate category of background is that due not to extraneous radiations but rather to the poor time response of the Ge(Li) detector. As

Table 4.2

Time Dependence of Photon Background

Time Independent

1. Cosmic Radiation, (1)
2. Accelerator Produced X-rays, (2a)
3. Induced Activity in Room Due to Neutron Capture, (3c)

Time Dependent

1. Gamma Burst Due to (p,n) Reaction at T = 0, (2a)
2. Fast Neutron Excitation and Capture in Detector and Nearby Auxilary Equipment (3a)
3. Fast Neutron Excitation and Capture in Room Environment (3b)

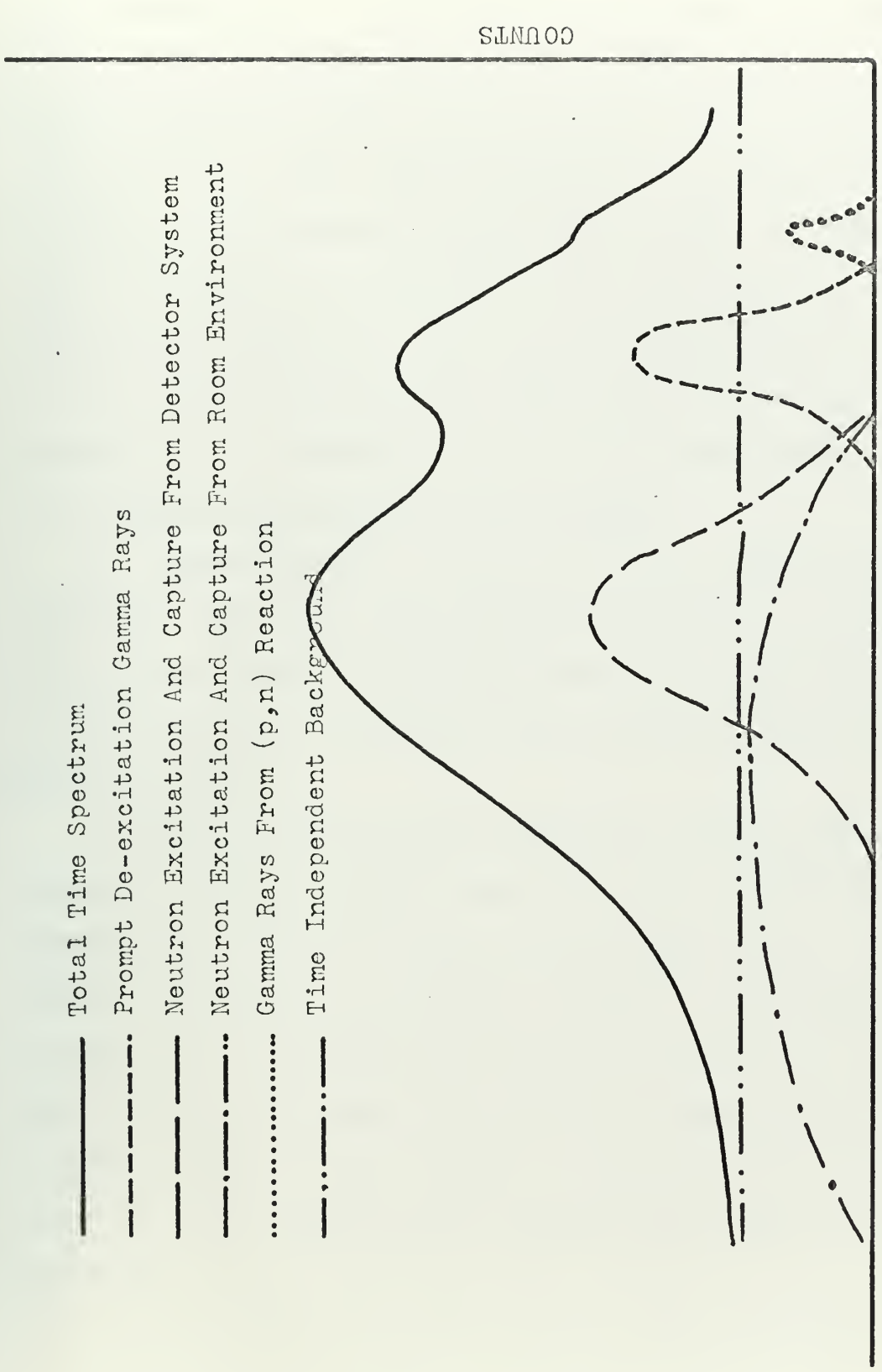

4.5 Time Spectrum Showing Background Contributions

discussed previously in section 3.4, the time spectrum for an instantaneous (on the order of a picosecond or faster) decay should be nearly a perfect guassian shaped peak. However because of the slow collection time of the solid state detector used, the time spectrum for such a decay exchibits an exponential tail (Figure 3.18). A relationship therefore has to be found which will yield the true experimental value of λ using the raw value measured by one of the above techniques and subtracting out the decay constant of the detector's exponential time response.

4.4.3 Methods of Background Subtraction

a. Carbon Sample: After the initial data run is completed, the ring sample being investigated is replaced by a carbon sample of identical geometry. The data run is repeated with the carbon and then subtracted from the initial sample spectrum.

Carbon is chosen as the background subtraction sample because its first excited level (4.43 MeV for C^{12} and 3.09 MeV for C^{13}) is a higher energy than the most energetic neutrons produced in the (p,n) targets. The carbon sample therefore will not introduce any new de-excitation gamma rays. During the carbon run, all the background sources listed in Table 4.1 are present. Only the de-excitation gamma rays will theoretically remain after complete subtraction.

The uncertainity over the length of time of the carbon sample subtraction run is perhaps the major contribution to background subtraction error. For the indirect mean life determination technique, the problem is not too great. In this case the carbon sample run is continued until a zero background level in the energy area of interest is reached. However in the direct mean life method, there may be no zero background level on the time spectrum and the decision as to when to stop subtracting is quite arbitrary. For the most part, the carbon subtraction runs on the time spectra were neutron normalized, that is each received the same number of incident neutrons. This neutron normalization method introduces an error since the microscopic scattering cross sections are different for the carbon and the investigated sample.

b. Background Subtraction by Energy Window Shift: This method for background reduction is used only with the direct mean life determination technique. After the initial time spectrum has been obtained, the energy discrimination window, which was previously placed around the de-excitation energy peak of interest is moved off the peak. A background spectrum is then taken and subtracted from the initial run.

Although the cross section and angular distribution

errors introduced by the carbon sample method have been eliminated, the placement of the energy window now becomes very critical in obtaining a good background subtraction. Changing the position of the energy window alters the ratio of time dependent to time independent background. The alteration of this ratio results in an erroneous time spectrum slope or decay constant after background subtraction.

The ratio change is explained by the following background properties. Due to its $1/E^2$ energy dependence, the time independent component of the gamma background is changed as the energy window is repositioned. As for the time dependent background component, movement of the energy window results in a different Compton scattering background level. There is also the possibility of accepting some background photopeaks or even the Compton edge of the de-excitation peak of interest if the window is moved to a lower energy. It is emphasized that the energy spectrum must be carefully scanned before repositioning the energy window for background subtraction.

If the amounts of time dependent and time independent background are approximately the same after repositioning the energy window, the length of the background subtraction run is controlled by neutron normalization. If the amounts of the background components are different than in the initial

run, a correction could be attempted by varying the subtraction time.

c. Reduction of Detector Time Response Background: To eliminate the detector time response background, a relationship must be derived which will separate the mean life of the solid state detector time response ($\tau_D = 1/\lambda_D$) from the mean life, τ , of the isomeric state.

For a theoretical case, the decay of an excited level can represented as shown in Figure 4.6. The number of nuclei which have decayed at any time t_i is

$$N_i = N_0 \left(1 - e^{-t_i/\tau}\right) \tag{4.1}$$

The number of nuclei which have decayed in the time period dt_1 , about t_1, that is the amplitude of the time spectrum at t_1 , is the time derivative of equation (4.1) or

$$\frac{dN_1}{dt_1} = + \frac{N_0}{\tau} e^{-t_1/\tau} . \tag{4.2}$$

Likewise at t_2 ,

$$\frac{dN_2}{dt_2} = + \frac{N_0}{\tau} e^{-t_2/\tau} . \tag{4.3}$$

However, due to the detector time response, the nuclei decaying in the time interval dt_1, about t_1 have an effect on the time spectrum amplitude, dN_2/dt_2 , at the time

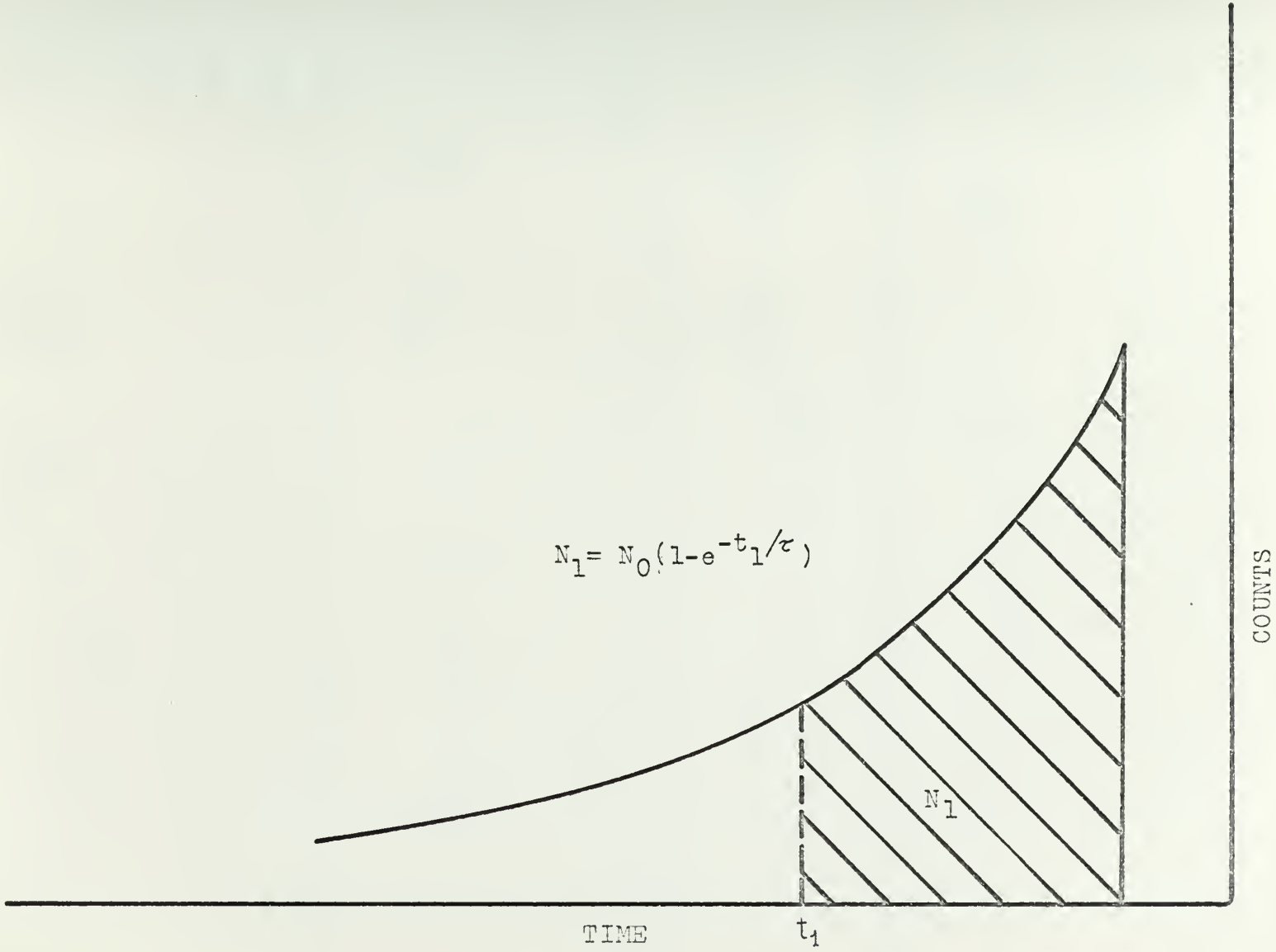

4.6 Exponential Decay

interal dt_2 about t_2 . Figure 4.7 shows the effect in the time interval at t_2 due to the detector exponential time response from a level decay detected in dt_1, about t_1. In equation form the effect on dN_2/dt_2 due to the decay in dt_1 about t_1 is

$$\frac{dN_{21}}{dt_2} = + \frac{dN_1}{\tau_D} e^{-(t_2-t_1)/\tau_D} \quad . \tag{4.4}$$

Substituting equation (4.2) into equation (4.4), one obtains

$$\frac{dN_{21}}{dt_2} = \frac{N_o}{\tau \tau_D} e^{(-t_1/\tau - t_2/\tau_D + t_1/\tau_D)} dt_1 \quad . \tag{4.5}$$

The total amplitude at t_2 due to all previous decays is obtained by integrating equation (4.5) from $t=0$ to $t=t_2$.

$$\frac{dN_2}{dt_2} = \frac{N_o e^{-t_2/\tau_D}}{\tau \tau_D} \int_0^{t_2} dt_1 \left[e^{-t_1/\tau + t_1/\tau_D} \right] . \tag{4.6}$$

The resulting relationship gives the amplitude of the time spectrum at any given time in terms of the known detector mean life, τ_D , and the unknown excited level mean life, τ .

$$\text{amplitude} = \frac{dN_i}{dt_i} = \frac{N_o}{\tau_D - \tau} \left(e^{-t_i/\tau} - e^{-t_i/\tau_D} \right) . \tag{4.7}$$

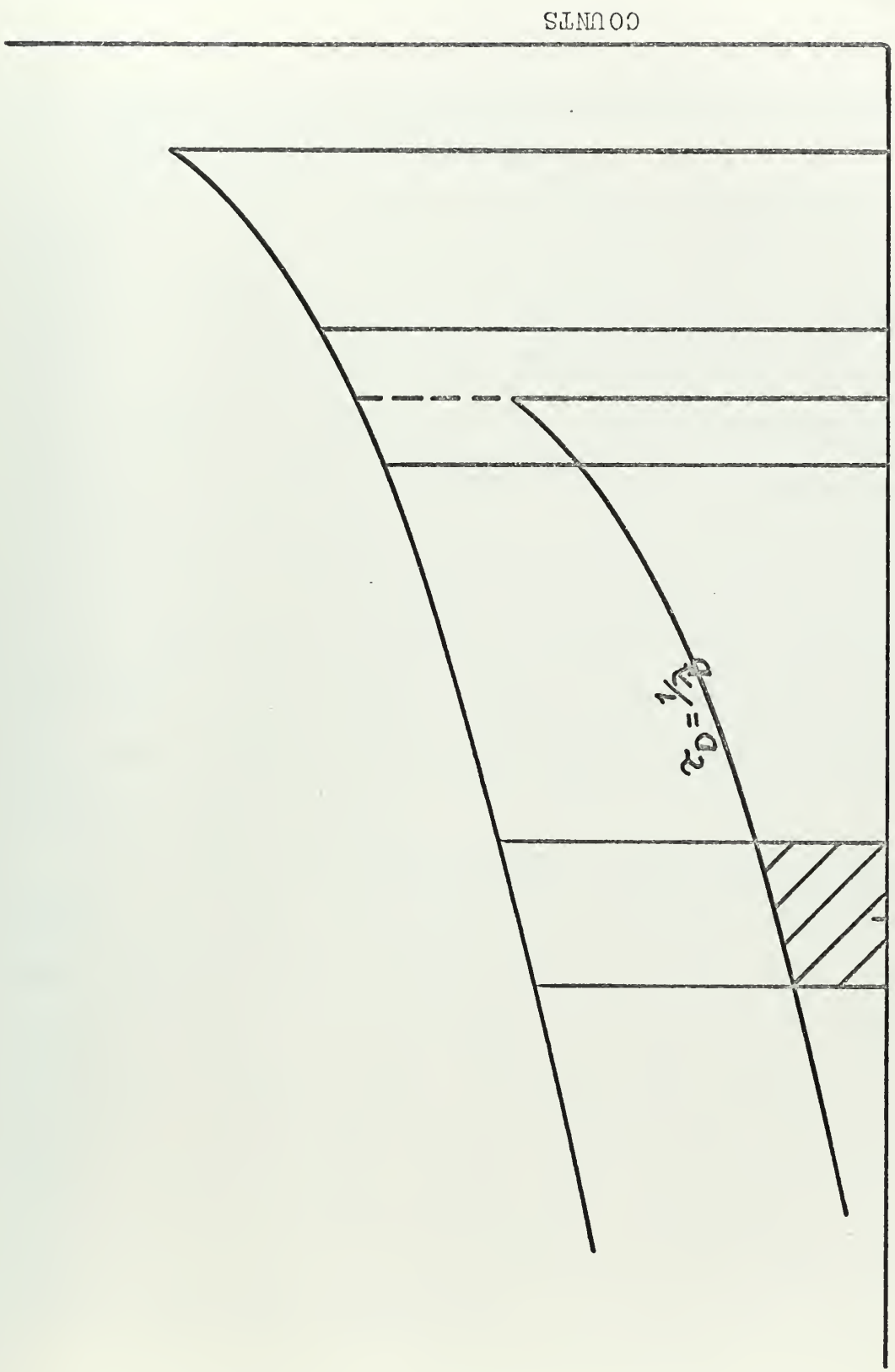

4.7 The Effects of the Detector Mean Life on the Amplitude of the Time Spectrum

Using the least squares method, one can fit experimentally measured time spectra to equation (4.7) and thus determine the best value for τ, the excited level mean life.

4.5 Analysis of the Two Mean Life Determination Techniques After Background Subtraction

The problem of errors introduced by background subtraction is less critical in the indirect mean life determination method. The gamma background can be effectively removed by judiciously selecting the photopeak area above the background on which it rides. Another advantage of this method is that other de-excitation gamma photopeaks can be studied since the entire energy spectrum can be obtained at each window. The primary inconvenience of this technique is the requirement of many experimental runs and the proponderance of data output. During these runs the accelerator beam characteristics must remain constant in order to insure accurate results.

At present the direct method for mean life determination suffers from large errors due to background subtraction. Even though thetime spectra are energy gated, the gamma background count is still almost as large as the prompt de-excitation gamma count. Thus when the background time spectrum is subtracted from the initial time spectrum, the resulting statistics are quite poor. Compounding the high statistical error is the uncertainity in the time duration of the background subtraction.

4.6 Quick Method for Determining the Presence of Long-Lived Excited Levels

The presence of long-lived excited levels can quickly be discerned by running two neutron normalized energy spectra, one time gated on the prompt de-excitation gamma peak and the other time gated 50 nanoseconds after the prompt de-excitation gamma peak (Figure 4.8). For both spectra, the time windows were the same width, 20 nanoseconds.

By comparing the areas under the de-excitation photopeaks in the two energy spectra, one can determine the ratio of gamma rays detected after a 50 nanosecond delay with respect to those detected promptly after excitation. If the ratio of the areas, that is the delayed photopeak over the prompt photopeak, is appreciable, it can be assumed that total de-excitation does not occur immediately and that a long-lived excited level has been found. Once such an excited level is identified, the mean life can be further investigated, by one of the two mean life determination techniques discussed above.

However, should the ratio of the areas effectively be zero, that is no de-excitation photopeak can be seen in the 50 nanosecond delayed energy spectrum, the mean life of that particular excited level is assumed to be less than thelimit of sensitivity of this technique, about 10 nanoseconds.

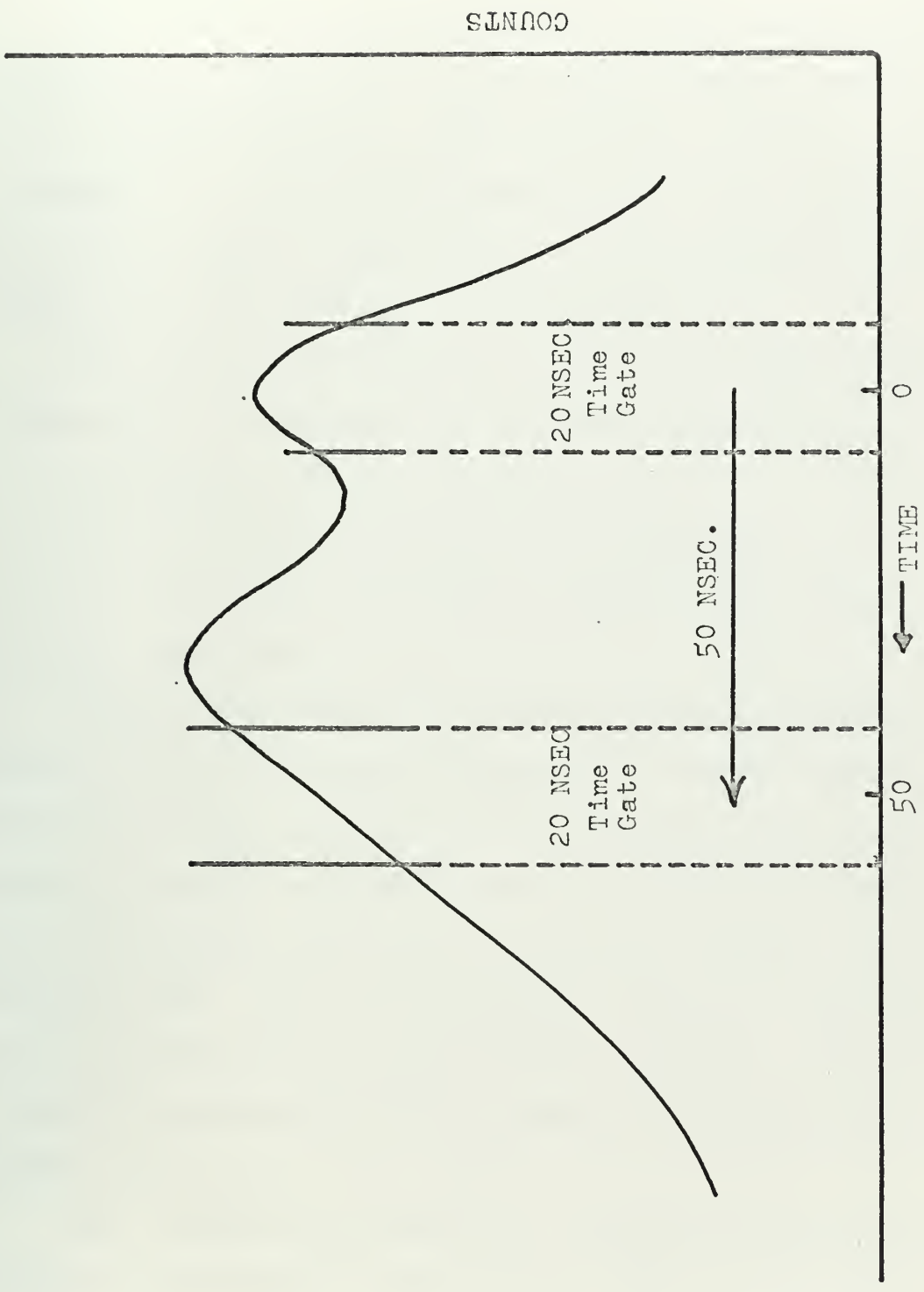

4.8 Time Spectrum With Prompt and 50 Nanosecond Delayed Time Gates

4.7 Errors Associated With Experimental Mean Life Measurements

The source of error presented in this section will be evaluated as a percentage of the experimentally determined time spectrum amplitude. This procedure allows for easy propagation of errors in determining the total uncertainty. The values given to the errors below are arrived at through experience, data analysis, and reference [3].

The primary uncertainties in the experimental time spectra can be attributed to the following effects:

1. changes in beam characteristics,
2. a variation in electronic properties,
3. difficulty in background subtraction, and
4. statistics.

During operation of the Van de Graaff accelerator the energy of the proton beam remains very steady because of a magnetic resonance control unit in the bending and analyzing magnet. However a geometry error of about 3% is introduced due to the slight drifting of the proton beam in the accelerating tube. This drifting causes the (p,n) reaction area to shift about on the Li^7 and H^3 targets. The 3% error evaluation assumes that the accelerator is operating in a stable condition.

The variation in electronic properties refers mainly to the non-uniformity of the timing signals which start the

TAC. The variation is inversely proportional to the energy of the detector output pulses. At energies around 200 keV, the error is about 10% while at higher energies, around 1 MeV, the error reduces to about 5%.

The background subtraction error is dependent on the method of mean life determination used. The least error is involved in the employment of the indirect, or time spectra reconstruction, technique. Here the background reduction is essentially performed when the area of the photopeak is measured. For prominent peaks the error in the area measurement is about 5 %.[3] . For very small photopeaks which hardly are discernable above the background, the errors maybe on the order of 100%. The uncertainity of the exact size and position of the time windows introduces another 3 to 5 % error in the time spectrum amplitude.

The direct mean life determination method is subject to the lack of an accurate means for determining the duration of the background subtraction run. An estimate of the uncertainty in the subtraction time is about 5 %, and this could lead to an error in the time spectrum amplitude as high as 50%. Other smaller errors in duplicating the geometry of the actual data runs, arebrought about by the use of a carbon scatterer. About an 8 % error is present due to the difference in the positioning and physical properties

of the two scattering samples.

Statistically, the error is the square root of the count rate of interest. Percentage-wise this error can be reduced by longer counting times. In the indirect method, the more prominent peaks of an energy spectrum may have a statistical error under 4 %. In the direct method, the statistical error is larger due to the subtraction of the background time spectrum from the initial time spectrum. The statistical error may be as high as 20%.

Under the most optimum conditions the cumlulative errors for the direct and indirect methods are 24 and 9 percent respectively. These errors refer to a percentage of the time spectrum amplitude, dN/dt . Translated to a percentage of the mean life, τ , the errors become 35 and 14 percent for the direct and indirect mean life determination methods respectively.

CHAPTER V

EXPERIMENTAL RESULTS AND DISCUSSION

5.1 Excited Level Mean Life Determination in F^{19}, Cd^{111}, and Ta^{181}

The procedure used to determine the mean lives of the excited levels investigated was to fit, using the method of least squares, the experimentally measured time spectra to the theoretical time spectra, equation (4.7) derived in section 4.4.3c.

The actual steps taken in arriving at a value for consisted of first, comparing the experimental time spectrum to a series of normalized time spectra (Figure 5.1) obtained from equation (4.7). From this comparison an approximate value of the mean life could be estimated. Having narrowed down the possible range for τ, one then conducted a trial and error, single variable (τ), least squares fit. The value of τ, which makes the sum of the squares of the deviations in the time spectrum amplitudes as small as possible, is considered, together with its appropriate error, to be the experimentally derived mean life of the particular excited level.

5.1.1 Indirect Method Results: The mean lives of excited levels in F^{19} and Cd^{111} were measured by the indirect method. Energy level diagrams [12] and de-excitation energy spectra

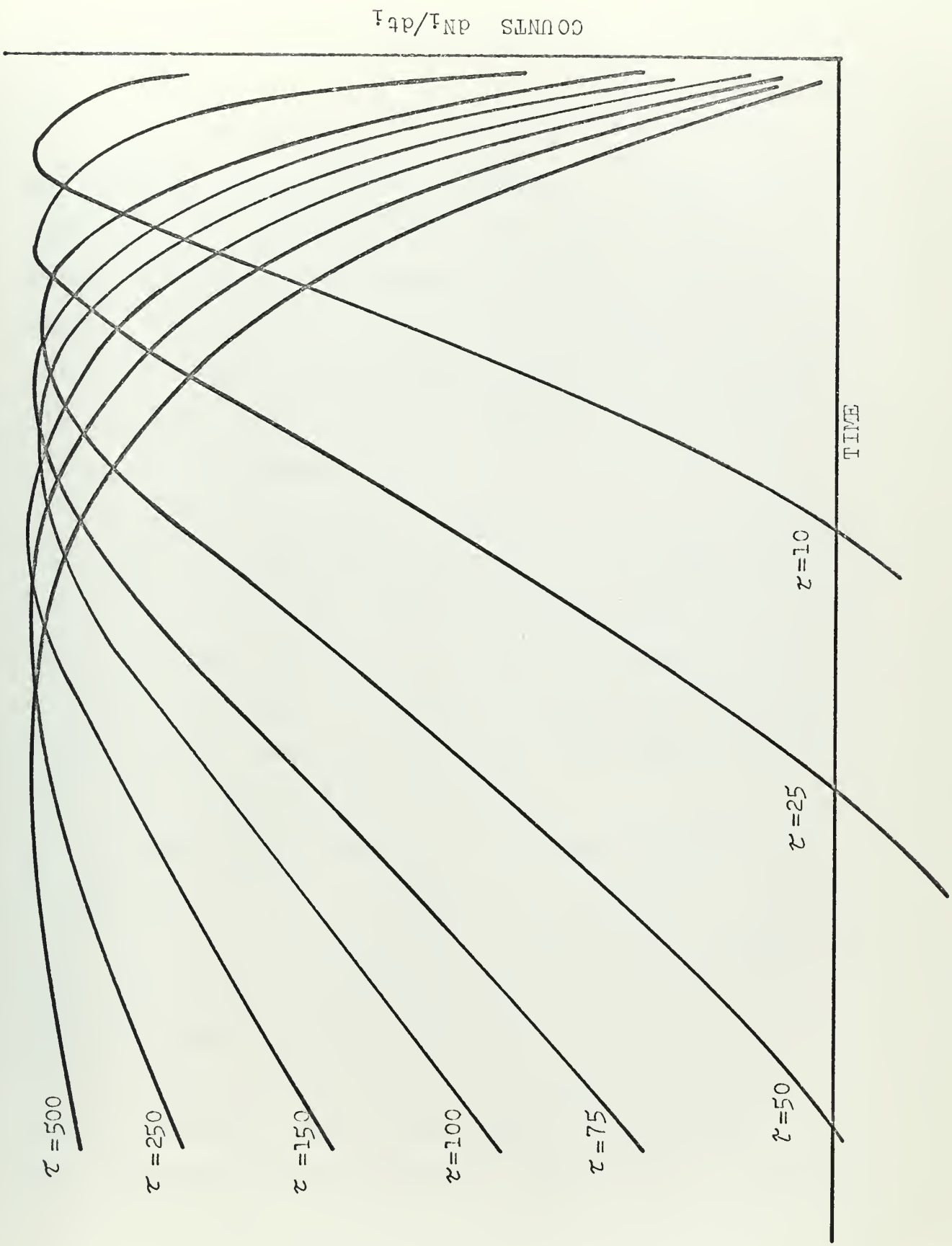

5.1 Normalized Theoretical Time Spectra

for these two isotopes are shown in Figures 5.2 through 5.5.

In fluorine the level of interest is that at .197 MeV. This excited level decays by emitting an isomeric .197 MeV. gamma ray. The photopeak areas and their respective time window positions are displayed in Figures 5.6 and 5.7. The reconstructed time spectrum is shown in Figure 5.8. Using the least squares procedure discribed above, the value of the mean life of the .197 MeV excited level in F^{19} was found to be 130 $\pm$ 25 nanoseconds.

In cadmium the level of interest is that at .247 MeV. The only decay from that level is a .247 MeV gamma ray to the ground state. The .247 MeV photopeak areas and respective time window positions are shown in Figures 5.9 and 5.10. After the resulting time spectrum (Figure 5.11) was least squares fitted, the mean life of the .247 level in Cd^{111} was found to be 110 $\pm$ 35 nanoseconds.

5.1.2 Direct Method Results: The direct method was used to determine the mean lives of excited levels at .197 MeV in F^{19} and at .482 MeV in Ta^{181}. Energy level diagrams [12] and de-excitation energy spectra for these isotopes are shown in Figures 5.2, 5.3, 5.12, and 5.13.

In fluorine, the energy discrimination window was placed around the .197 MeV photopeak. The resulting time spectrum, without background subtraction, is depicted

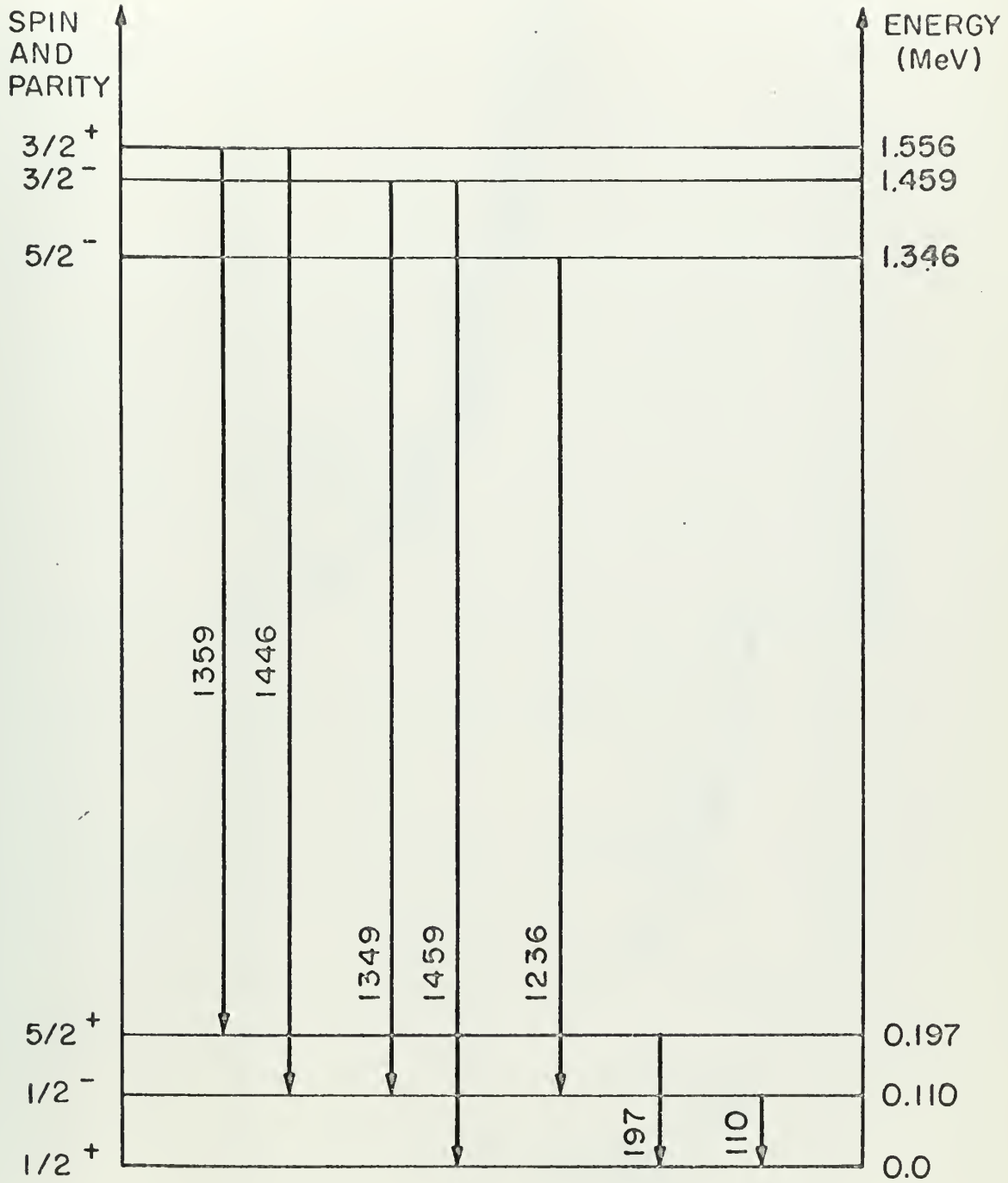

5.2 F^{19} Energy Level Diagram

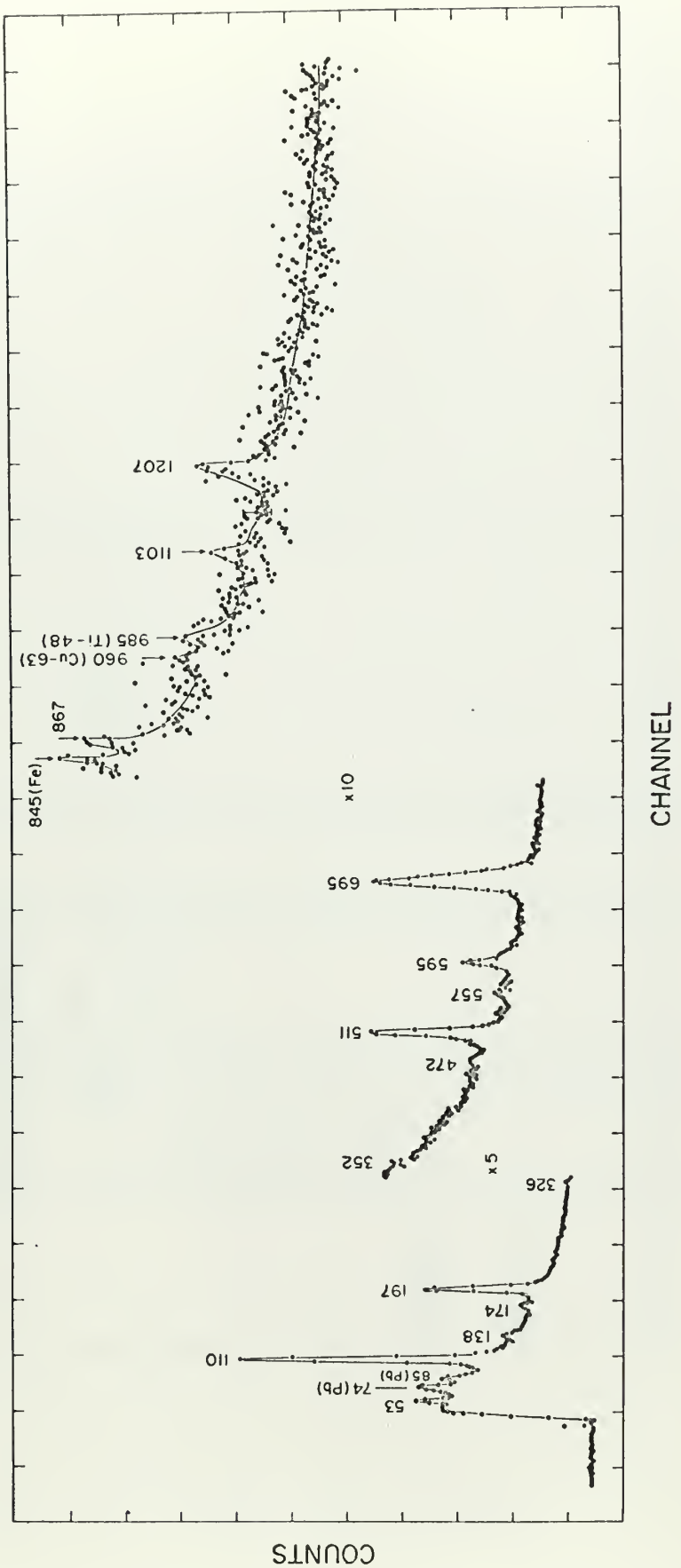

5.3 F^{19} Time Gated Energy Spectrum, Neutron Energy, 1.41 MeV

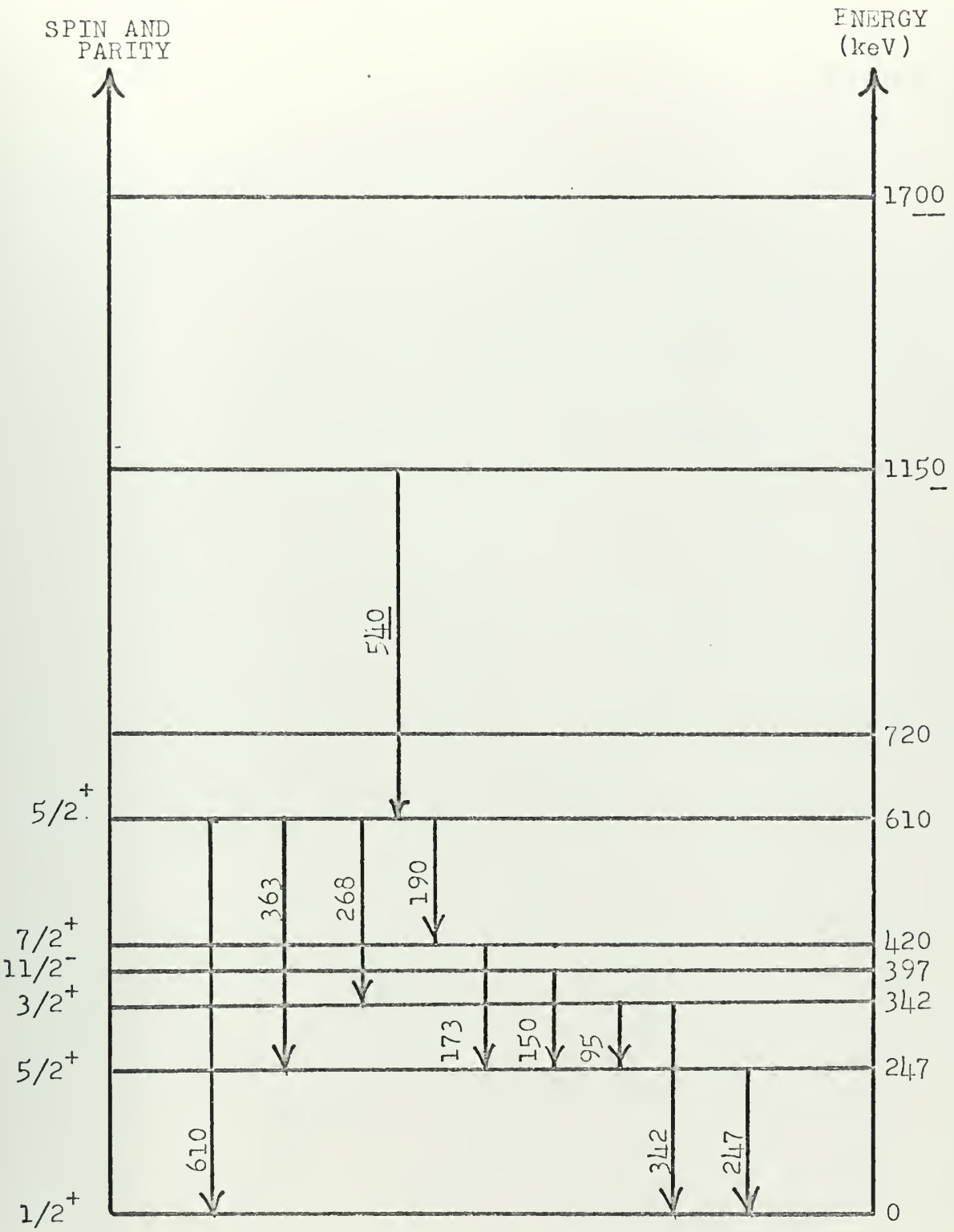

5.4 Cd^{111} Energy Level Diagram

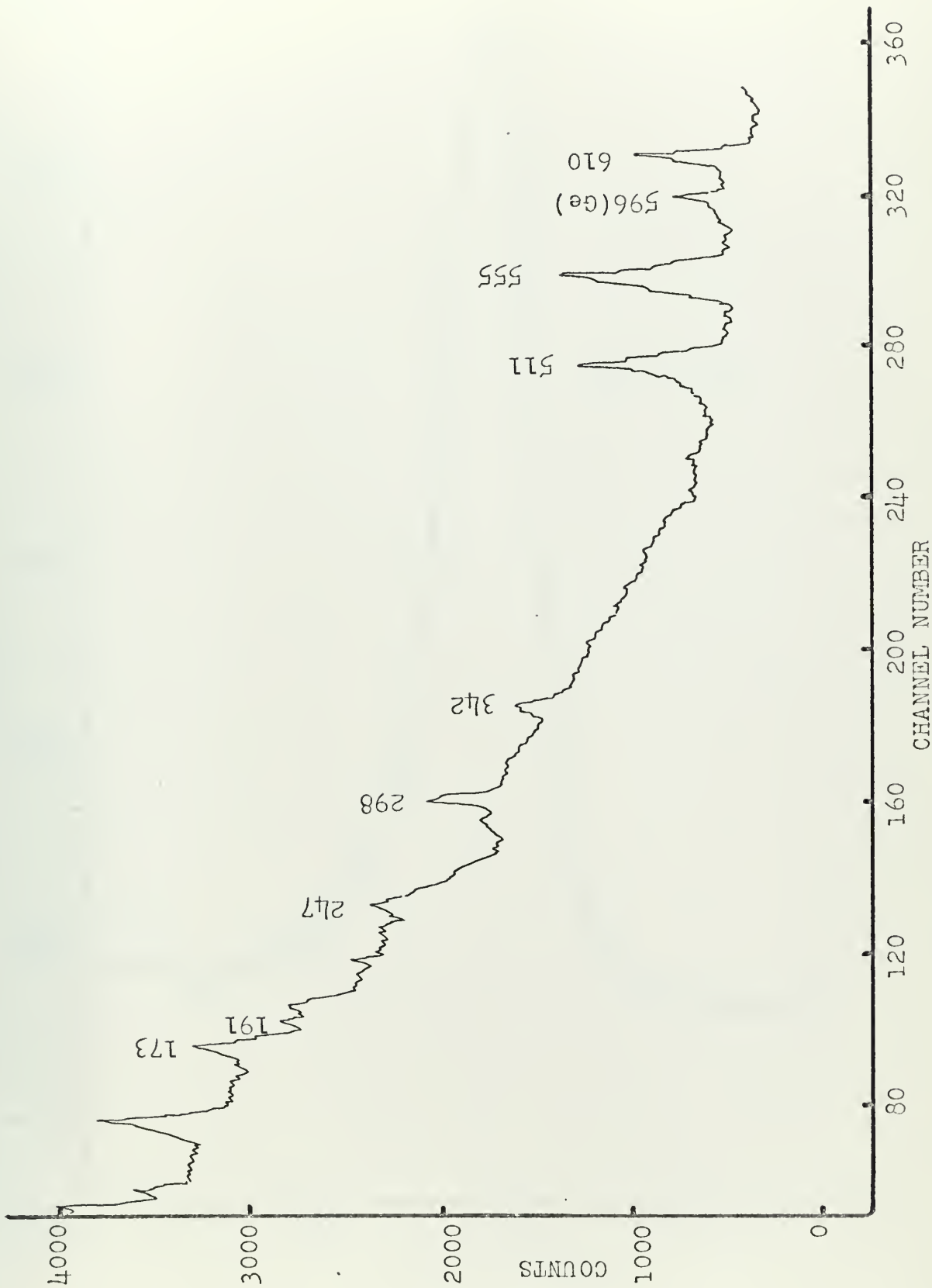

5.5 Cd111 Time Gated Energy Spectrum, Neutron Energy, 1.5 MeV

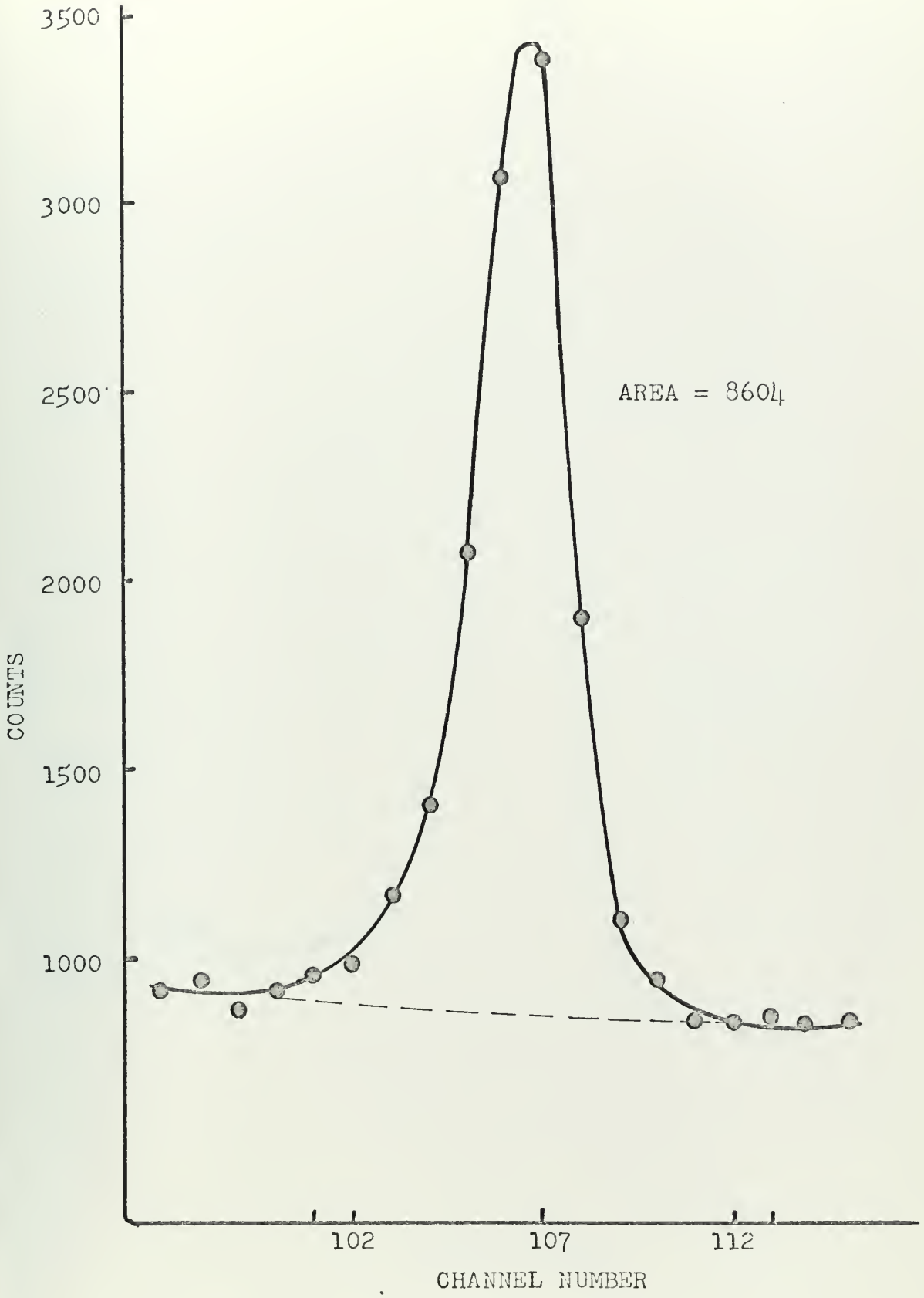

5.6a Timed Gated Photopeaks for the .197 MeV Gamma Decay in F^{19} (at t = 20 nsec.)

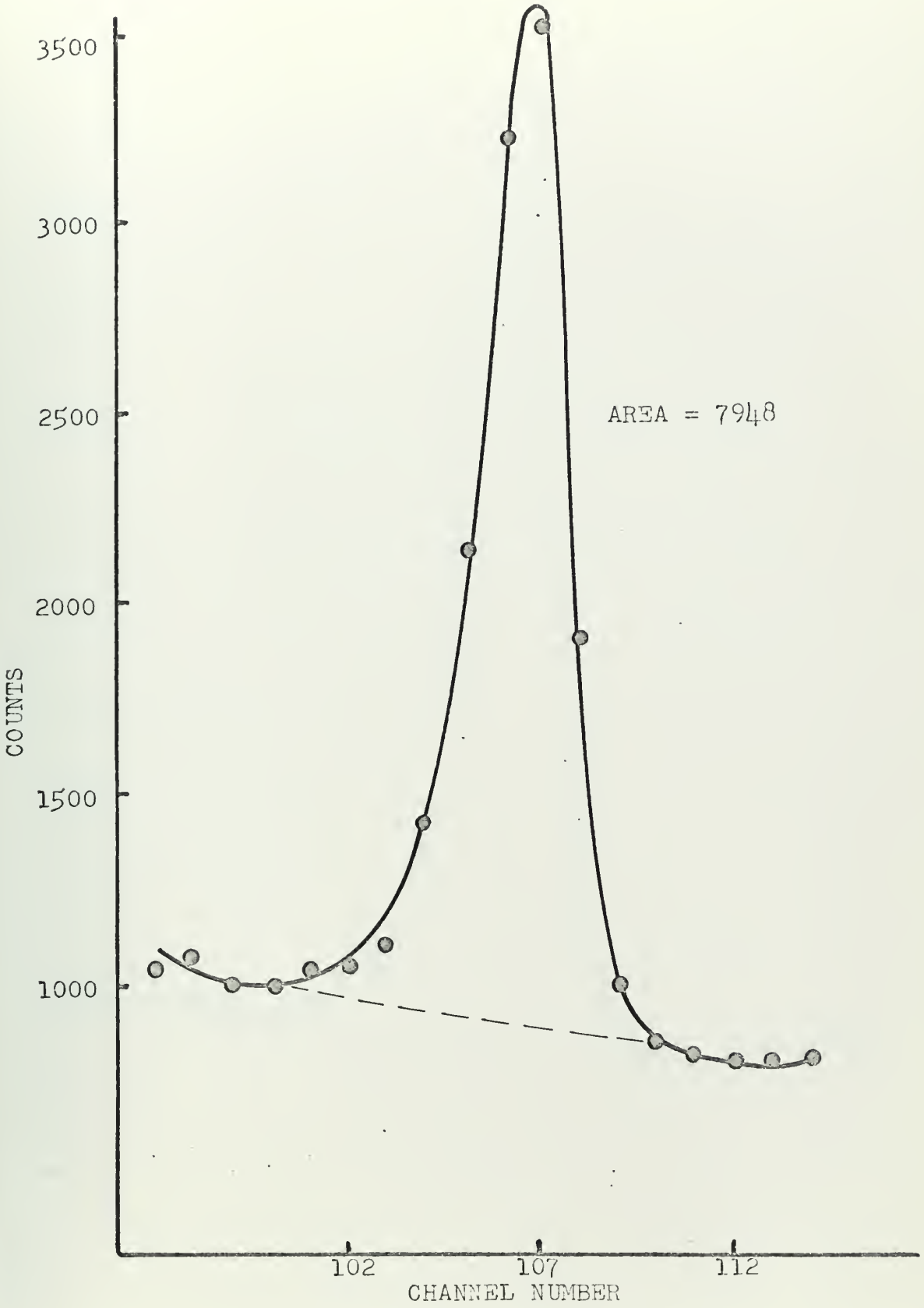

5.6b Timed Gated Photopeaks for the .197 MeV Gamma Decay in F^{19} (at t = 31 nsec.)

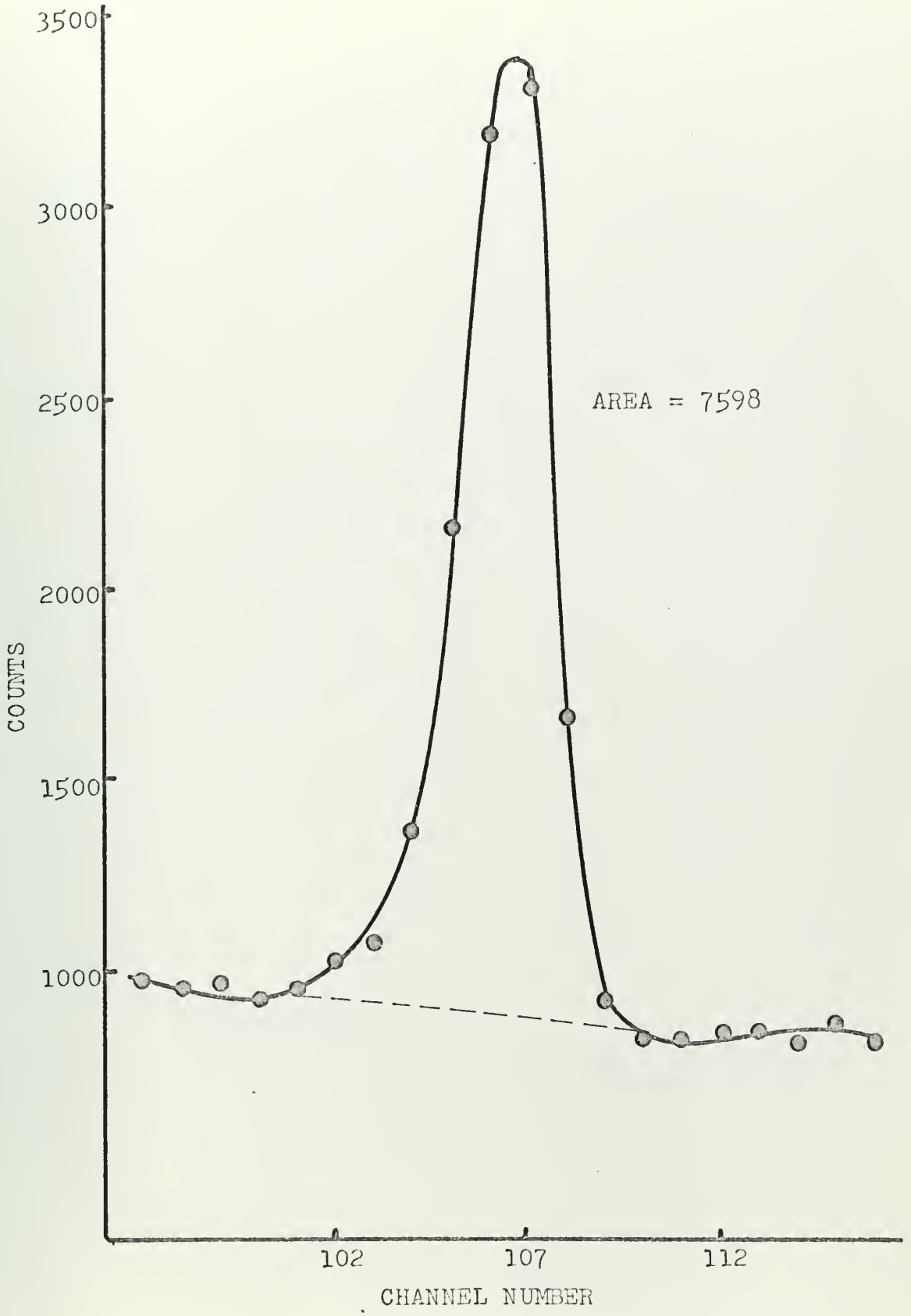

5.6c Timed Gated Photopeaks for the .197 MeV Gamma Decay in F^{19}
(at t = 43 nsec.)

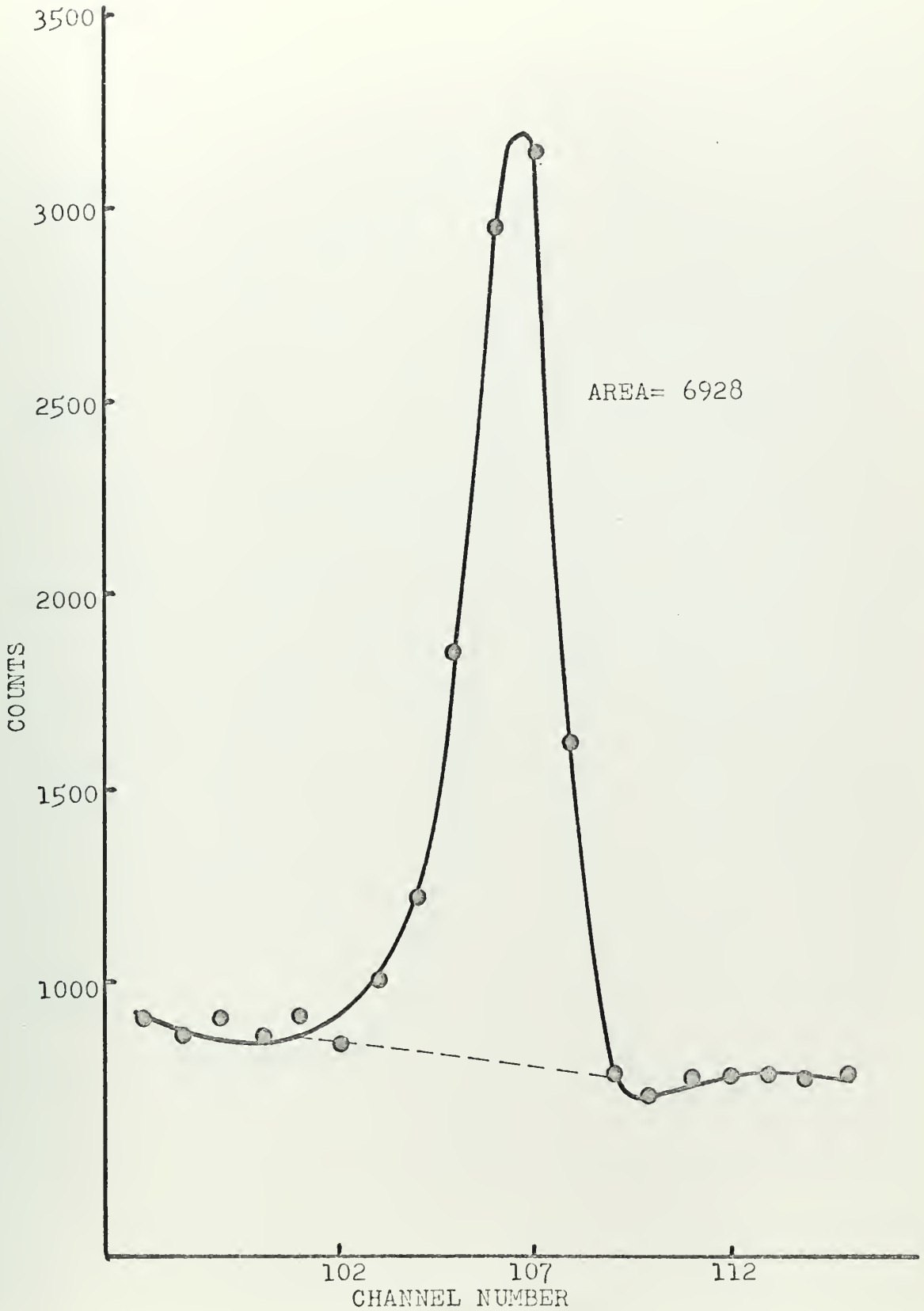

5.6d Timed Gated Photopeaks for the .197 MeV Gamma Decay in F^{19} (at t = 54 nsec.)

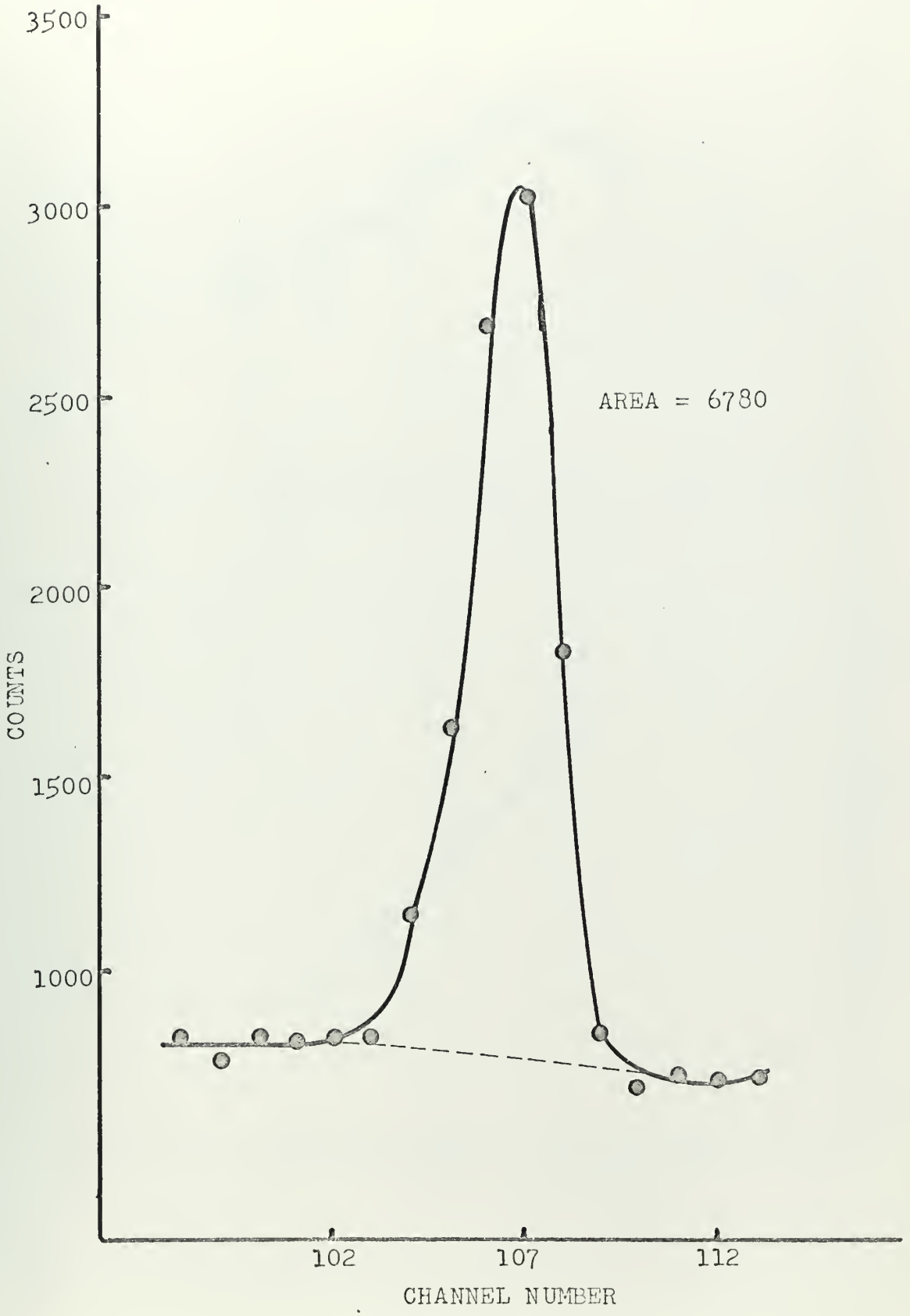

5.6e Timed Gated Photopeaks for the .197 MeV Gamma Decay in F^{19} (at t = 70 nscc.)

5.7 F^{19} Time Gate Positions on 125 Nanosecond Period Time Spectrum

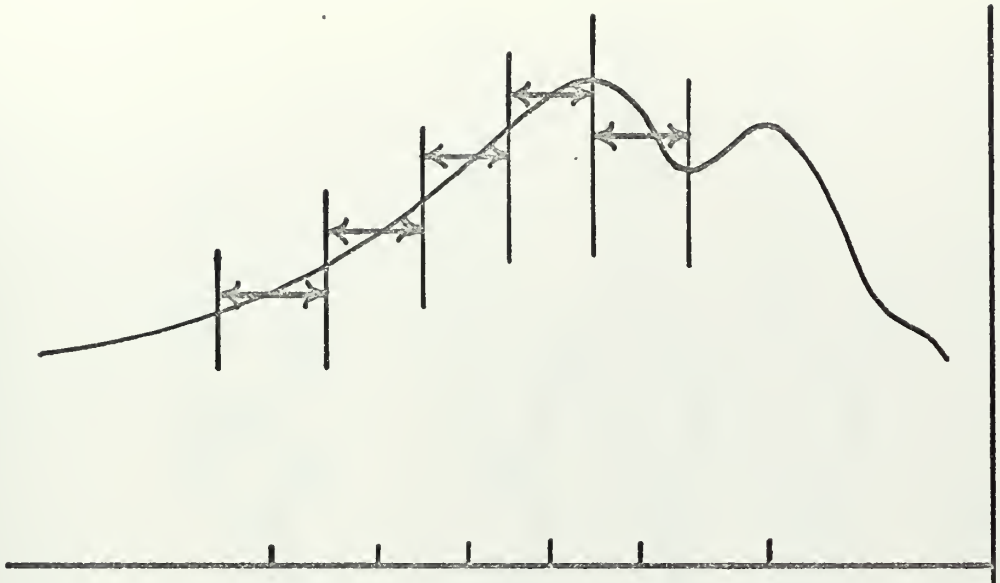

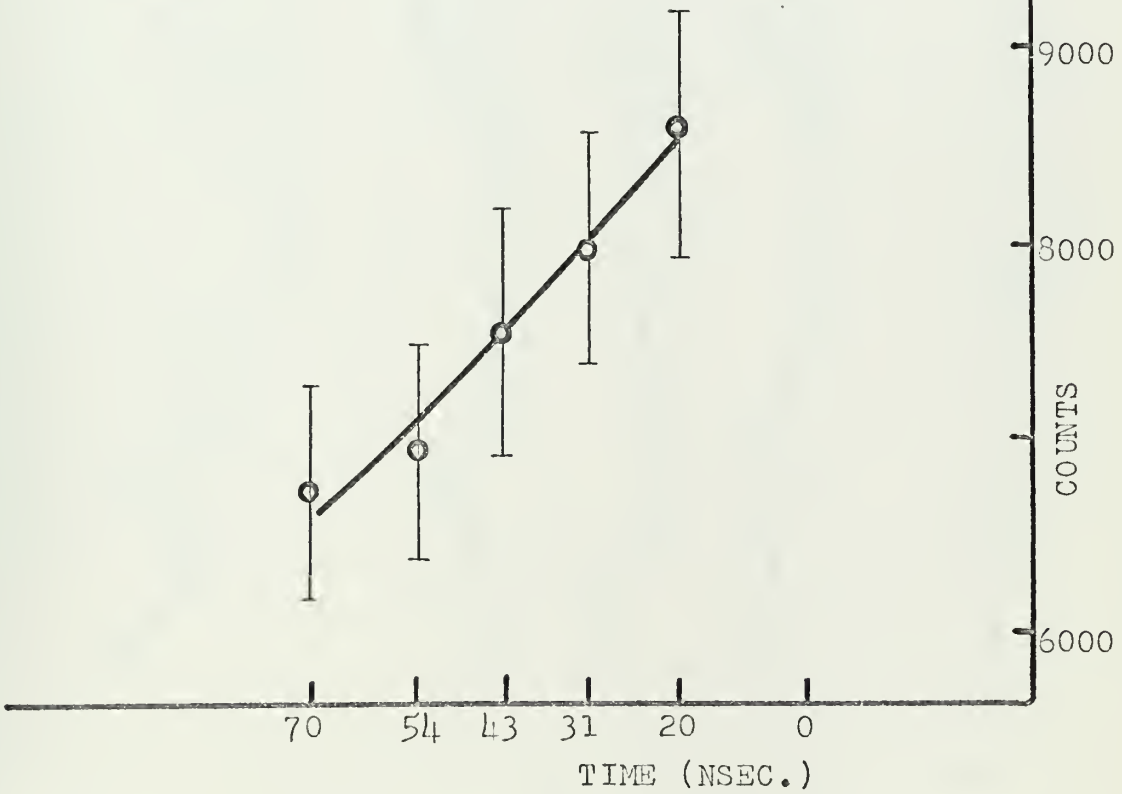

5.8 F^{19} Reconstructed Time Spectrum

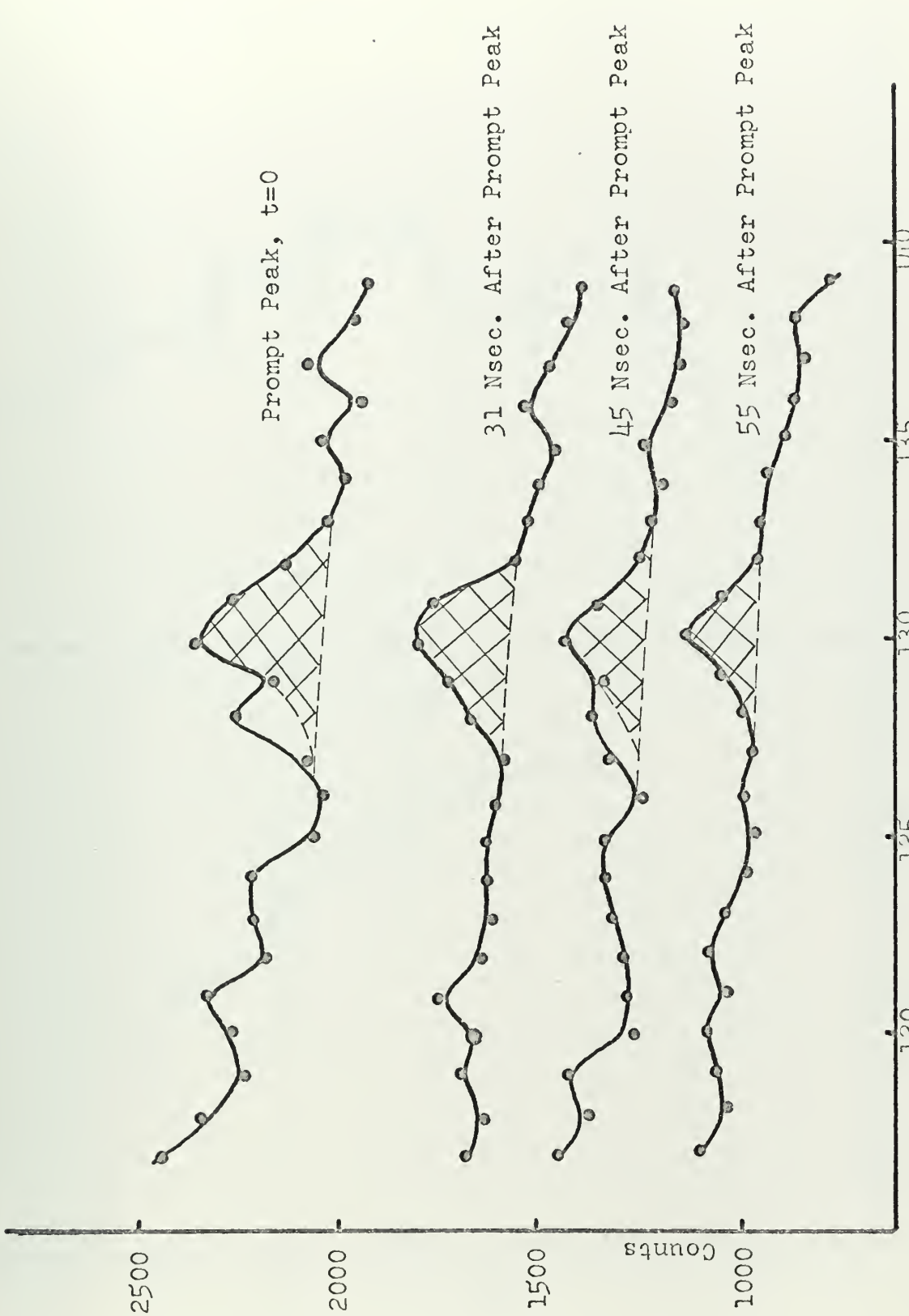

5.9 Time Gated Photopeaks for the .247 MeV Gamma Decay in Cd^{111}

5.10 Cd^{111} Time Gate Positions on 125 Nanosecond Period Time Spectrum

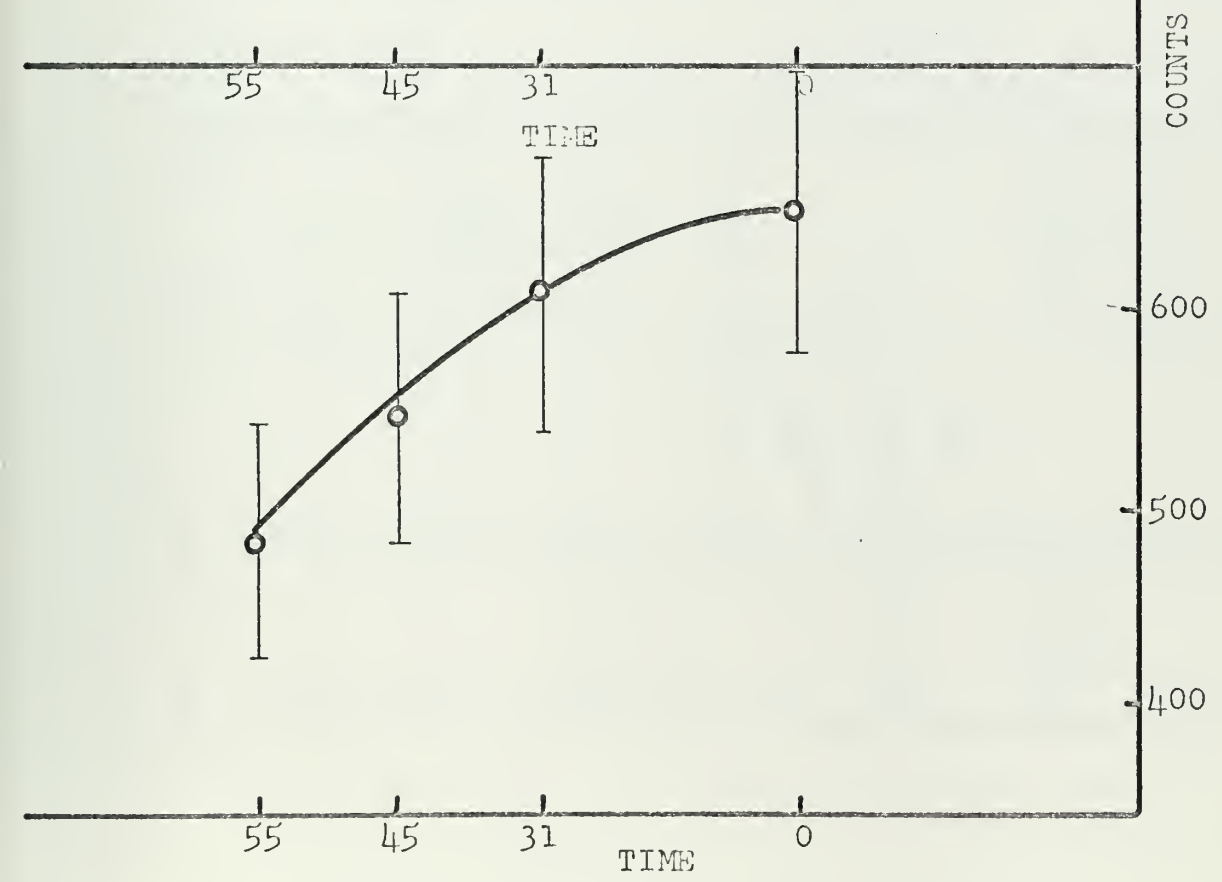

5.11 Cd^{111} Reconstructed Time Spectrum

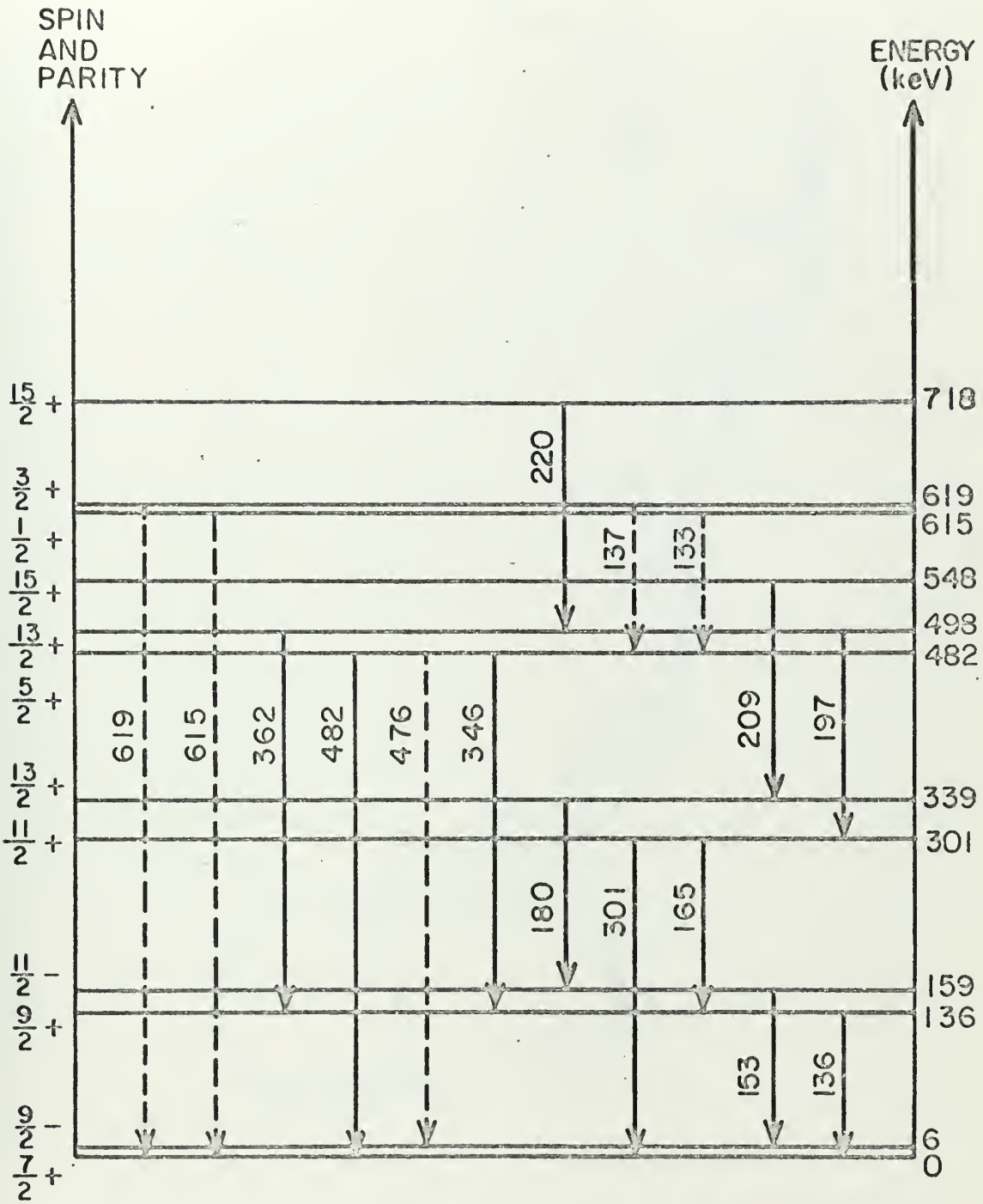

5.12 Ta^{181} Energy Level Diagram

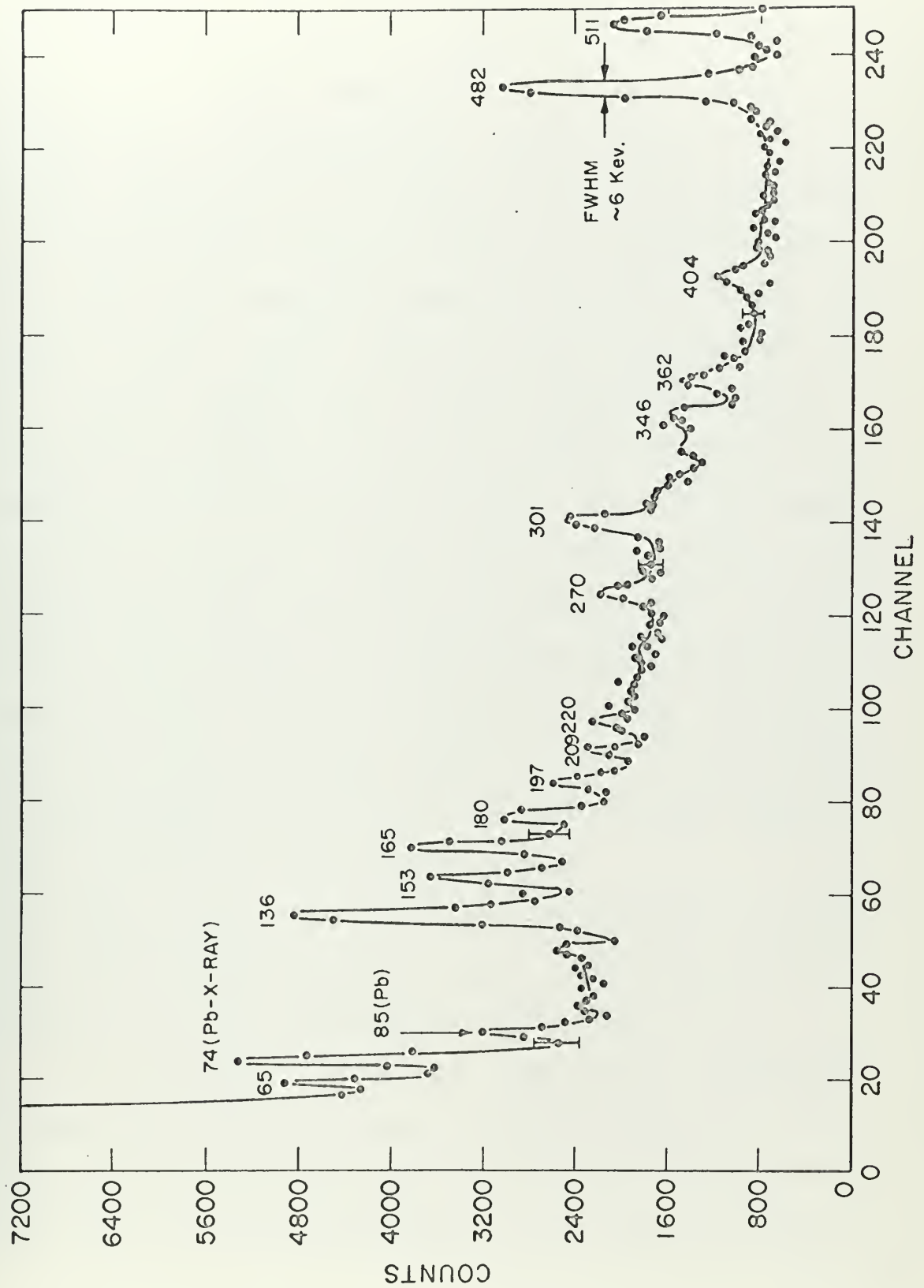

5.13 Ta^{181} Time Gated Energy Spectrum, Neutron Energy, 1.41 MeV

in Figure 5.14. After background subtraction using the carbon subtraction method, the time spectrum is shown in Figure 5.15. A least squares fit to the equation (4.7), revealed that the experimentally measured mean life of the .197 level in F^{19} was found to be 74 ± 60 nanoseconds.

In Ta^{181} the level of interest is located at .482 MeV. This level decays by gamma rays of .482 MeV (to ground state), .346 MeV (to the .136 MeV level) andpossibly .476 MeV [3] (to the 6 keV level). Since the branching ratio highly favors the decay to ground, the energy window was placed around the .482 MeV photopeak. The .346 MeV gamma ray could, of course, be used, however the smaller photopeak to background ratio would cause a greater error. Figures 5.16 and 5.17 present the experimental Ta^{181} time spectrum, before and after background subtraction using the energy window shift method. As a result of the least squares fit, the experimental value of the mean life for the .482 MeV level in Ta^{181} was 10 ± 8 nanoseconds.

5.1.3 Discussion: The experimental measurements of the mean lives compare favorably with the known values [12] of the excited levels investigated above (Table 5.1).

In the indirect method the effect of the uncertainty in photopeak area measurements is aptly revealed. The photopeak to background ratio for the .197 MeV gamma ray in fluorine is relatively large. This allows for ease in

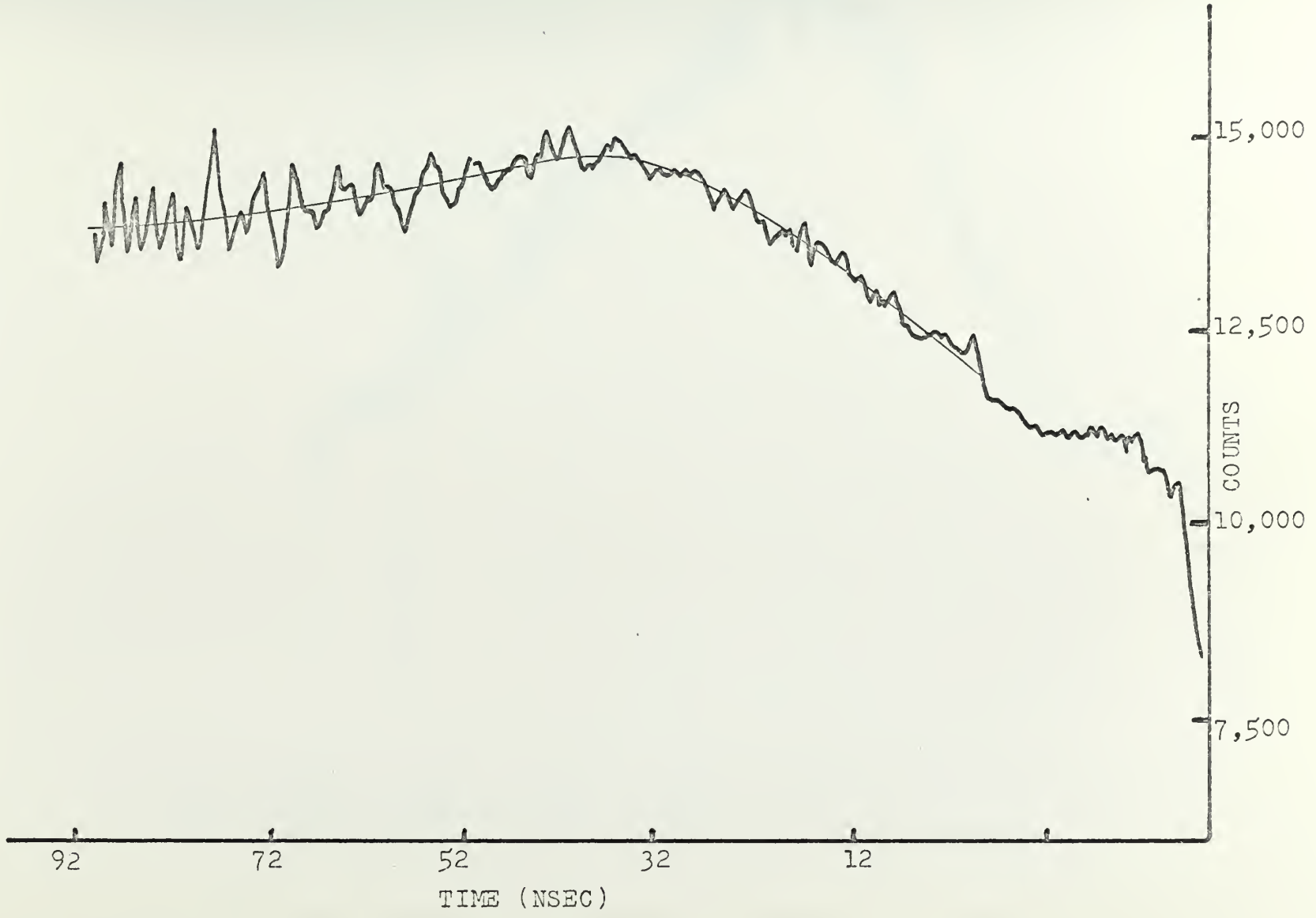

5.14 F^{19} Direct Method Time Spectrum, No Background Subtraction

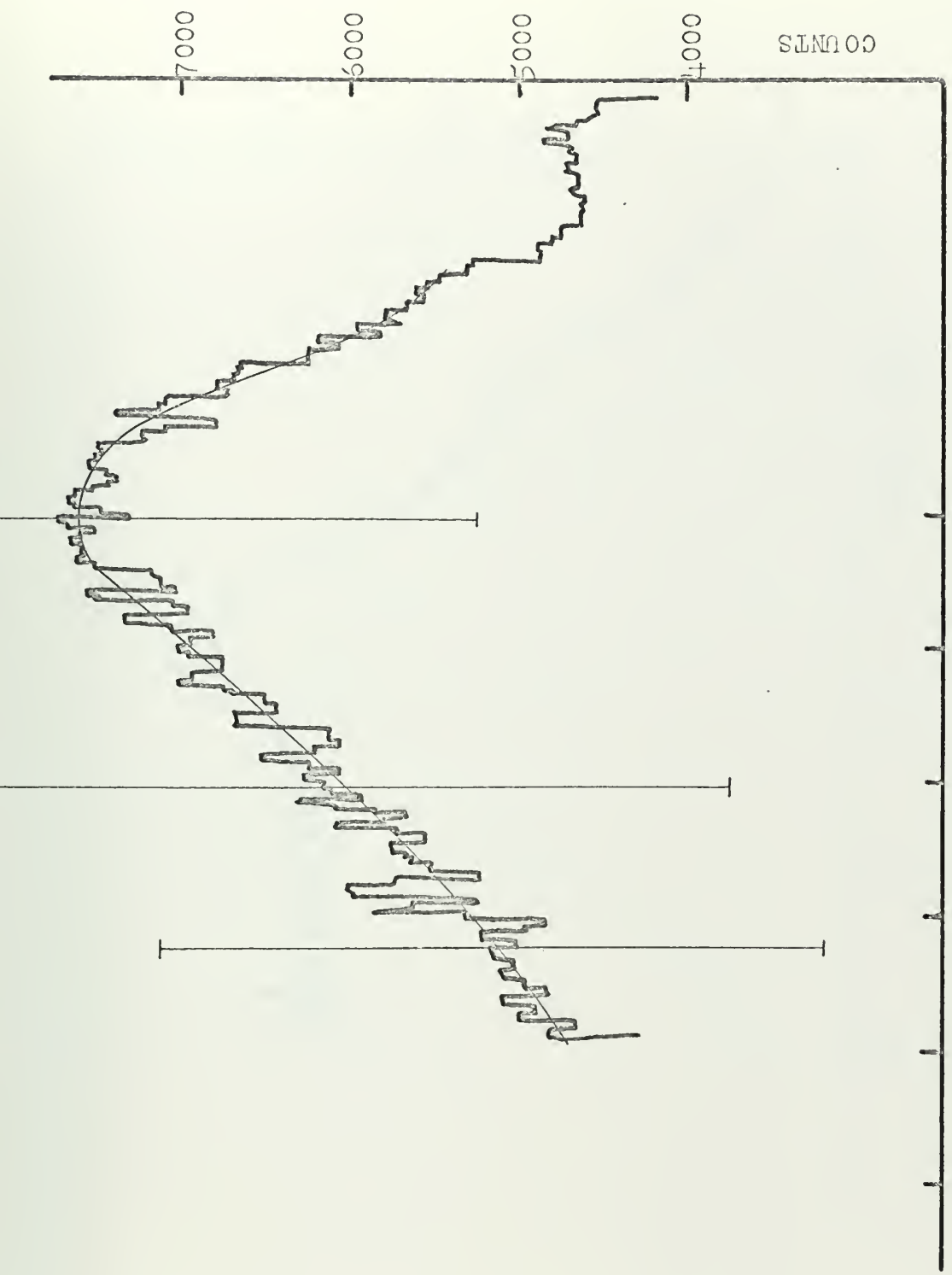

5.15 F^{19} Direct Method Time Spectrum, Background Subtracted

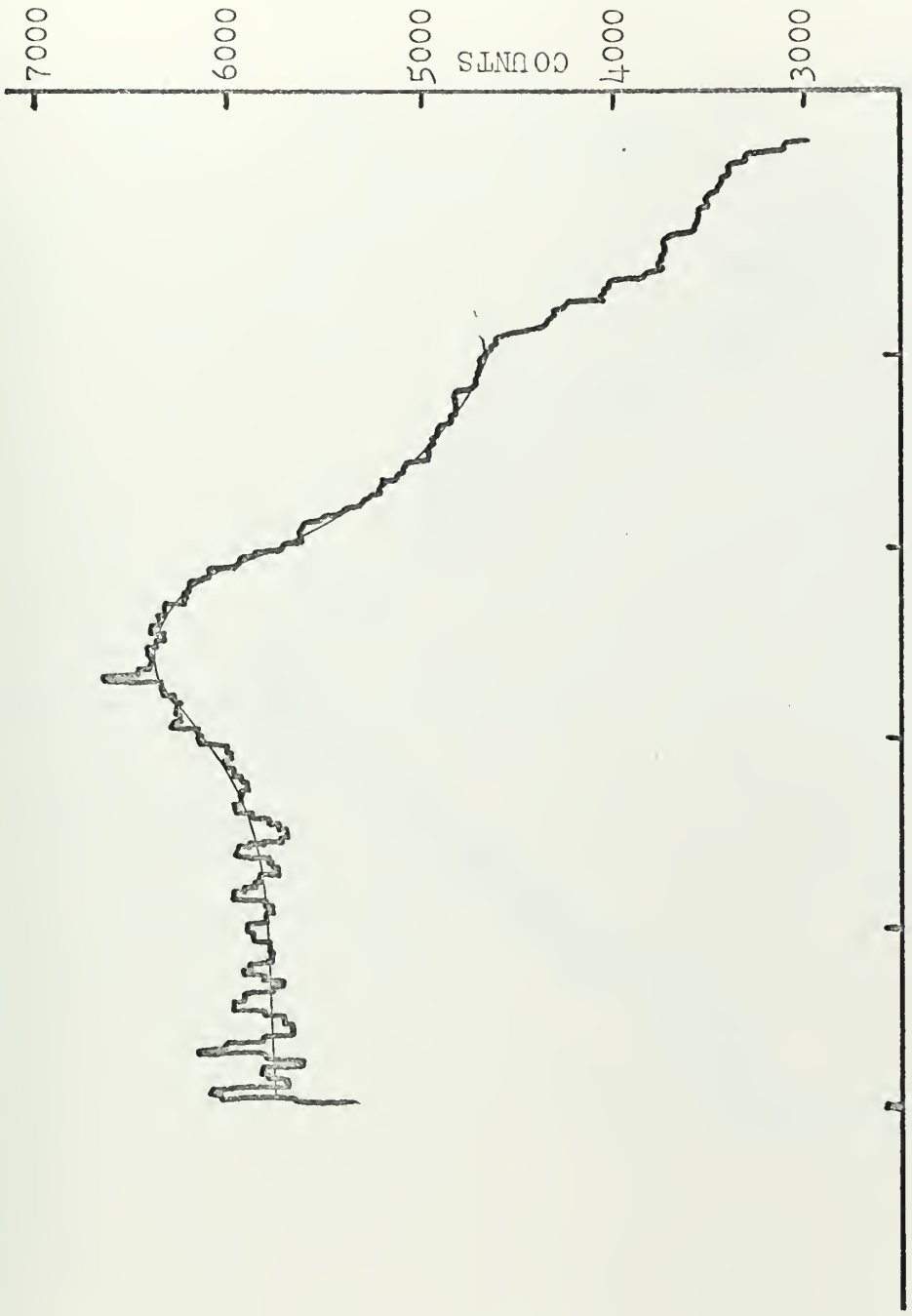

5.16 Ta^{181} Direct Method Time Spectrum, No Background Subtraction

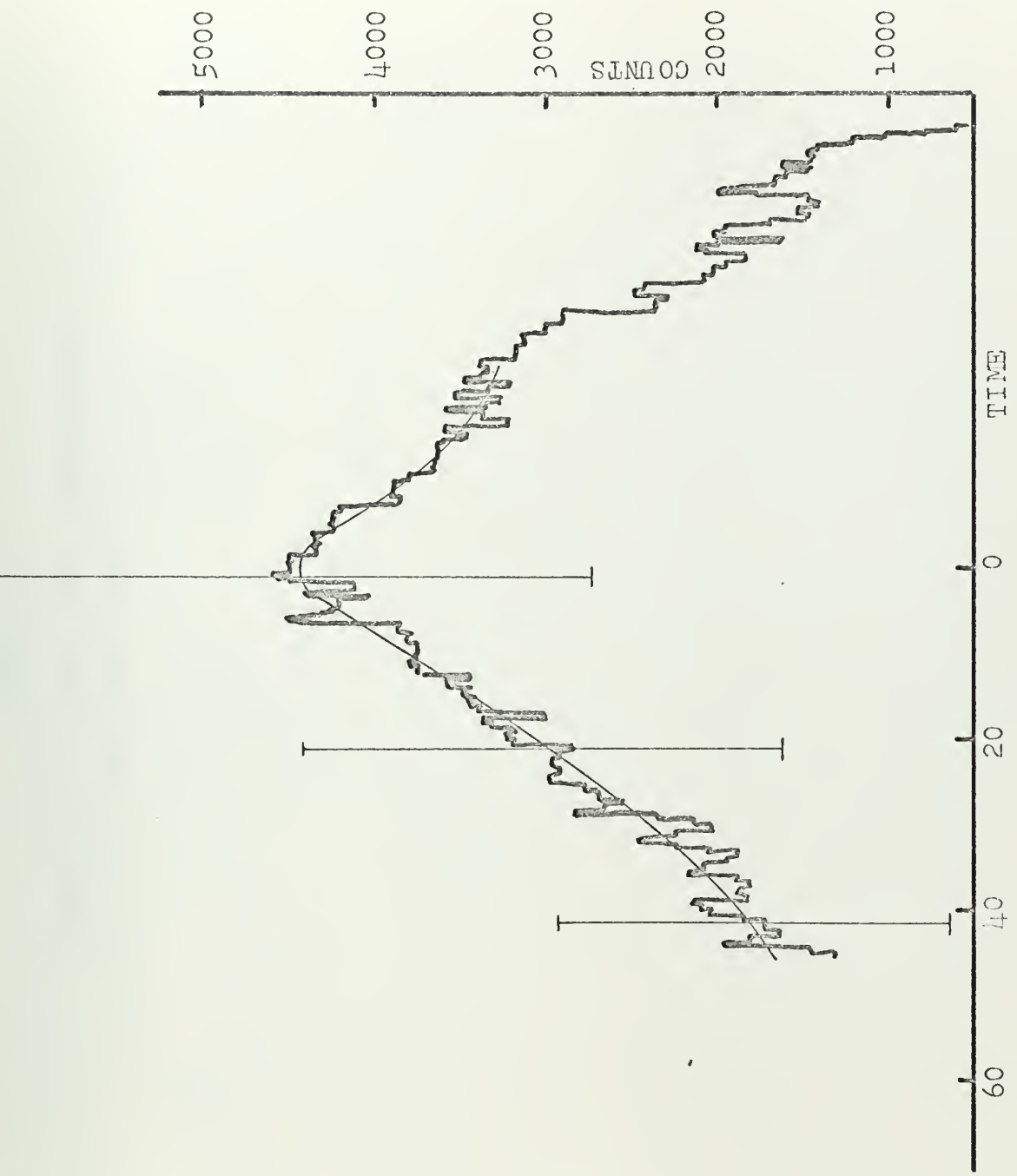

5.17 Ta^{181} Direct Method Time Spectrum, Background Subtracted

Table 5.1

Comparison of Experimental Measurements
to Well Determined Mean Life Values

Isotope	τ (ns) other experiments	τ (ns) this experiment direct method	τ (ns) this experiment indirect method	τ_w Weisskopf single particle estimate
F^{19}	125 [13, 14]	74 ± 60	130 ± 25	~1000 ns.
Cd^{111}	85 [15, 16]	--	110 ± 35	~50 ns.
Ta^{181}	15 [17]	10 ± 8	--	346, E2 ~5 ns. 482, M1 $\sim 10^{-16}$ sec.

calculating the areas under the energy peaks and, in the case of fluorine, the uncertainty in these areas was only about 5%. Conversely, for the gamma ray from the .247 MeV level in cadmium, the photopeak to background ratio was very small (Figure 5.9) and the uncertainty in the area determination was about 30%. The greater accuracy in the flourine mean life measurement verifies this effect.

The direct method results are present with a large uncertainty due to the background subtraction. The higher accuracy of the Ta^{181} value is most probably caused by a better choice for the duration of the background subtraction run.

Table 5.1 also compares the known values of the mean lives of the excited levels investigated above to their respective Weisskopf extreme single particle estimates [7]. Considering the simplicity of the single particle model, the accuracy of the Weisskopf estimates is astonishing. Indeed, over the entire mean lifetime range, Weisskopf's extreme single particle estimates are generally found to agree within several orders of magnitude [7].

5.2 The Search for Long Lived Excited Levels in Nb^{93} and Sc^{45}

Unlike those in the isotopes investigated in section 5.1, the mean lives of the excited levels in Nb^{93} and Sc^{45} have not yet been established. Due to the work of V. Rogers [3] in experimental measurements of the neutron inelastic scat-

tering cross sections for Nb^{93} and Sc^{45}, it was necessary to determine if the mean lives of any of the excited levels in Nb^{93} or Sc^{45} were long enough ($\sim > 5$ nanoseconds) to warrant a correction in the gamma ray production cross sections (reference chapter I).

The energy level diagrams [12] and de-excitation energy spectra for Nb^{93} and Sc^{45} are depicted in Figures 5.18 through 5.21.

As discussed in section 4.6, the technique used to search for these long lived excited levels is to compare prompt time gated energy spectra against 50 nanosecond delayed time gated energy spectra. Figures 5.22 through 5.34, show the results from such energy spectra for F^{19}, Nb^{93}, and Sc^{45}. The diagrams represent a comparison between the prompt and delayed photopeak areas of the gamma ray decay from the excited levels of interest. The .197 MeV level in fluorine is included as an example of a level with a relatively long mean life (τ = 125 nanoseconds).

5.2.1 Niobium Results: The levels in Nb^{93} which could be successfully investigated using the comparison between the prompt and delayed photopeak areas are those at .742 MeV (Figure 5.23), .808 MeV (Figure 5.24), .809 MeV (Figure 5.25), .952 MeV (Figure 5.26), 1.080 MeV (Figure 5.27), 1.295 MeV (Figure 5.28) and 1.337 MeV (Figure 5.29).

The evidence from each of these levels shows that,

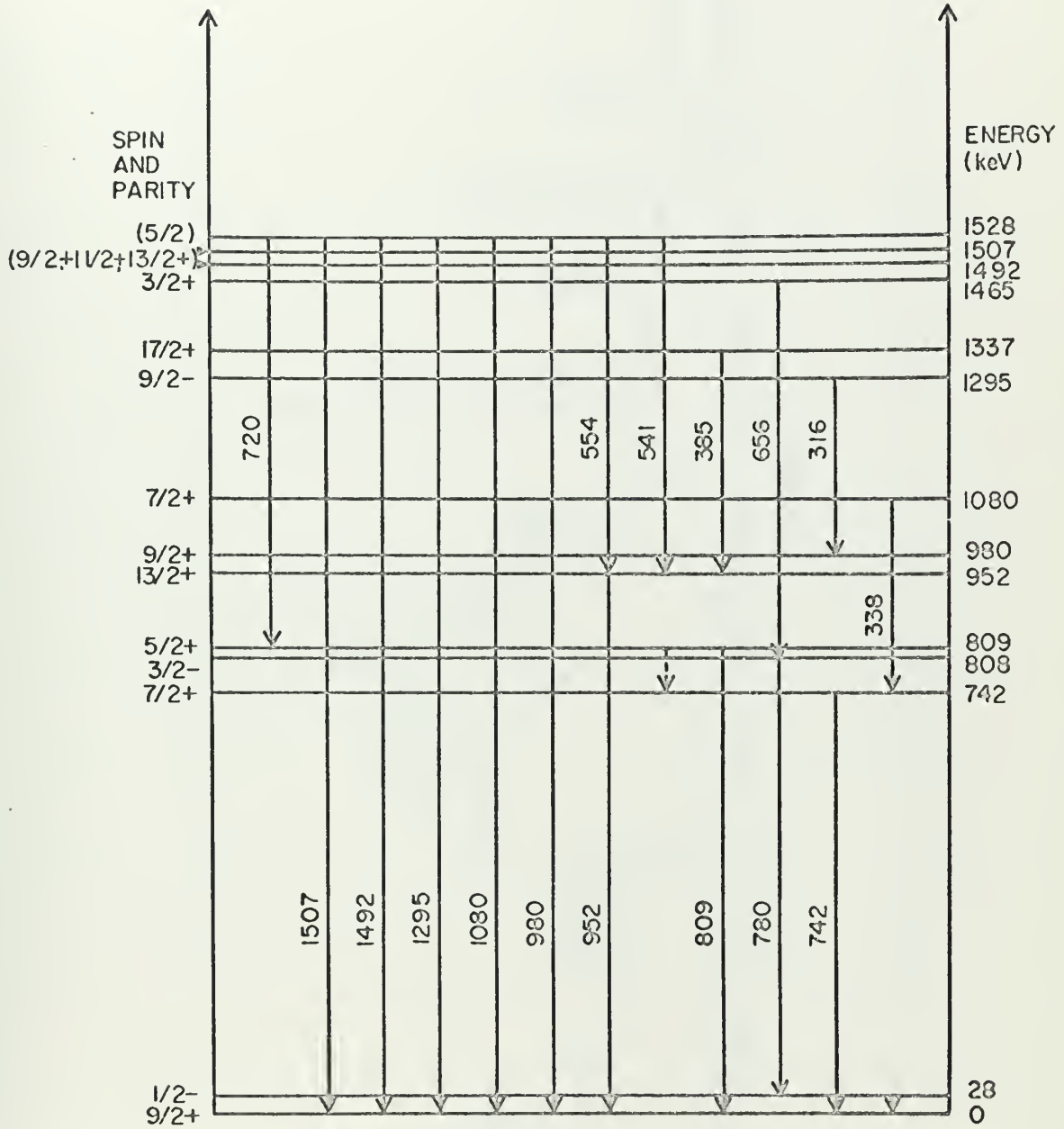

5.18 Nb^{93} Energy Level Diagram

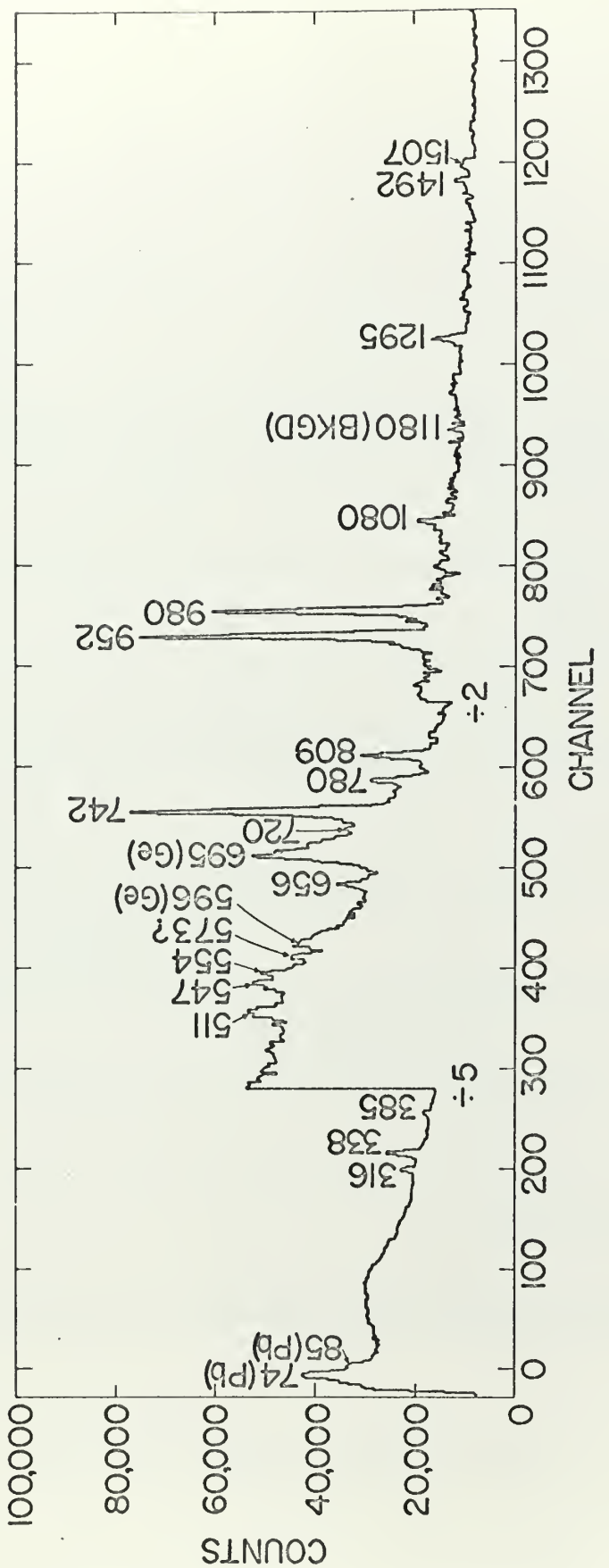

5.19 Nb^{93} Time Gated Energy Spectrum, Neutron Energy, 1.79 MeV

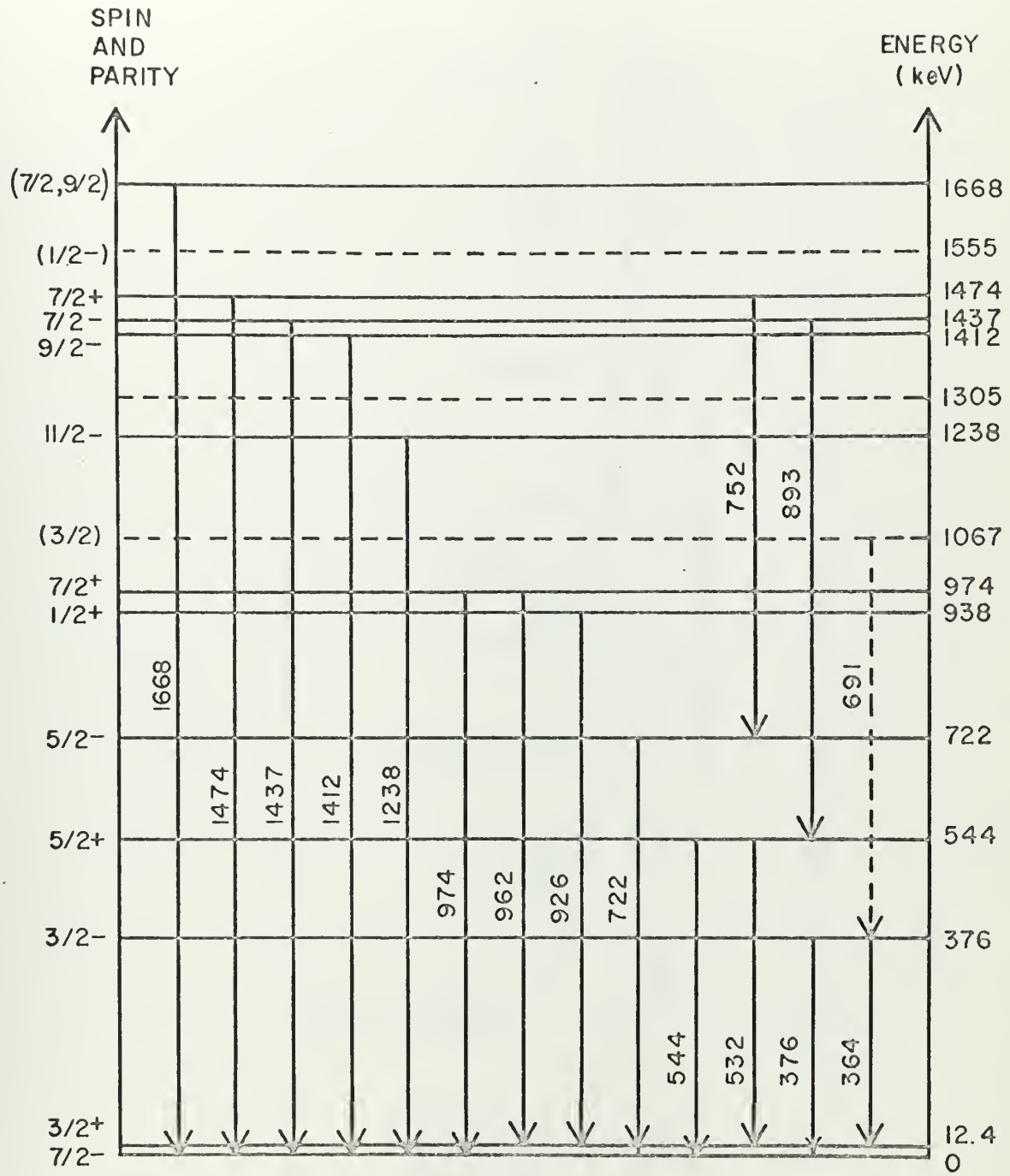

5.20 Sc^{45} Energy Level Diagram

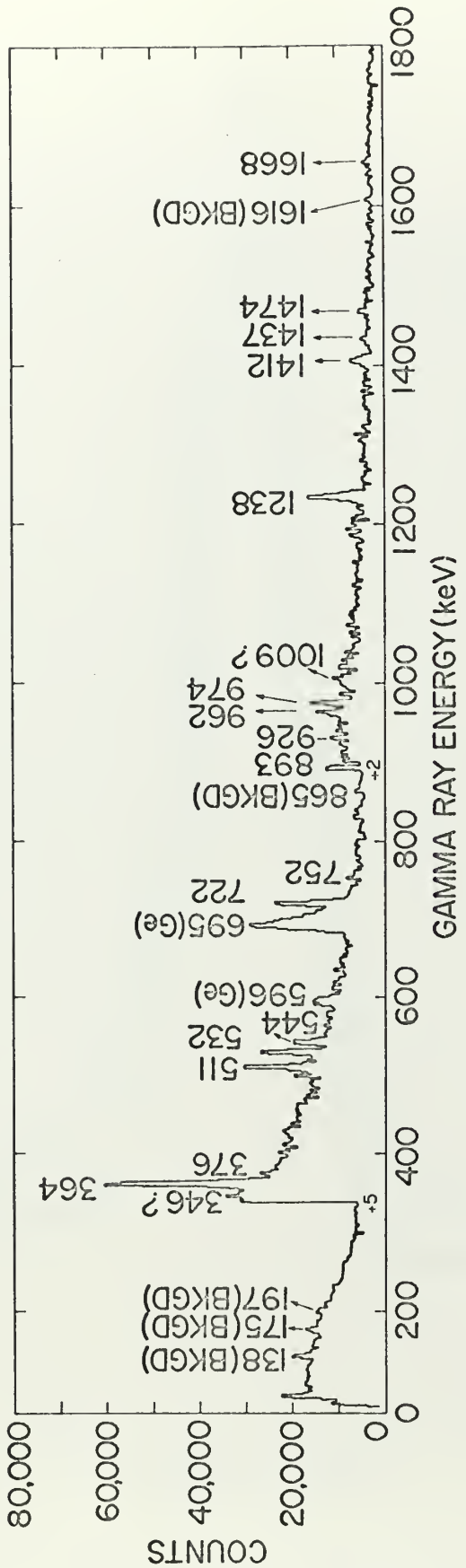

5.21 Sc^{45} Time Gated Energy Spectrum, Neutron Energy, 1.69 MeV

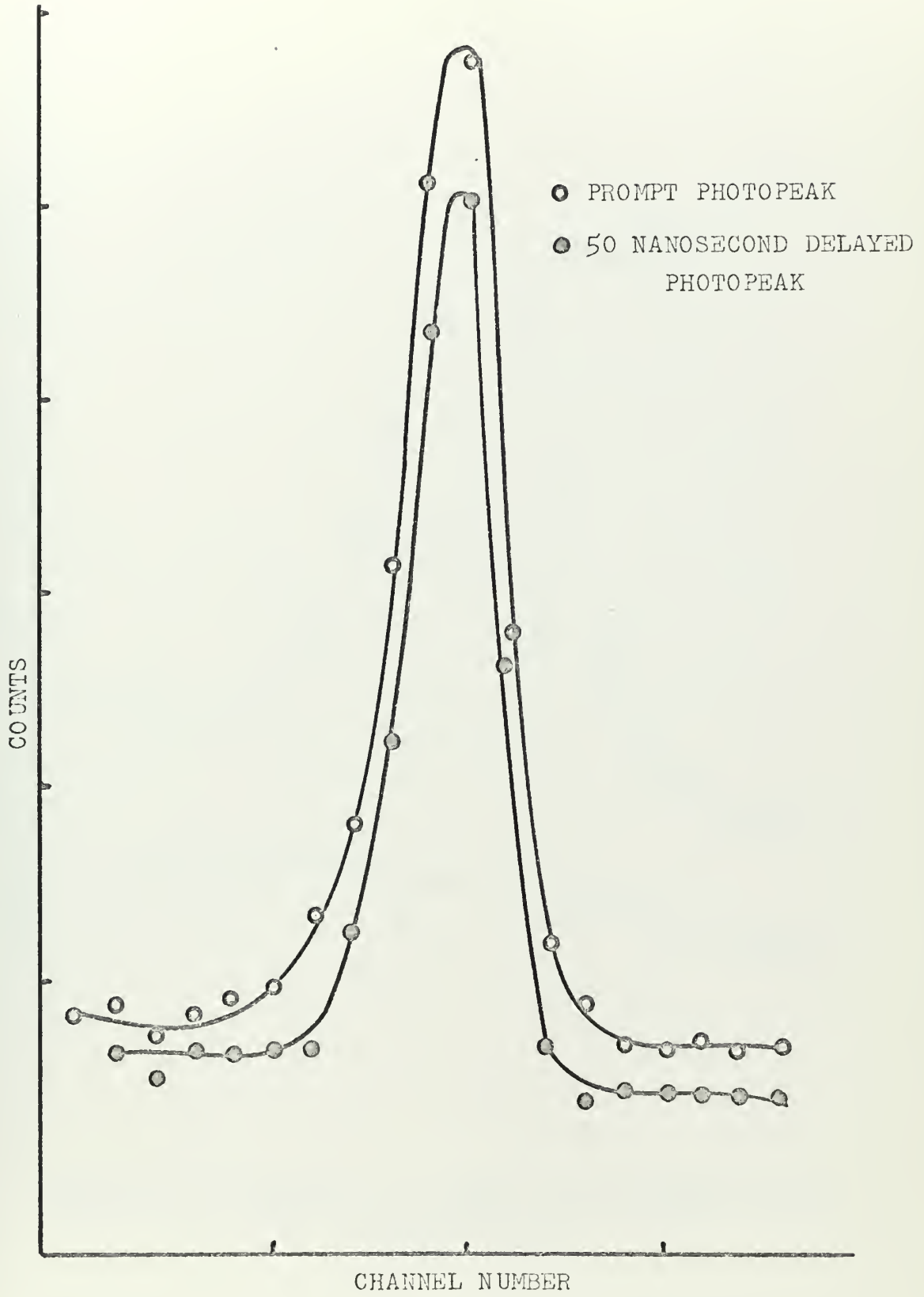

5.22 F^{19}, 197 keV Level, Prompt Versus Delayed Photopeaks

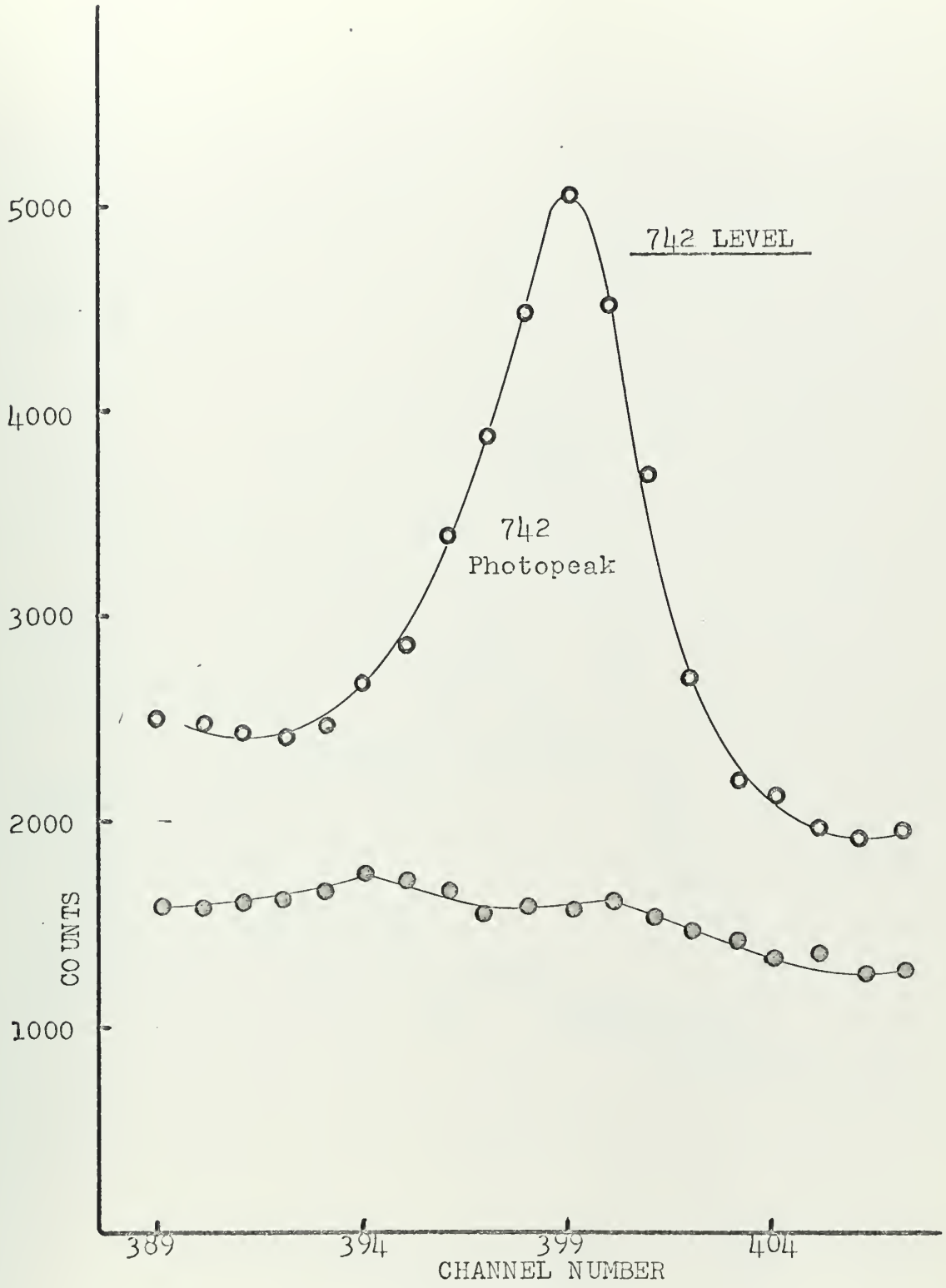

5.23 Nb^{93}, 742 keV Level, Prompt Versus Delayed Photopeaks

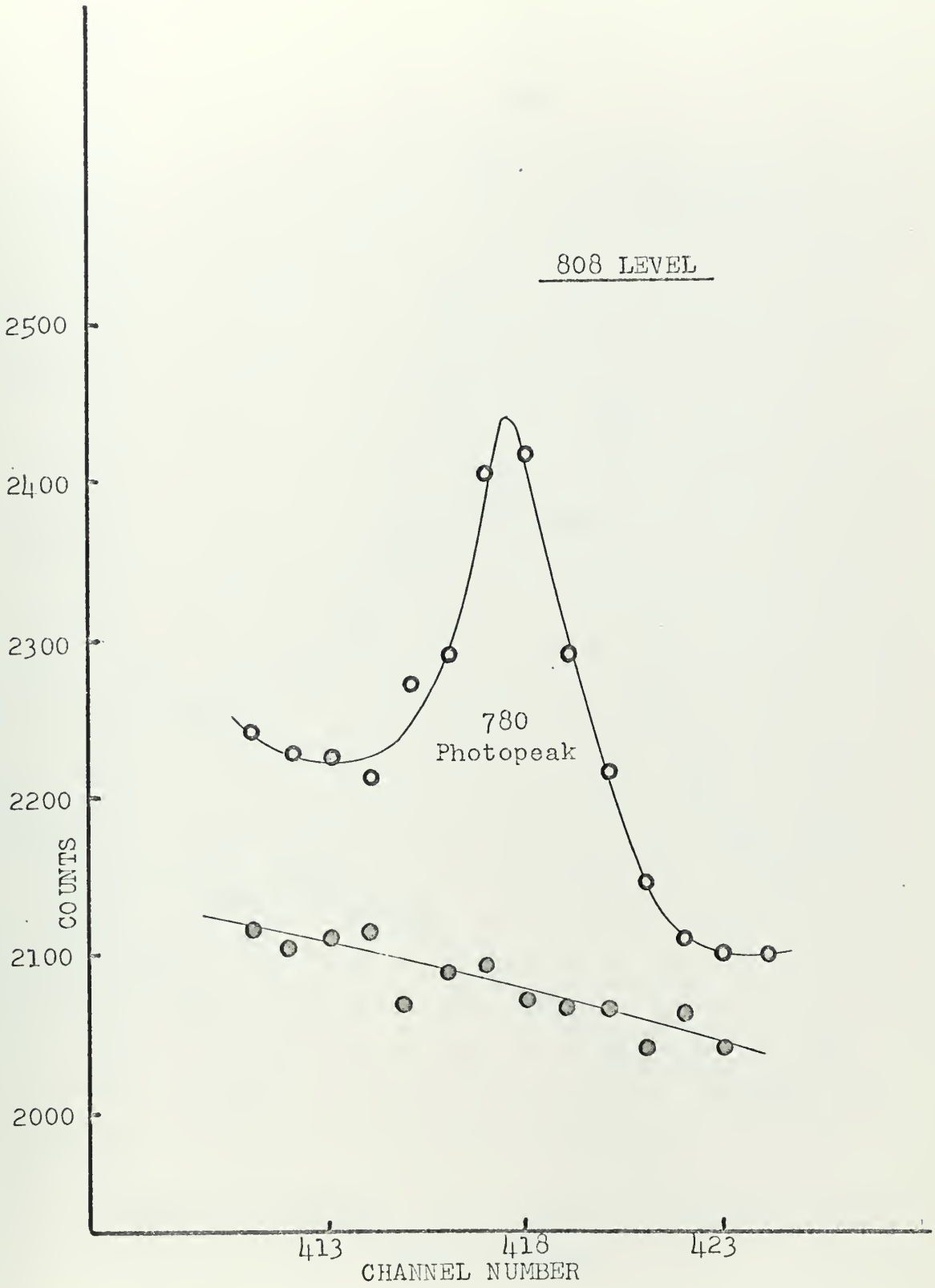

5.24 Nb^{93}, 808 keV Level, Prompt Versus Delayed Photopeaks

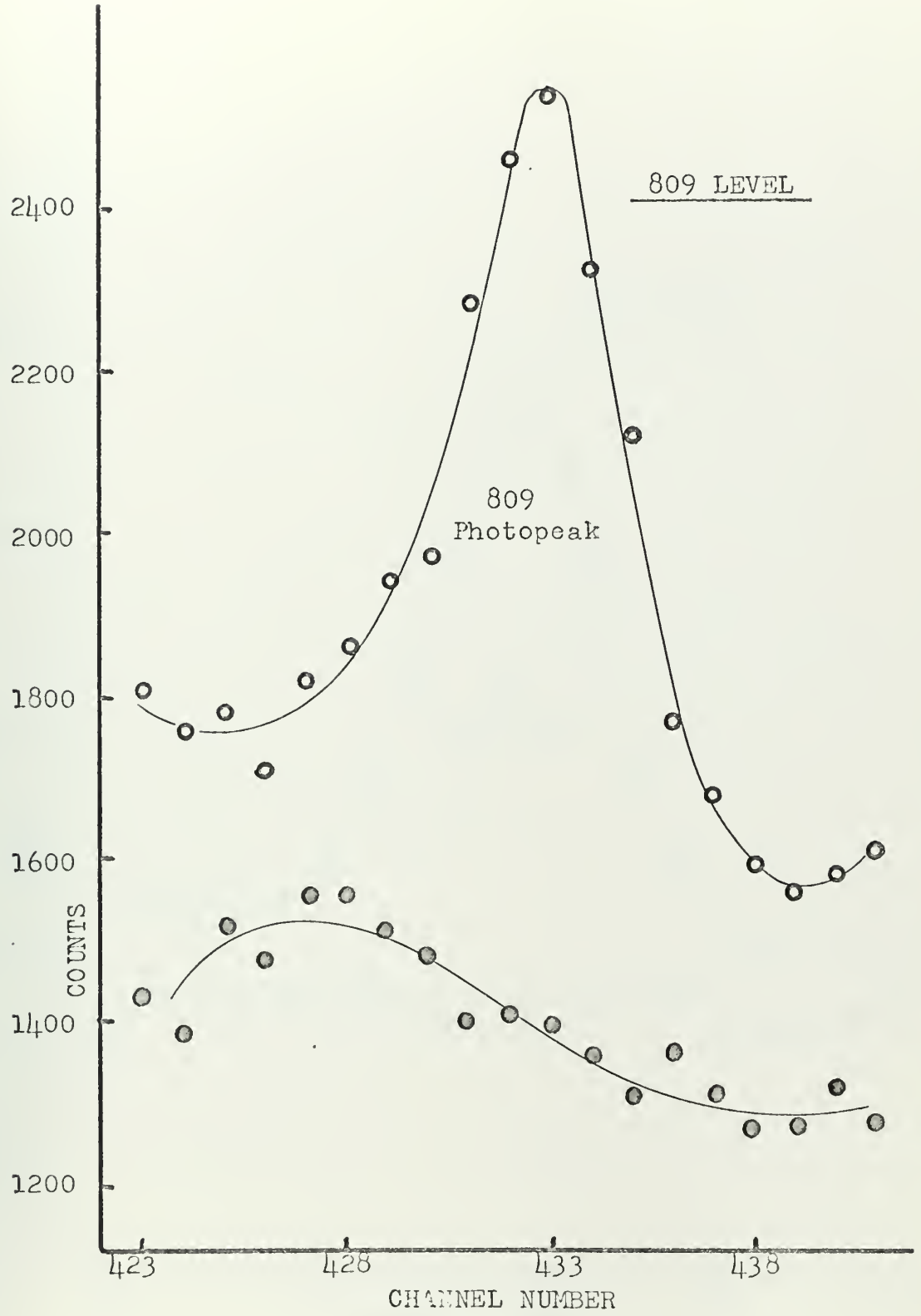

5.25 Nb^{93}, 809 keV Level, Prompt Versus Delayed Photopeaks

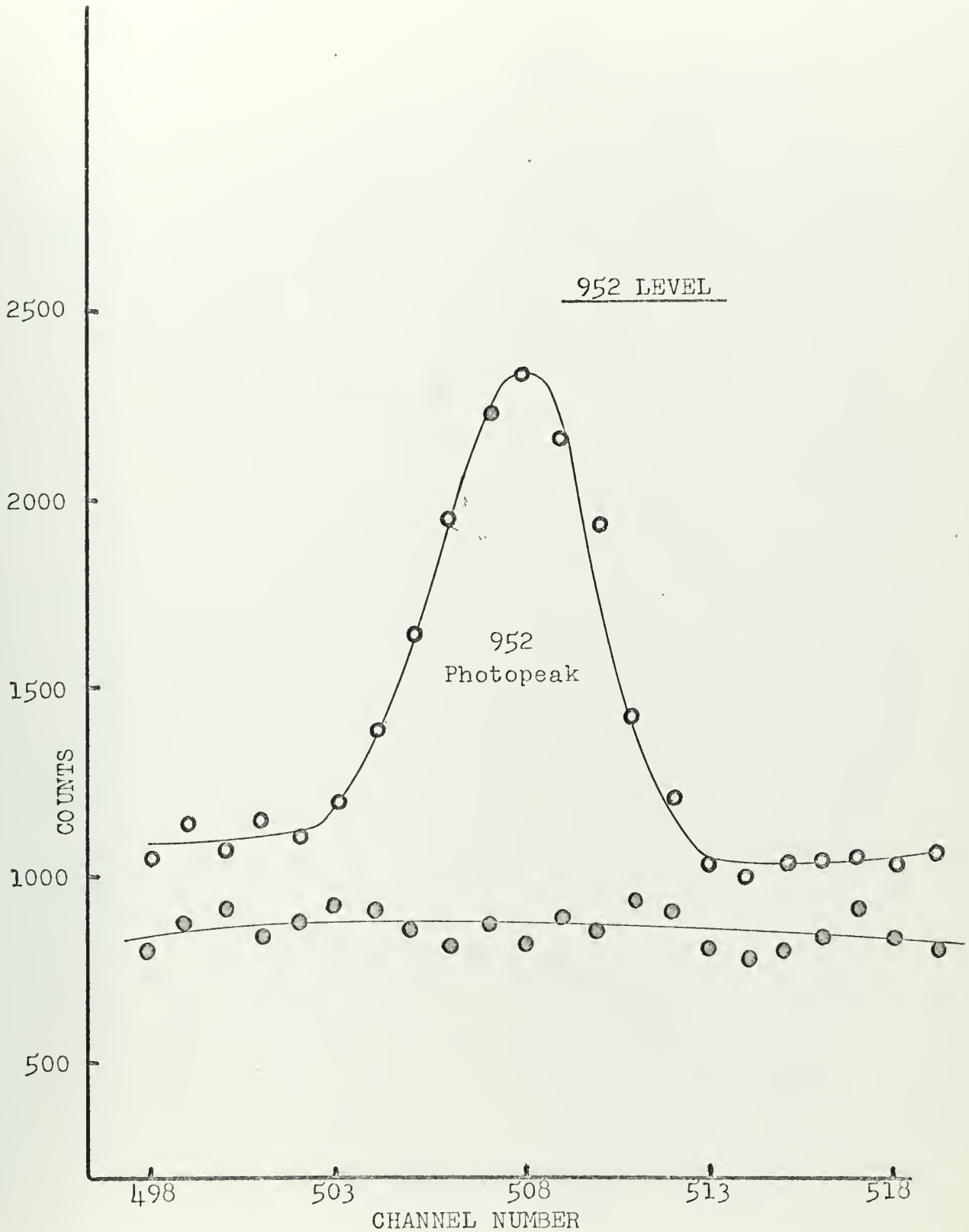

5.26 Nb^{93}, 952 keV Level, Prompt Versus Delayed Photopeaks

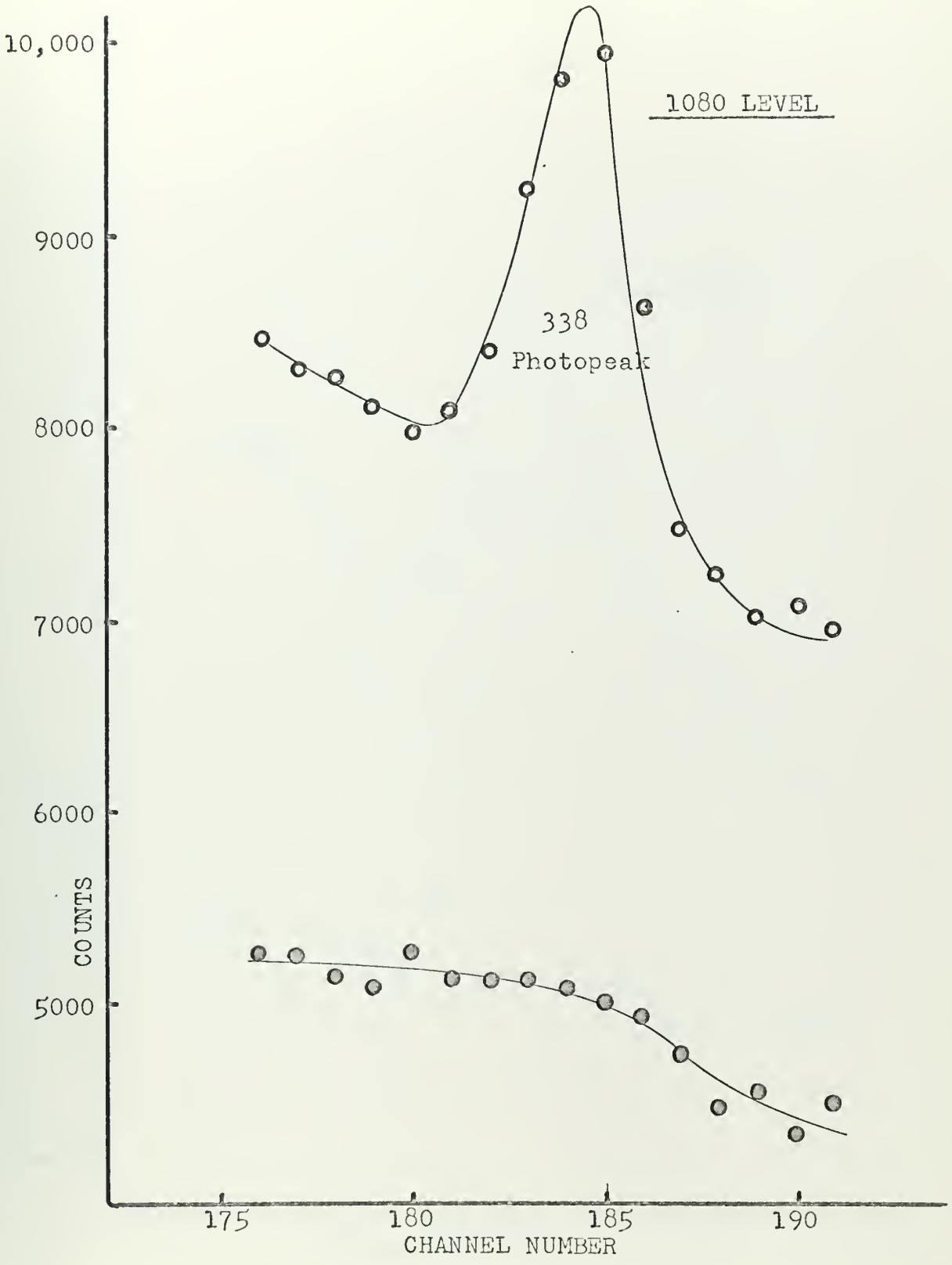

5.27 Nb^{93}, 1080 keV Level, Prompt Versus Delayed Photopeaks

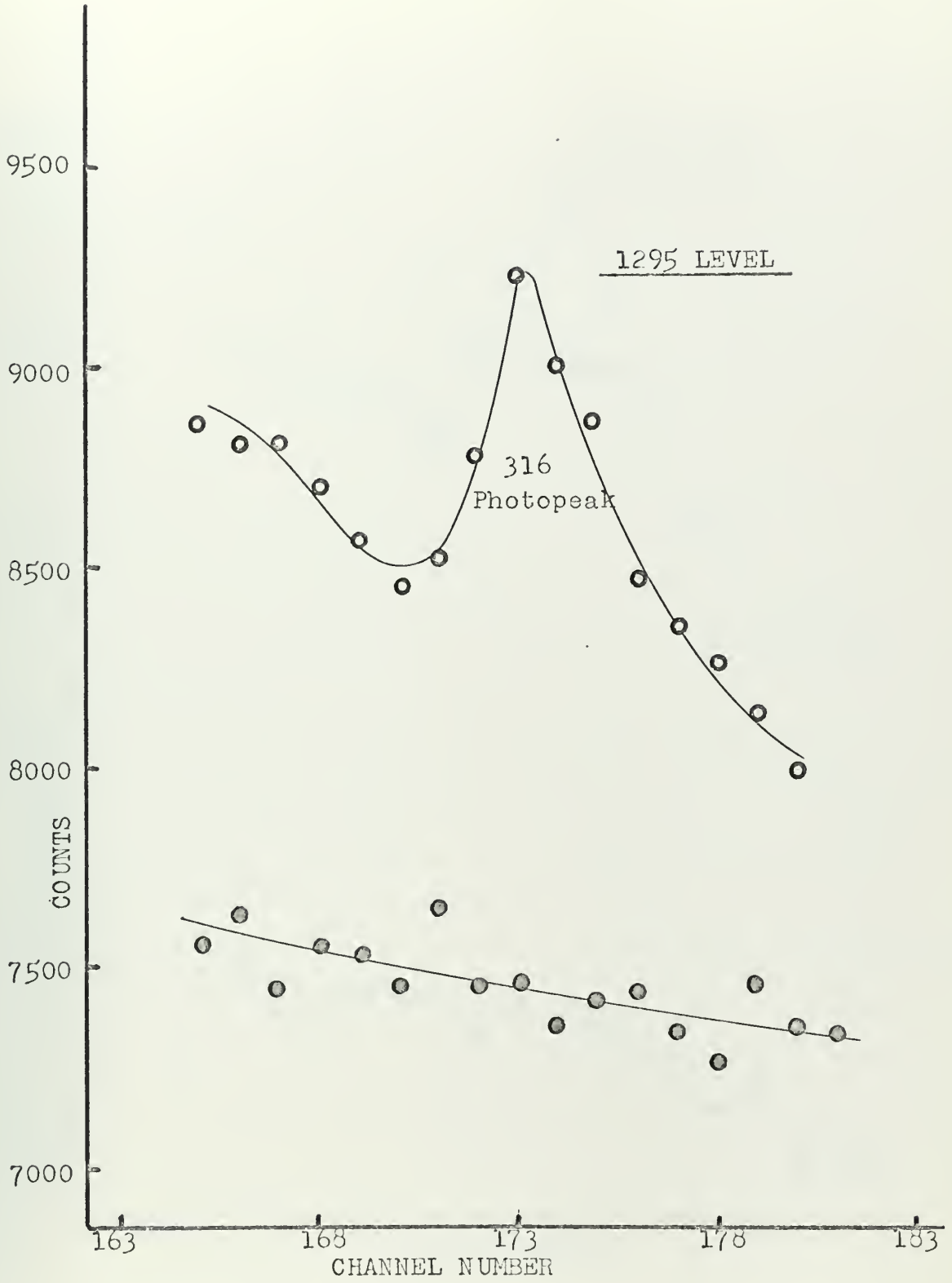

5.28 Nb^{93}, 1295 keV Level, Prompt Versus Delayed Photopeaks

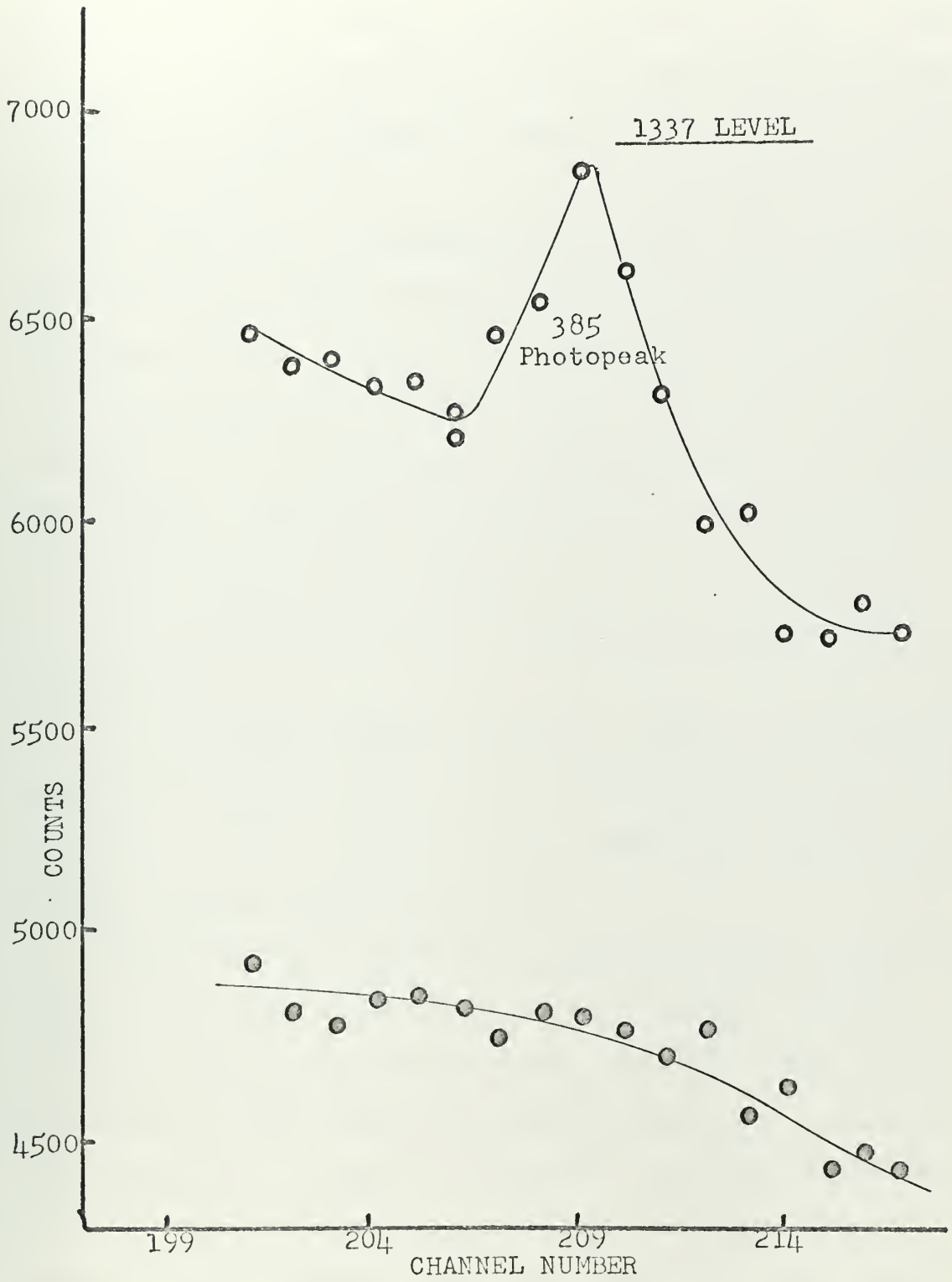

5.29 Nb^{93}, 1337 keV Level, Prompt Versus Delayed Photopeaks

within statistical accuracy, the photopeak areas from the 50 nanosecond delayed energy spectra are zero. This indicates that for the above excited levels the mean lives are all below the detection limit of this technique, about 10 nanoseconds.

A comparison of photopeak areas could not be made on the remaining levels because of the poor photopeak to background ratio. These small photopeak areas are caused by a low gamma ray production cross section for the particular excited level. A low cross section may be due to a large spin change necessary for excitation or the possibility that the energy of the neutrons from the accelerator is lower than the threshold for significant excited level production.

All the Nb^{93} excited levels of interest, that is those investigated by V. Rogers, are listed in Table 5.2. Beside each level, is an estimate of its mean life using Weisskopf's extreme single particle model.[7]

Weisskopf's estimates are verified by the results from the excited levels that were experimentally evaluated. With the exception of the 28 keV level, the only level for which Weisskopf's single particle estimate predicts a relatively long mean life is that at 1.337 MeV. The predicted mean life for this E2 transition is about 10 nanoseconds. However experimentation has shown that for actual E2 transistions the mean lives are usually shorter or enhanced [7]

Table 5.2

Excited Levels Investigated [3] in Nb^{93}

EVEL ENERGY (keV)	GAMMA DECAY ENERGIES (keV)	τ EXPERIMENTAL RESULT	τ_w (sec) WEISSKOPF ESTIMATE
742	742	<10 ns.	10^{-10} - 10^{-16}
808	780	<10 ns.	10^{-10} - 10^{-16}
809	809	<10 ns,	10^{-10}
952	952	< 10 ns.	10^{-10}
980	980	--	10^{-16}
1080	1080, 338	<10 ns.	10^{-16}
1295	1295, 316	<10 ns.	10^{-14} - 10^{-16}
1337	385	<10 ns.	10^{-8}
1465	656	--	10^{-14}
1492	1492, 541	--	10^{-15} - 10^{-17}
1507	1507, 554	--	10^{-16}
1528	720	--	10^{-15}

by factors of from 10 to 300 with respect to the Weisskopf single particle estimates. This enhancement, coupled with the fact that a 10 nanosecond mean life is on the limit of the sensitivity of this mean life detection technique, accounts for the experimental determination that the mean life of the 1.337 MeV level was less than 10 nanaoseconds.

For the levels which could not be experimentally investigated, Weisskopf'f estimates probably give a value to within several orders of magnitude. Therefore it appears that for each excited level in Nb^{93}, studied by V. Rogers, the mean life is sufficiently short so that no further corrections are necessary in the experimentally determined gamma ray production cross sections.

5.2.2 Scandium Results: The levels in Sc^{45} which proved conducive to experimental investigation were those at .376 MeV (Figure 5.30), .544 MeV (Figure 5.31), .722 MeV (Figure 5.32), and 1.238 MeV (Figure 5.33). Comparison of the photopeak areas revealed that for all levels, with the exception of that at .376 MeV, the mean lives were shorter than the 10 nanosecond sensitivity limit of the detection technique.

In the case of the .376 MeV level, the experimental results (Figure 5.30) show that there is a small photopeak at .364 MeV in the 50 nanosecond delayed energy spectrum. Comparison of the photopeak areas gives an experimentally

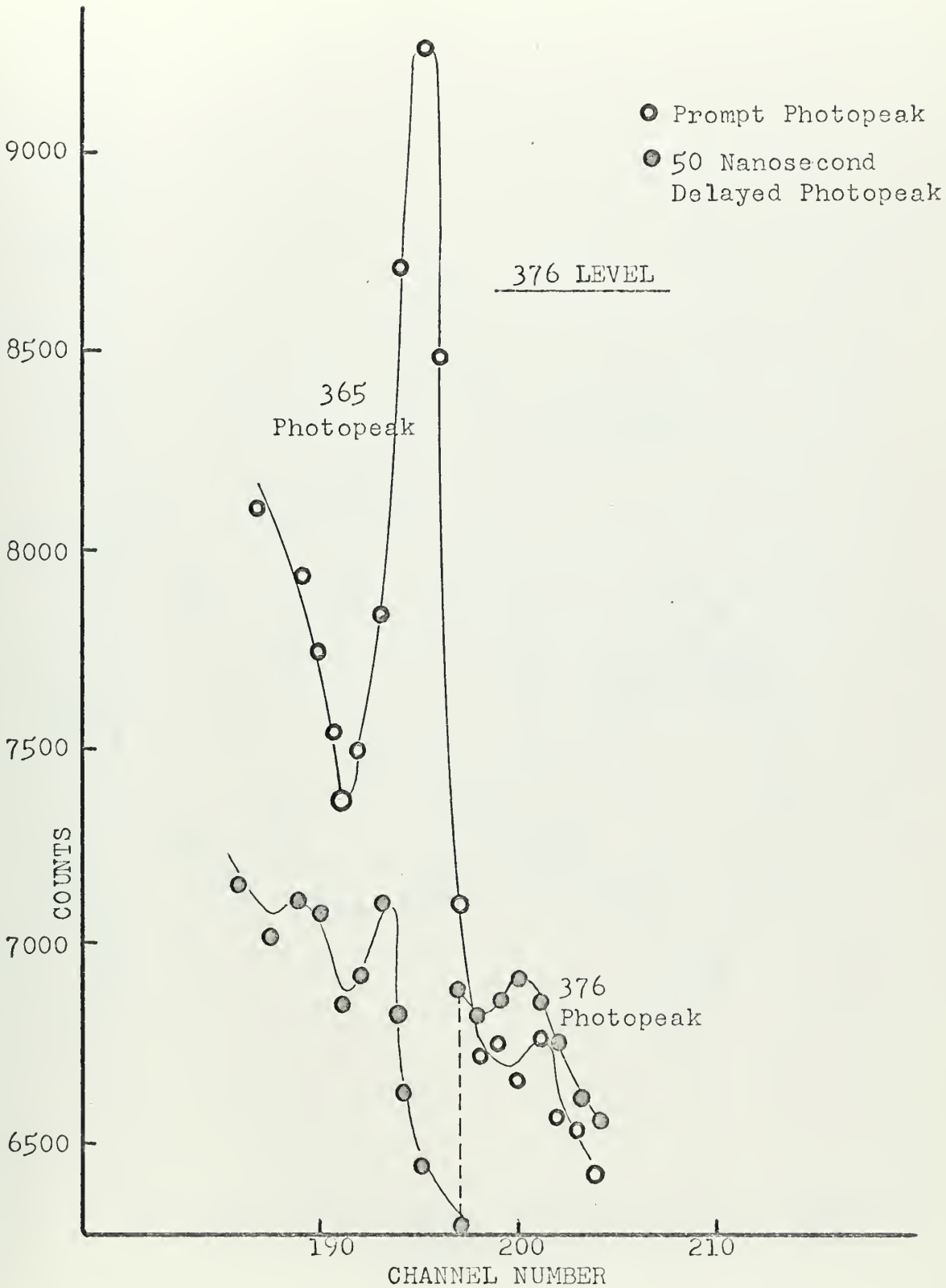

5.30 Sc^{45}, 376 keV Level, Prompt Versus Delayed Photopeaks

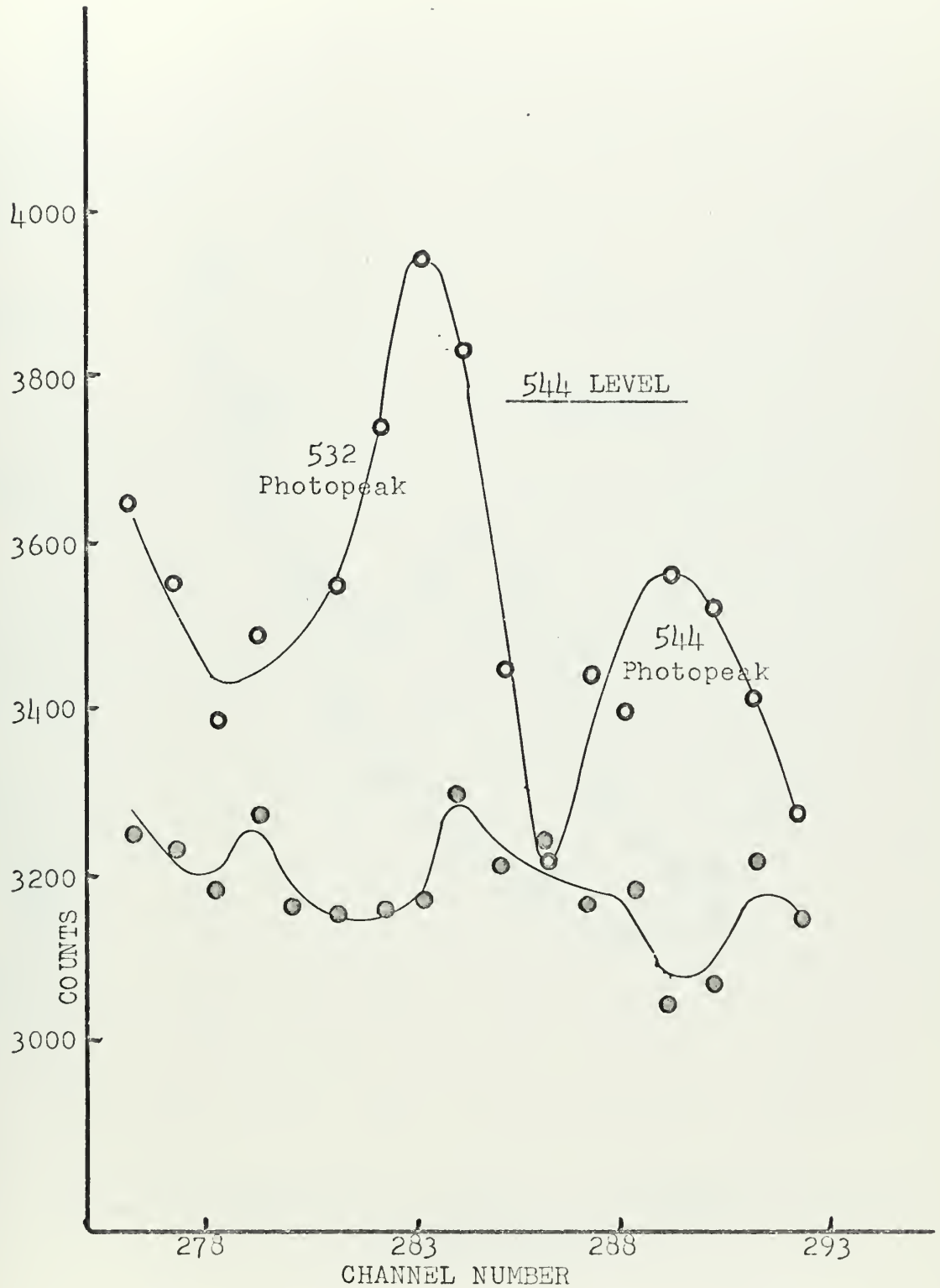

5.31 Sc^{45}, 544 keV Level, Prompt Versus Delayed Photopeaks

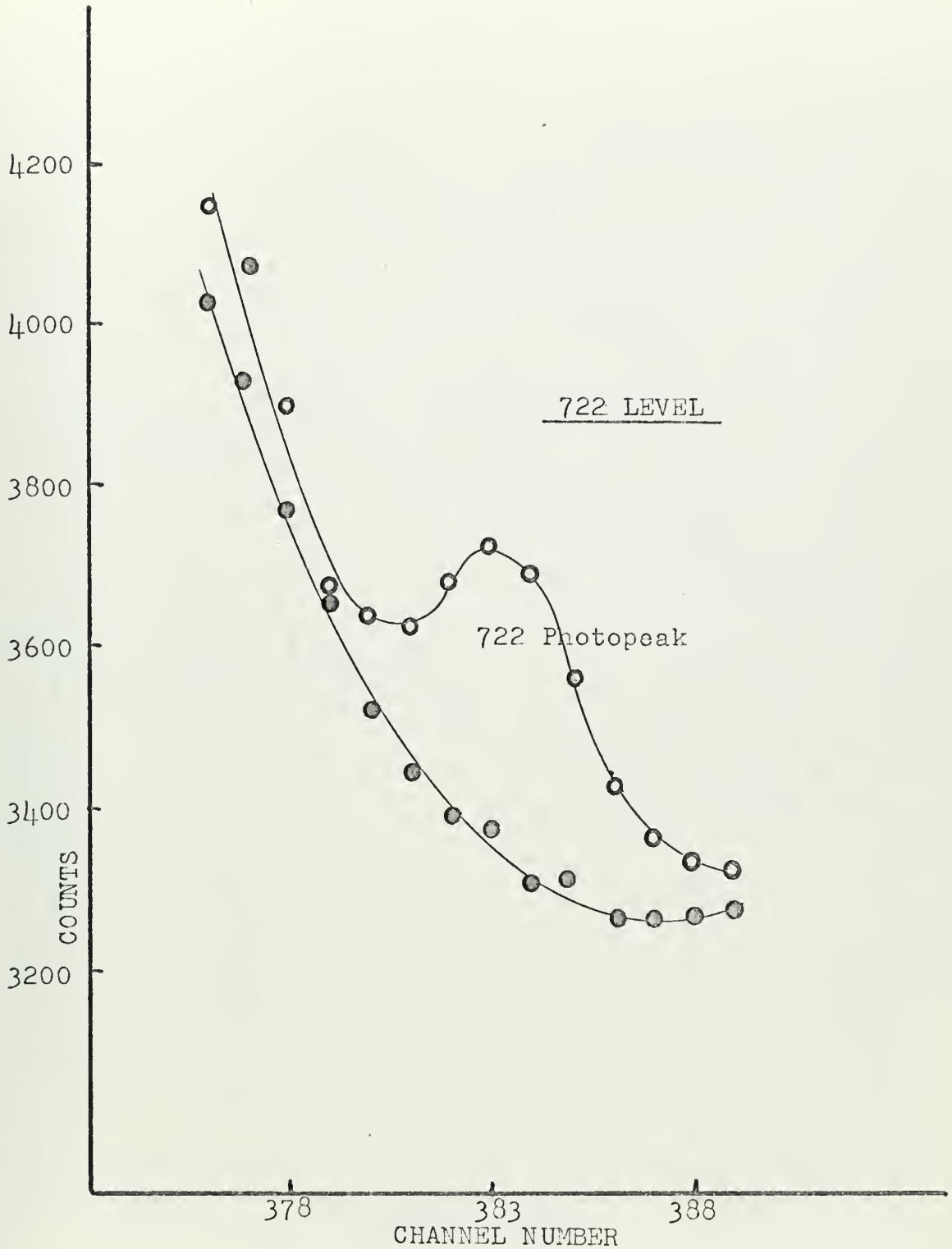

5.32 Sc^{45}, 722 keV Level, Prompt Versus Delayed Photopeaks

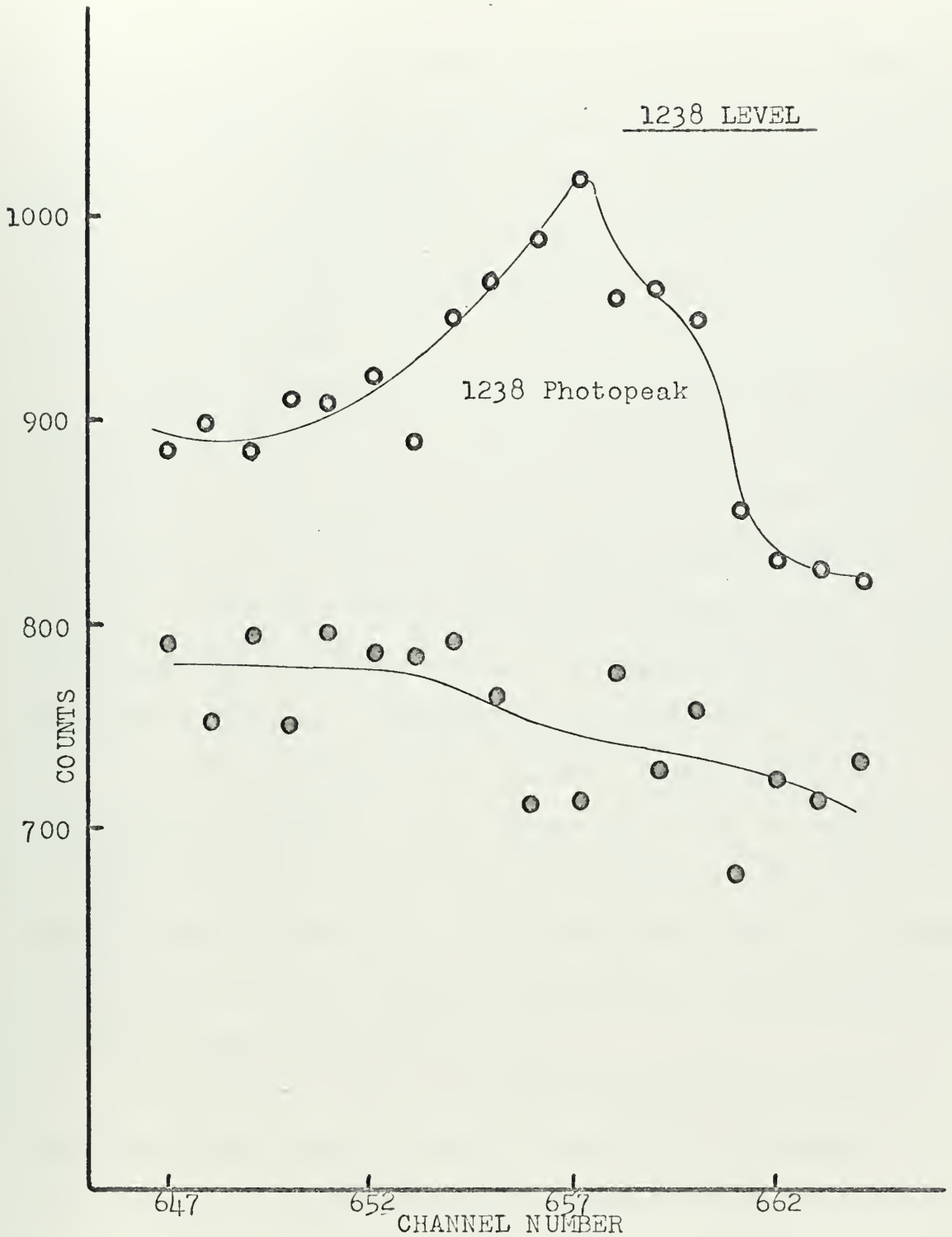

5.33 Sc^{45}, 1238 keV Level, Prompt Versus Delayed Photopeaks

observed mean life for the .376 MeV level of 10 ± 10 nanoseconds.

The .376 MeV level decays by emission of .376 and .364 MeV gamma rays. The possible transistion multipolarities are (for the .376 MeV decay) E1, M2, E3 and (for the .364 MeV decay) E2, M3, E4 and M5. The most probable Weisskopf estimates (for E2 and E1) are between 10^{-8} and 5×10^{-14} seconds.

Further investigation of the .376 MeV level is needed to confirm the results of this experiment. If indeed the mean life of the .376 MeV level was approximately 10 nanoseconds, the value of the experimentally measured total neutron inelastic scattering cross section for Sc^{45} would be about 10% to 15% greater at energies lower than 1 MeV and about 5% to 10% greater at energies above 1 MeV.

All the excited levels in Sc^{45} investigated by V. Rogers, including those which could not be experimentally evaluated because of reasons discussed in section 5.2.1, are listed in Table 5.3. For each level there is presented an estimate of its mean life calculated from Weisskopf's extreme single particle model [7].

The results from the experimentally investigated excited levels tend to verify Weisskopf'f estimates. In all cases, the predicted mean lives were below 10 nanoseconds.

Table 5.3

Excited Levels Investigated [3] in Sc^{45}

EVEL ENERGY (keV)	GAMMA DECAY ENERGIES (keV)	τ EXPERIMENTAL RESULT	τ_W WEISSKOPF ESTIMATE
376	364, 376	$\sim 10 \pm 10$ ns.	$10^{-8} - 5 \times 10^{-14}$
544	544, 532	< 10 ns.	10^{-14}
722	722	< 10 ns.	10^{-13}
938	926		10^{-14}
974	974, 962	--	10^{-10}
1238	1238	< 10 ns.	10^{-11}
1412	1412	--	10^{-14}
1437	1437, 893	--	10^{-16}
1474	1474, 752	--	10^{-15}
1668	1668	--	10^{-16}

Assuming the Weisskopf estimates for the levels not experimentally evaluated are within several orders of magnitude of the actual values, it can be concluded that, for each excited level studied by V. Rogers with the exception of that at .376 MeV, the mean life is sufficiently short so that no further corrections are necessary in the experimentally determined gamma ray production cross sections.

CHAPTER VI

CONCLUSIONS AND RECOMMENDATIONS FOR FURTHER WORK

6.1 Conclusions

The detection of de-excitation gamma rays produced by pulsed, fast neutron bombardment has shown to be an effective technique for measuring the mean lives of certain nuclear excited levels. Of the mean life determination methods investigated in this thesis, the indirect method, that of reconstructing the time spectrum from a series of time gated energy spectra, proved the most accurate. It is in the indirect method that, by determining the mean life by measuring the photopeak areas, the greater advantage is taken of the high resolution in the Ge(Li) detector. At present, the major problem in the direct method is the uncertainty in the duration of background subtraction.

It is also the determination of this thesis that for the excited levels investigated by V. Rogers, all in Nb^{93} and all, with the exception of the level at .376 MeV., in Sc^{45} have mean lives of such short duration as to require no further corrections in the experimentally measured neutron inelastic scattering cross sections. The experimentally observed mean life for the .376 MeV level in Sc^{45} was found to be 10 ± 10 nanoseconds. However, further work must be done to verify this measurement.

The range of the mean lives which can be determined using the equipment discussed in chapter III, is limited by the fixed repetition rate and maximum proton energy of the accelerator and the time response of the Ge(Li) detection system. Due to these limitations, the mean lives which can be successfully measured must be for an excited level less than 2 MeV and must be in the range of 200 to 10 nanoseconds.

6.2 Recommendations for Further Work

The .376 MeV level in Sc^{45} must be further investigated in order to establish its mean life. The indirect method, coupled with long counting times, could determine if the mean life is indeed in the nanosecond region.

The accuracies of the mean life measurements could be further optimized by the recommendations below.

6.2.1 Leading Edge Timing: It appears that leading edge timing using the fast output from the first stage of the detector preamplifier may improve the detector time response by over a factor of two (Figure 6.1). Further work with the electronic equipment in the area of leading edge timing could result, not only in improving the uniformity of the timing signal, but also in decreasing the lower limit of the measurable mean life range.

6.2.2 Double Variable Least Squares Fit: The method used in this thesis to fit the experimental data to equation (4.7)

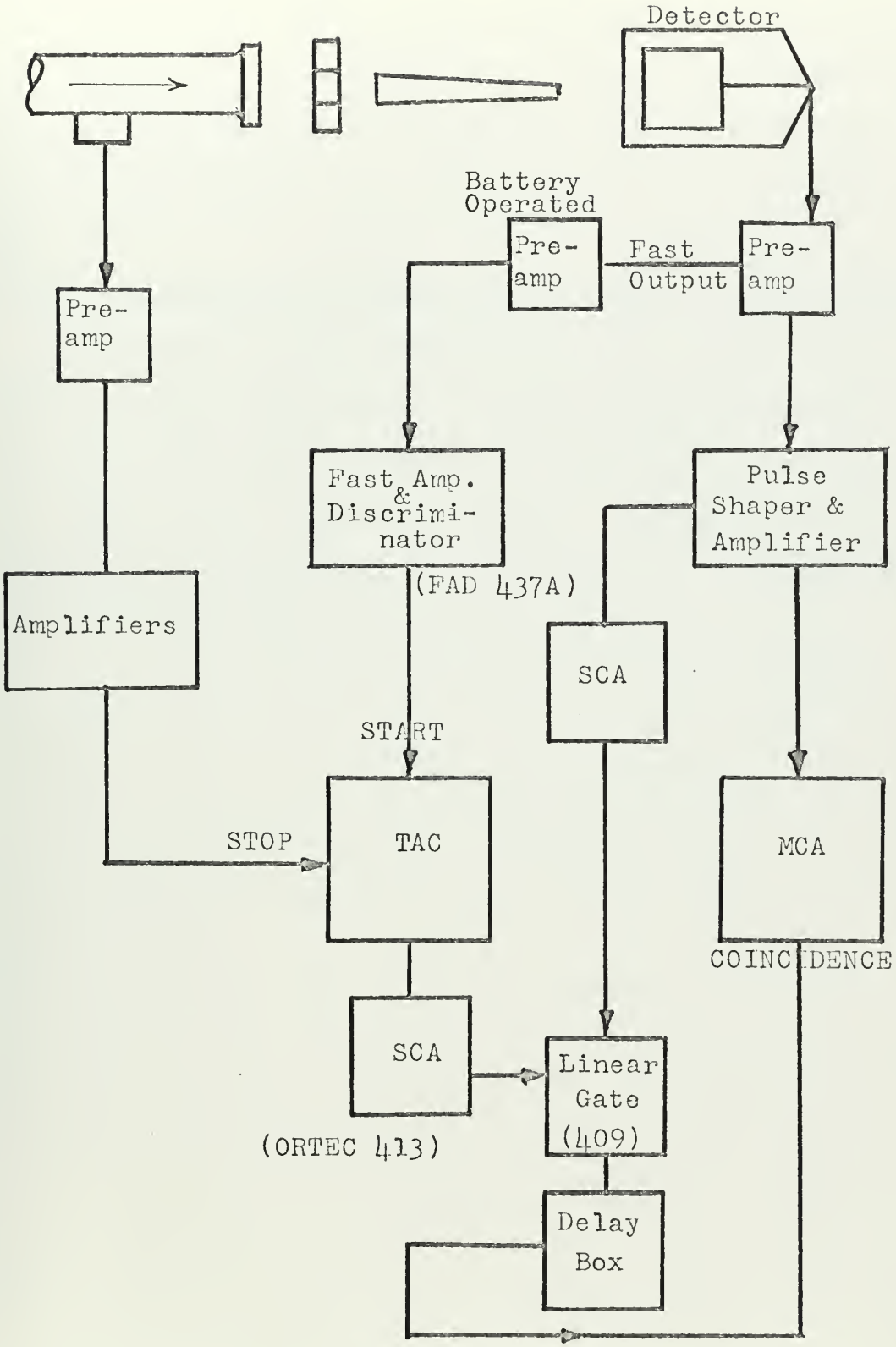

6.1 Improved Leading Edge Timing

was to normalize $\frac{dN}{dt}_{MAX}$ and then perform a least squares fit using only one variable, τ . However a more accurate fit by the method of least squares could be realized by varying both N_o and τ . This would require computer work.

6.2.3 Improvements of Theoretical Detector Time Response

In section 4.4.3c the detector time response was assumed to be a prompt jump, followed by an exponentical decay. In actuality, the time response is a combination of a guassian-type peak and an exponential decay. Incorporation of the guassian and exponential time responses will improve the accuracy of the theoretical time spectra.

REFERENCES

1. Hofmann, F., "The Application of Pulsed Neutron Techniques of the Measurement of Inelastic Scattering Cross Section," Sc.D. Thesis, M.I.T. (1966).

2. Mahoney, F.J., "Gamma Rays From Fast Neutron Scattering," Ph.D. Thesis, M.I.T. (1967).

3. Rogers, V.C., "Neutron Inelastic Scattering Cross Sections," Ph.D. Thesis, M.I.T. (1969).

4. Weisskopf, V.F., Physical Review 83, 1073 (1951).

5. Blatt, J.M. and V.F. Weisskopf, Theoretical Nuclear Physics, John Wiley and Sons, New York (1952).

6. Enge, H.A., Lecture Notes, 8.053 Introduction to Nuclear Physics, M.I.T. (1964).

7. Wilkinson, D.H., Nuclear Spectroscopy, Part B, ed.by F. Ajzenberg - Selove, Academic Press, New York (1960).

8. Evans, R.D., The Atomic Nucleus, McGraw Hill, New York (1955).

9. Graham, R.L. and G.T. Ewan, AECL-2505 (1965).

10. Graham, R.L., I.K. MacKenzie and G.T. Ewan, "Timing Characteristics of Large Coaxial Ge(Li) Detectors for Coincidence Experiments," IEEE Transactions on Nuclear Science, February, 1966.

11. Hopper, V.D., Cosmic Radiation and High Energy Interactions, Prentice-Hall, Englewood Cliffs, New Jersey (1965).

12. Nuclear Data Sheets, National Research Council, Washington, D.C. NRC 60-1, 2.

13. Johnson, C.M.P., Philosophical Magazine 1, 573 (1956).

14. Fiehrer, M., et. al., Comptes rendus 241, 1746 (1955).

15. Rietjens, L.H., et. al., Physica 21,899 (1955).

16. Simms, P.L. and R.M. Steffen, Physical Review 108, 1459 (1957).

17. Kantele, J. and O. Tannilla, Nuclear Data 4, July 1968.

thesP383
Measurements of half lives of isomeric s
3 2768 001 98015 4
DUDLEY KNOX LIBRARY